University of Padua

Department of Information Engineering
Master of Science in Electronic Engineering

Impedance spectroscopy for the study of interface phenomena in polymeric solar cells

Candidate:
Jonny Favaro

Supervisor:
Andrea Cester
Co-Supervisor:
Nicola Wrachien

Academic Year 2014/2015

Abstract

My thesis work concerns the possibility to use the Impedance Spectroscopy technique to study the interface phenomena that occur in a polymeric solar cell, focusing on the identification of the interfaces with the aim to obtain an electrical model for the studied devices.
All the tested samples come from the *Solar Cell group* of the *Energy Conversion Department* of DTU (Technical University of Denmark).
After a small introduction about the renewable electricity sources and the operation of the Standard Solar Cells, in the third chapter i present the basic principles of the *Molecular and Organic Electronic*, starting from the mechanisms that regulate the formation of bands and the conduction in organic materials and ending with a brief description of the typical production methods of the organic devices.
The chapter four describes the structure and the operation of the Organic Photovoltaic devices with a summary of standard Figures of Merits.
The fifth chapter is about the measurement technique used to characterise the devices with a description of the setup and a brief introduction on the basic principles of the Impedance Spectroscopy technique and on the methods to use the data obtained to model a device.
Chapter six present all the results i obtained on the DTU samples. The first section is about the *Switching* procedure, a technique used by DTU to activate the cell after the production using a high-voltage pulse; i analysed the impact that the length of this pulse has on the Impedance of the cells. The second section present a series of different experiments made to identify the interfaces that affect the Impedance Spectroscopy measure.
In the chapter seven i present a summary of the activity i did at DTU mostly concerning the production the devices and their basic characterization.

Index

Chapter 1

Introduction

Renewables are steadily becoming a greater part of the global energy mix, in particular in the power sector and in regions that have put in place measures to promote their deployment.

Double-digit growth rates have been observed in the last decade for some renewable energy technologies and renewables are projected to continue to grow strongly, provided that the necessary support measures are kept in place. However, the situation is nuanced across the three main energy uses: electricity, heat and transport.

Electricity generation from renewable sources is growing rapidly for most technologies while renewable energy use for heat is growing more slowly and remains under-exploited. In Europe, rapid expansion of renewable power generation, particularly wind and solar, has occurred in recent years, driven by the requirements of the European Union's Renewable Energy Directive and national targets. However, low rates of power demand growth and a difficult economic situation raise doubts about the timelines of future investments and policymakers in several countries have started to express concerns about the affordability of high shares of certain types of renewable power generation.

These concerns relate,particularly, to higher than anticipated rates of deployment of solar photovoltaic (PV) systems, driven, in some countries, by generous and unlimited subsidy schemes and rapidly falling PV system cost. Difficulties about integrating high levels of variable renewables into the electricity system are also emerging in some European countries.

In the United States, the market for renewables has been growing strongly,

in large part due to the continuation of stimulus policies directed at renewable energy, such as the provision of cash grants (instead of a tax credit) of up to 30% of investment costs for eligible renewable energy projects.
This programme expired at the end of 2012, but many projects were able to pre-qualify and will receive this support if completed by the end of 2016.
With rapidly growing power demand and concerns over energy security and local pollution, deployment of renewables has been accelerating and is expected to continue to do so in non-OECD countries.
In China, the energy development plan, published in January 2013 as part of the 12th Five-zear Plan, sets ambitious renewables targets with mandatory 2015 targets for non-fossil energy use, energy intensity, carbon intensity and particulate emissions. India's 12th Five-zear Plan foresees an increase in grid-connected renewable generation capacity of 11GW from large hydropower and 30GW from other renewable sources by 2017.
Major increases in renewables capacity are planned in the coming years in Brazil, led by hydropower, bioenergy and onshore wind.
Tendering schemes in South Africa, the United Arab Emirates and Morocco are prompting investment in wind, solar PV and concentrating solar power, and many other countries with rising power demand are also embarking on large-scale deployment (Figure 1.1).

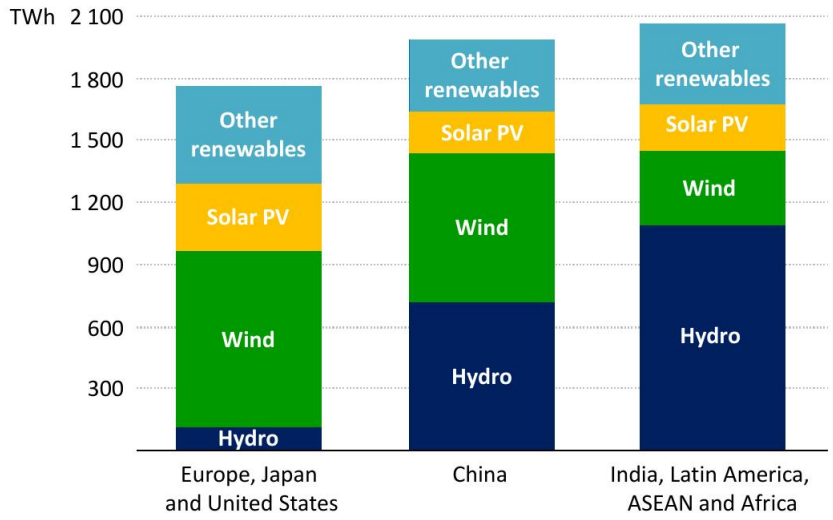

Figure 1.1: Growth in electricity generation from renewable sources, 2011-2035

1.1 Solar Energy

Unlike dispatchable power generation technologies, which may be ramped up or down to match demand, the output from solar PV is tied to the availability of the resource.
Since their availability varies over time, they are often referred to as variable renewables, to distinguish them from the dispatchable power plants.

The relevant properties include:

Variability Power generation from solar is bound to the variations of the levels of solar irradiance but remains a element of unpredictability, such as the extent of cloud cover or interference through snow, sand or dust cover

Resource location Solar resources may be located far from load centres.

Modularity Solar PV systems have capacities that are typically on the order of tens of kilowatt to megawatt, much smaller than conventional power plants that have capacities on the order of hundreds of MW.

Uncertainty The accuracy of forecasting solar irradiance levels diminishes the earlier the prediction is made for a particular period, though forecasting capabilities for the relevant time-frames for power system operation are improving.

Low operating costs Once installed,solar power systems generate electricity at very low operating costs, as no fuel costs are incurred.

Non-synchronous generation Power systems are run at one synchronous frequency:most generators turn at exactly the same rate (commonly 50 Hz or 60 Hz), synchronized through the power grid.Solar generators are mostly non-synchronous, that is, not operating at the frequency of the system.

The extent to which these properties of variable renewables pose challenges for system integration largely depends on site-specific factors, such as the correlation between the availability of solar generation with power demand the flexibility of the other units in the system available storage and interconnection capacity and the share of variable renewables in the overall generation mix.

The last ten years brought important technology progress, with significant cost reductions.
Newer technologies, such as thin film technologies, are gaining growing market shares and bring further potential for cost reductions.
Systems which include sun tracking systems can reduce variability, as can an array of panels with differing orientations, but in both cases costs are increased.
Solar PV generation expanded by 50 % per year worldwide over the last decade, reaching almost 100 TWh in 2012.
In this year, total installed capacity of solar PV increased by 43 %, or 29.4 GW, representing 15 % of the total growth in global power generation capacity. In the New Policies Scenario, electricity produced from solar PV rises to 950 TWh in 2035, as its share of global electricity generation increases from 0.4% to 2.6%.
Europe remains the world's leading region in terms of cumulative installed capacity, with more than 70 GW as of 2012.
This represents about 70% of the world's cumulative PV capacity (compared to about 75% of the world's capacity in 2011).
Next in the ranking are China (8.3 GW) and the USA (7.8 GW), followed by Japan (6.9 GW). Many of the markets outside EU-in particular China, the USA and Japan, but also Australia (2.4 GW) and India (1.2 GW)-have addressed only a very small part of their enormous potential; several countries from large Sunbelt regions like Africa, the Middle East, South East Asia and Latin America are on the brink of starting their development.
Even so, the cumulative installed capacity outside Europe reached 30 GW as of 2012, demonstrating the ongoing rebalancing between Europe and the rest of the world and reflecting more closely the patterns in electricity consumption (Figure 1.2). Europe's market has progressed rapidly over the past decade: from an annual market of less than 1 GW in 2003 to a market of over 13.6 GW in 2010 and 22.4 GW in 2011 - even in the face of difficult economic circumstances and varying levels of opposition to PV in some countries.
But the record performance of 2011, driven by the fast expansion of PV in Italy and again a high level of installations in Germany, was not repeatable in 2012 and the market went down to 17.2 GW.

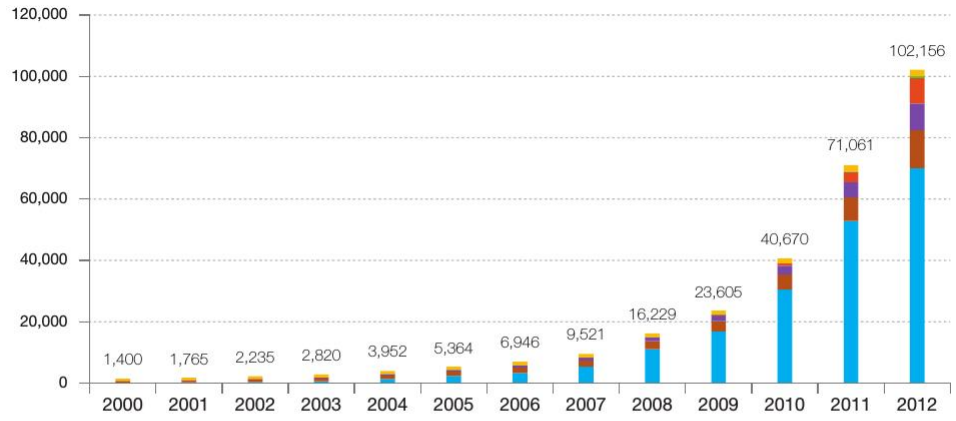

	2000	2001	2002	2003	2004	2005	2006	2007	2008	2009	2010	2011	2012
ROW	751	807	887	964	993	1,003	1,108	1,150	1,226	1,306	1,590	2,098	2,098
MEA	n/a	n/a	n/a	n/a	1	1	1	2	3	25	71	192	601
China	19	24	42	52	62	70	80	100	140	300	800	3,300	8,300
Americas	146	178	225	290	394	501	650	863	1,209	1,752	2,780	4,959	8,717
APAC	355	495	686	916	1,198	1,500	1,825	2,096	2,631	3,373	4,956	7,628	12,397
Europe	129	262	396	598	1,305	2,289	3,281	5,310	11,020	16,850	30,472	52,884	70,043
Total	**1,400**	**1,765**	**2,235**	**2,820**	**3,952**	**5,364**	**6,946**	**9,521**	**16,229**	**23,605**	**40,670**	**71,061**	**102,156**

Figure 1.2: Evolution of global PV annual installations 2000-2012 (MW)

For the first time in the last 12 years, the PV market in Europe decreased in terms of new connected capacity.
For the seventh time in the last 13 years, Germany was the world's top PV market, with 7.6 GW of newly connected systems; China was second with an assumed 5 GW, followed closely by Italy (3.4 GW), the USA (3.3 GW) and Japan with an estimated 2 GW. The geographical split of the PV market in Europe is linked to the speed at which the technology developed in recent years. Germany saw steady growth for nearly a decade and represents clearly the most developed PV market. But some countries that got a later start - the Czech Republic, Italy, Greece and Belgium - quickly reached high levels.
Next to these leaders, Spain now appears quite low since its market has been constrained; the French and British results continue to reveal an untapped potential in both countries (Figure 1.3). Together, Germany, China, Italy, the USA and Japan accounted for nearly 21.3 GW, or two-thirds of the global market during last year.
Regionally, Europe is followed by the Asia-Pacific (APAC) region, which in addition to Japan and China includes Korea, Australia, Taiwan and Thai-

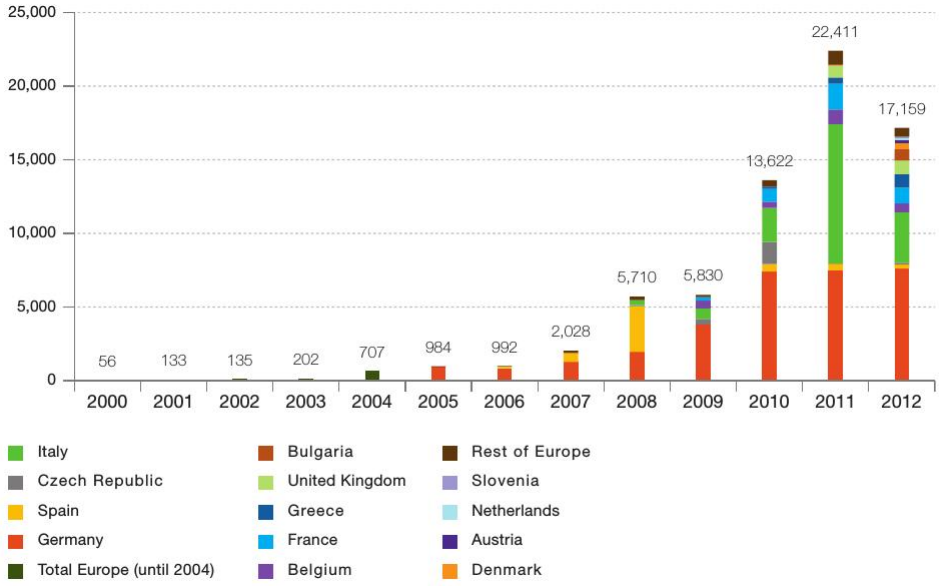

Figure 1.3: Evolution of European new grid-connected PV capacities 2000-2012 (MW)

land.

The third leading region is North America, with Canada developing steadily alongside the USA.

From a PV perspective, Europe's development is unrivalled. The USA and Japan, once PV pioneers, are now years behind Europe in terms of PV penetration and China has caught up to their level in just a few years of fast development.

Apart from Australia, the rest of the world scores quite low in terms of PV markets, though in many countries there remains great untapped potential.

Chapter 2

Solar Cell

2.1 Hystory of Solar Cells

In the year 1767 a Swiss scientist named Horace-Benedict de Saussure created the first solar collector - an insulated box covered with three layers of glass to absorb heat energy.
Saussure's box became widely known as the first solar oven, reaching temperatures of 111 C.
In 1839 the French scientist Edmond Becquerel discovered and defined the photovoltaic effect: when a photon of sufficient energy strikes a material, the photon is absorbed and an electron can pass from the valence band to the conduction band.
He used an electrolytic cell and a platinum electrode coated with silver.
In 1873, Willoughby Smith discovered photoconductivity of a material known as selenium. The discovery was to be further extended in 1876 when the same man discovered that selenium produces solar energy. Attempts were made to construct solar cells using selenium.
The cell did not work out well but an important lesson was learned - that solid could convert light into electricity without heat or moving parts. The discovery laid a strong base for future developments in the history of solar power.
In 1914 Goldman and Brodsky hooked up the photovoltaic effect with the presence of an energy barrier at the interface and with rectifying effect of the junctions.
In 1953, Bell Labs set up a research project for devices to provide energy

source to remote parts of the world where no grid power was available. The leading scientist, Darryl Chapin, suggested using solar cells, and his proposal was approved by his supervisors.
At that time, the photovoltaic effect in selenium, discovered in the 1870s, was already commercialized as a device for the measurement of light intensity in photography.
A layer of Se is applied on a copper substrate, then covered by a semitransparent film of gold. When the device is illuminated by visible light,a voltage is generated, which in turn generates a current (Figure 2.1a). The intensity

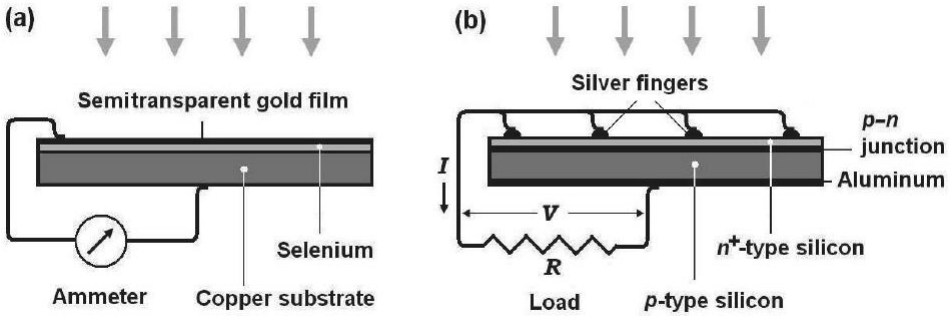

Figure 2.1: Selenium solar cell and silicon solar cell. (a) The selenium photovoltaic cell was discovered in the middle of the nineteenth century and was used for measuring light intensity in photography. (b) The silicon photovoltaic cell was invented at Bell Labs in 1954 using the technology for silicon transistors.

of electric current depends on the intensity of light. It has been a standard instrument in the first half of the twentieth century for photographers to measure light conditions. Chapin started his experiment with selenium photocells. He found that the efficiency, 0.5%, is too low to generate sufficient power for telephony applications. Then, a stroke of unbelievable luck, two Bell Lab scientists involved in the pioneering effort to develop silicon transistors, Calvin Fuller and Gerald Pearson, joined Chapin in using the nascent silicon technology for solar cells;in 1954, a solar cell with 5.7% efficiency was demonstrated (Figure 2.1b). The silicon solar cell was made from a single crystal of silicon. By judicially controlling the doping profile, a p-n junction is formed. The n-side of the junction is very thin and highly doped to allow light to come to the p-n junction with very little attenuation, but the lateral electric conduction is high enough to collect the current to

the front contact through an array of silver fingers.
The back side of the silicon is covered with a metal film, typically aluminum.
The initial demonstration of the solar cell to the public in New York City was a fanfare. The cost of building such solar cells was very high.
From the mid 1950s to the early 1970s, photovoltaics research and development were directed primarily toward space applications and satellite power. In 1976, the U.S. Department of Energy (DOE) was established. A Photovoltaics Program was created. The DOE, as well as many other international organizations, began funding research in photovoltaics at appreciable levels. A terrestrial solar cell industry was quickly established. Economies of scale and progress in technology reduced the price of solar cells dramatically (Figure 2.2).

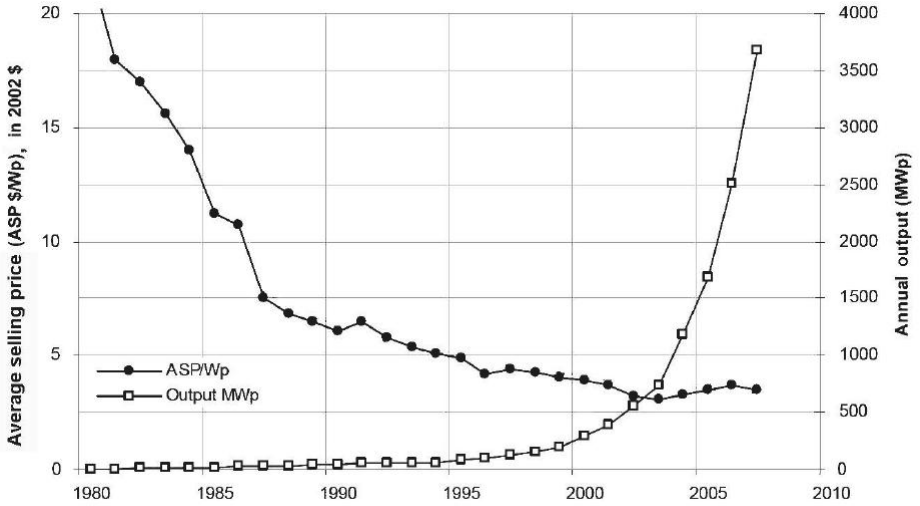

Figure 2.2: Average price and installation of solar cells: 1980-2007. The average price of solar cells dropped threefold from more than $ 20 per peak watt in 1980 to $ 6.5 per peak watt in 1990.

2.2 Semiconductor

The main difference between semiconductor and other material (conductor and insulator) is the different distribuition and configuration of the energy bands. In particular for this type of application the most important bands are:

Conductive Band The conduction band quantifies the range of energy required to free an electron from its bond to an atom. Once freed from this bond, the electron becomes a 'delocalized electrons', moving freely within the atomic lattice of the material to which the atom belongs

Valence Band The valence band is the highest range of electron energies in which electrons are normally present at absolute zero temperature.

Various materials may be classified by their band gap: this is defined as the difference between the valence and conduction bands (Figure 2.3)

Insulator The conduction band is higher than that of the valence band and the Energy Gap is big so it takes infeasibly high energies to delocalize their valence electrons. They are said to have a non-zero band gap.

Semicondutors Is primarily an insulator at 0K but the Energy band gap is small. The valence band is slightly thermally populated at room temperature, whereas the conduction band is slightly depopulated and thus it isn't a insulator but the conductivity is small.

Metals Conduction bands and valence bands are not separated and there is therefore no energy gap. The conduction band is then partially occupied, resulting in a "high" electrical conductivity.

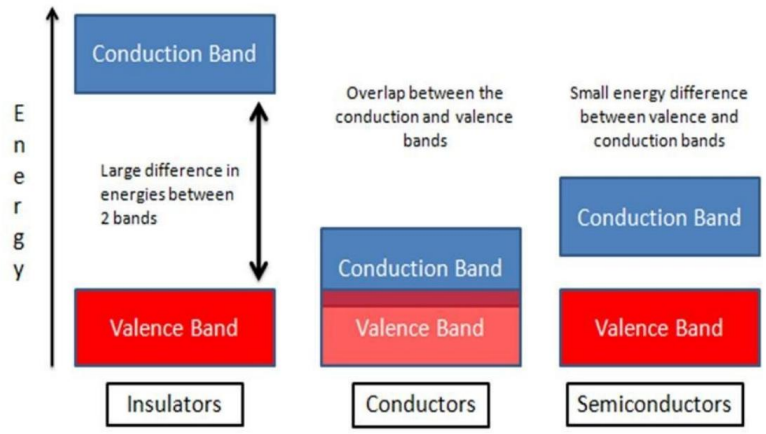

Figure 2.3: Energy Bands in Semiconductor, insulator and conductor

2.3 Working Principles of Inorganic Solar Cell

Semiconductor solar cells are fundamentally quite simple devices. Semiconductors have the capacity to absorb light and to deliver a portion of the energy of the absorbed photons to carriers of electrical current - electrons and holes. A semiconductor diode separates and collects the carriers and conducts the generated electrical current preferentially in a specific direction. Thus, a solar cell is "simply" a semiconductor diode that has been carefully designed and constructed to efficiently absorb and convert light energy from the sun into electrical energy.
A simple conventional solar cell structure is depicted in Figure 2.4.
Sunlight is incident from the top on the front of the solar cell. A metallic

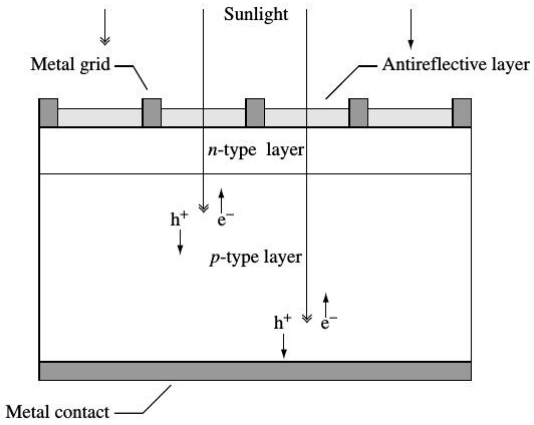

Figure 2.4: A schematic of a simple conventional solar cell. Creation of electron-hole pair, respectively, is depicted

grid forms one of the electrical contacts of the diode and allows light to fall on the semiconductor between the grid lines and thus be absorbed and converted into electrical energy. An antireflective layer between the grid lines increases the amount of light transmitted to the semiconductor. The semiconductor diode is fashioned when an n-type semiconductor and a p-type semiconductor are brought together to form a metallurgical junction. This is typically achieved through diffusion or implantation of specific impurities (dopants) or via a deposition process.
The diode's other electrical contact is formed by a metallic layer on the back of the solar cell.

All electromagnetic radiation, is composed of particles called photons, which carry specific amounts of energy determined by the spectral properties of their source.
Photons also exhibit a wavelike character with the wavelength,λ, being related to the photon energy, E_λ by

$$E_\lambda = \frac{\hbar c}{\lambda} \tag{2.1}$$

where $\hbar$ is Plank's constant and c is the speed of light. Only photons with sufficient energy to create an electron-hole pair, that is, those with energy greater than the semiconductor band gap (EG), will contribute to the energy conversion process (Figure 2.5).

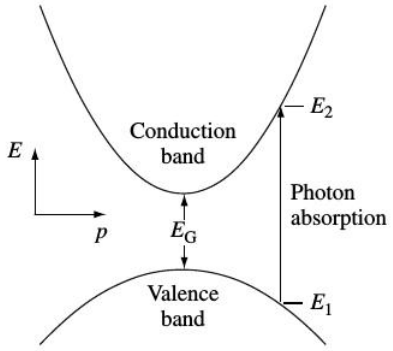

Figure 2.5: Photon absorption in a direct band gap semiconductor for an incident photon with energy hν = E2-E1>EG

When a p-n junction is illuminated the additional electron-hole pairs are generated in the semiconductor.
The concentration of minority carriers (electrons in the p-type region and holes in the n-type region) strongly increases. This increase in the concentration of minority carriers leads to the flow of the minority carriers across the depletion region into the quasi-neutral regions. Electrons flow from the p-type into the n-type region and holes from the n-type into the p-type region. The flow of the photo-generated carriers causes the so-called photo-generation current.
When no external contact between the n-type and the p-type regions is established, which means that the junction is in the open-circuit condition, no net current can flow inside the p-n junction. It means that the current

resulting from the flux of photo-generated and thermally-generated carriers has to be balanced by the opposite recombination current (Figure 2.6a) . Under illumination, when the n-type and p-type regions are short circuited, the photo-generated current will also flow through the external circuit. Under the short-circuit condition the electrostatic-potential barrier is not changed, but from a strong variation of the quasi-Fermi levels inside the depletion region one can determine that the current is flowing inside the semiconductor (Figure 2.6b).

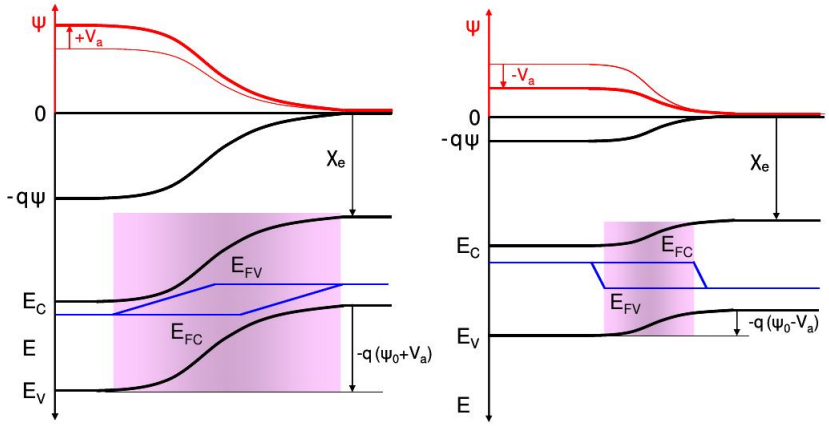

Figure 2.6: Energy band diagram and potential profile (in red colour) of a p-n junction under a) reverse bias, and b) forward bias.

2.4 Solar Cell External Parameter

The main parameters that are used to characterize the performance of solar cells are the peak power, P max, the short-circuit current density, J_{sc} , the open-circuit voltage, V_{oc} , and the fill factor, FF. These parameters are determined from the illuminated J-V characteristic (Figure 2.7).

Open-circuit voltage The open-circuit voltage is the voltage at which no current flows through the external circuit.

It is the maximum voltage that a solar cell can deliver. The V_{oc} corresponds to the forward bias voltage, at which the dark current compensates the photo-current.

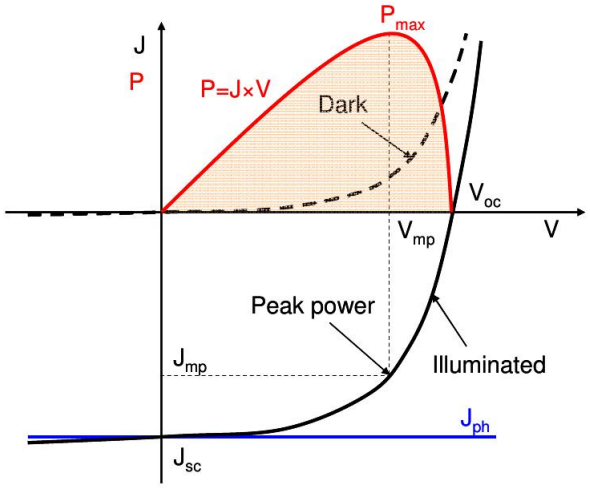

Figure 2.7: J-V characteristics of a p-n junction in the dark and under illumination.

Short-circuit current The short-circuit current,I_{sc}, is the current that flows through the external circuit when the electrodes of the solar cell are short circuited.

The short-circuit current of a solar cell depends on the photon flux density incident on the solar cell, that is determined by the spectrum of the incident light. The I_{sc} depends on the area of the solar cell. In order to remove the dependence of the Isc on the solar cell area, the short-circuit current density is often used to describe the maximum current delivered by a solar cell.

Fill Factor The fill factor is the ratio between the maximum power ($P_{max} = J_{mp}V_{mp}$) generated by a solar cell and the product of V_{oc} and J_{sc}.

$$FF = \frac{J_{mp}V_{mp}}{J_{sc}V_{oc}}$$

Conversion Efficiency The conversion efficiency is calculated as the ratio between the generated maximum power and the incident power. The irradiance value, P_{in}, of 1000 W/m^2 of AM1.5 spectrum hasbecome a standard for measuring the conversion efficiency of solar cells.

2.5 Solar Spectrum

The range of electromagnetic energy emitted by the sun is known as the solar spectrum, and lies mainly in three regions: ultraviolet, visible, and infrared. The solar spectrum extends from about or 290 nm in the longer wavelengths of the ultraviolet region, to over 4000 nm in the far infrared.
The power density just outside the earth's atmosphere is about 135 mW / cm^2 but before reaching the surface, the solar spectrum is altered due to phenomena of reflection (about 25% of the incidente radiation is reflected) and absorption (part of the radiation is absorbed by the atmosphere). The remaining part of the radiation reach the surface in two different components: direct component (light that reach the surface without deviation) and diffuse component (light that reach the surface after scattering phenomena).
The total intensity of the sun radiation that reach the surface is about 100mW/cm^2 . The unit of measure used for the sun radiation is the **SUN**, the average incident power density with an angle of 90 degrees at ground level (1 SUN=100 mW/cm^2).
The attenuation of the radiation intensity depends on the incidence angle; lower is the angle, larger is the thickness of atmosphere that the light has to pass through and thus lower is the radiation that reach the surface.

Air Mass

The Air Mass is the path length which light takes through the atmosphere normalized to the shortest possible path length (that is, when the sun is directly overhead). The Air Mass quantifies the reduction in the power of light as it passes through the atmosphere and is absorbed by air and dust. The Air Mass is defined as (Figure 2.8).

$$AM = \frac{1}{cos\theta}$$

If θ=0°, AM=1 (it's the standard atmosphere thickness).
If θ=48°, AM=1.5, the standard laboratory test value (Figure). The standard spectrum at the Earth's surface is called AM1.5G, (the G stands for

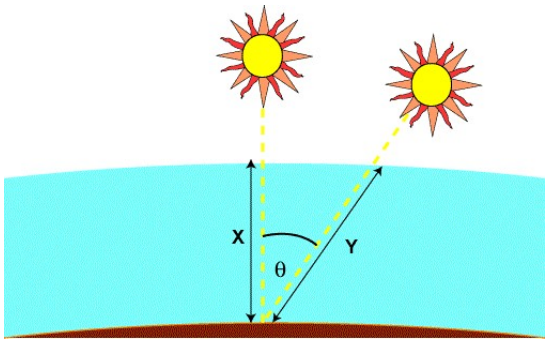

Figure 2.8: The air mass represents the proportion of atmosphere that the light must pass through before striking the Earth relative to its overhead path length, and is equal to Y/X.

global and includes both direct and diffuse radiation) or AM1.5D (which includes direct radiation only). The intensity of AM1.5D radiation can be approximated by reducing the AM0 spectrum by 28% (18% due to absorption and 10% to scattering) (Figure 2.9).

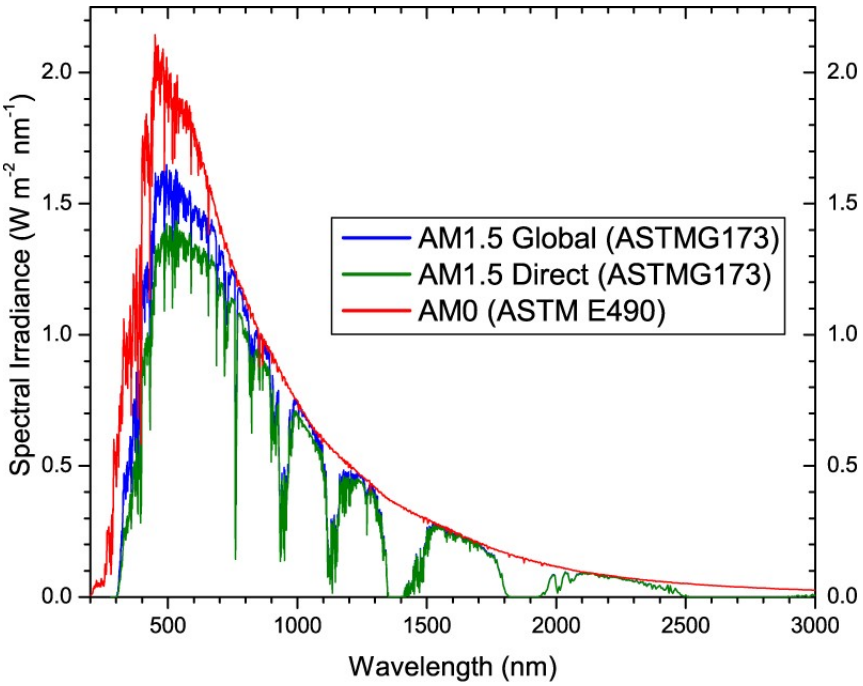

Figure 2.9: Standard Solar Spectra for space and terrestrial use.

Chapter 3

Molecular and Organic Electronics

The term "molecular electronics" is regarded as an interdisciplinary field that relies primarily on aspects of materials science, chemistry and physics. Knowledge from each of these disciplines is required when creating key molecules that can be utilized as the active (switching, sensing) or passive (current rectifiers, resistive wires) elements in electronic devices.
Traditional electronics (top-down technology) has already started to approach a practical size limit. Molecular Electronics (bottom-up strategy) has the potential to dramatically extend the miniaturization that has propelled the density and speed advantages of the integrated circuit phase per Moore's Law. The remarkable growth of molecular electronics in the last two decades is a direct reflection of the synthetic capabilities arising from surface functionalization and bonding at interfaces, in tandem with the invention/development of scanning probe technology that permits both manipulation and measurement at the nanoscale.
Research in organic electronics has witnessed similar explosive growth. The notion of creating electronic circuits and devices on plastic platforms, as apposed to a silicon foundation, provides researchers the possibility of circumventing issues such as cost, weight, widespread adoption and fragility. Global development of small molecules and polymers that are used throughout the field has accelerated, primarily in response to these advantages. The materials function as semiconductors, conductors and light emitters finding use in a myriad of applications such as smart windows, electronic paper,

printed electronics inks, low-cost flexible photovoltaic devices, lasers and solar cell.
The major advantages of organic electronics are

Variety of Substrate It's possible to use different type of substrate, obtaining trasparent and flexible devices

Molecules Functionalization Molecules can be modified in the laboratory to obtain certain physical and chemical properties

Low-Cost Production The techniques used for the production of this type of devices are low-cost.
You can use printing techniques (similar to those used for the production of the books) that do not require a controlled atmosphere or high temperatures; new low-cost techniques have been also developed for the production of organic devices

The disadvantages related to this technology are instead

Fast degradation the organic devices are sensitive to temperature (over 50 C) and tend to degrade quickly in the presence of oxygen and water; it is therefore necessary to encapsulate the devices

Poor Performance The performance of these devices will never reach the performance of silicon devices; the electronic and optical properties of these devices are related to the morphology, the quality, the orientation and the uniformity of the organic layers.

3.1 The Carbon Atom

The organic molecules are based on carbon and they also contain other atom like hydrogen, oxygen, nitrogen and other element. The Carbon atom has six electrons. Two electrons are found in the 1s orbital close to the nucleus. The next two will go into the 2s orbital. The remaining ones will be in two separate 2p orbitals (Figure 3.1a).
This configuration is called $1s^2 2s^2 2p^2$.

The carbon atom has only 2 unpaired electrons therefore should form a maximum of 2 bonds; instead, normally it forms 4 bonds. This is due to the fact that the 2s and 2p orbitals have similar energy; thus an electrons

of the 2s orbital can be "promoted" in the 2p orbital with a low energy contribution (Figure 3.1b).

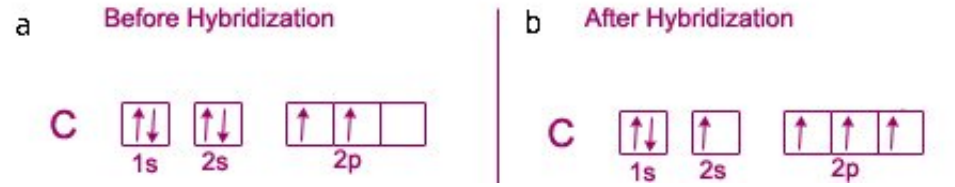

Figure 3.1: a)Non-Excited state of the carbon atom b)Excited state of the carbon atom

The energy spent to "promote" an electron in an higher energy level is compensated by the creation of two additional bonds.
This process is called hybridization.

3.2 Hybridization Of Carbon

There are a lot of possible combination for the atomic orbitals.
The complexity and the types of resulting orbitals depend on number and types of starting obitals; carbon has only s and p orbitals thus three type of hybridization are possible.

- sp^3 Hybridization
- sp^2 hybridization
- sp Hybridization

3.2.1 sp^3 Hybridization

In the sp^3 hybridization the s orbital and the three p orbitals combine in order to obtain four sp^3 hybrid orbitals.
Each orbitals has 1/4 of the characteristics of the s orbital and 3/4 of the characteristic of the p orbitals. The four sp3 hybrid orbitals will arrange themselves in three dimensional space to get as far apart as possible (to minimize repulsion). The geometry that achieves this is tetrahedral geometry, where any bond angle is 109.5 degrees (Figure 3.2).

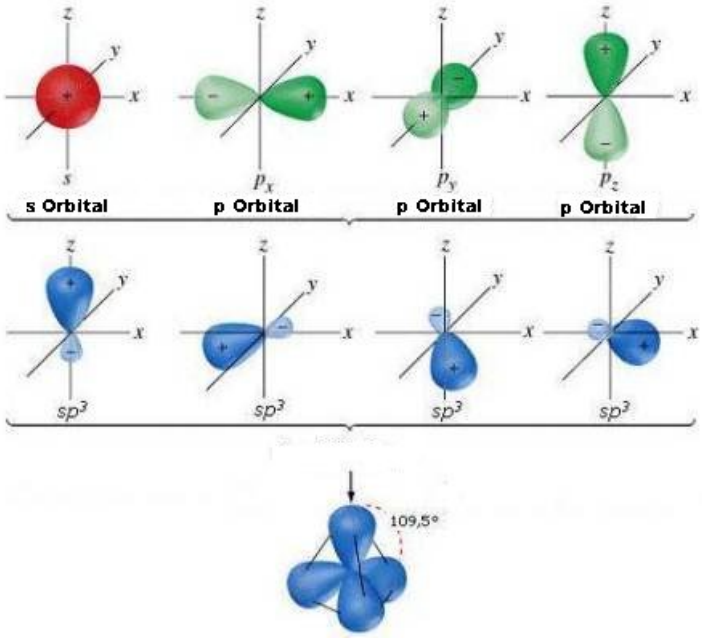

Figure 3.2: sp^3 orbitals

Each hybrid orbital contains 1 electron. A hydrogen 1s orbital will come in and overlap with the hybrid orbital to form a sigma bond.
In the metano molecule the four sp3 orbitals overlap with the 1s orbitals of four different atom of hydrogen (Figure 3.3).

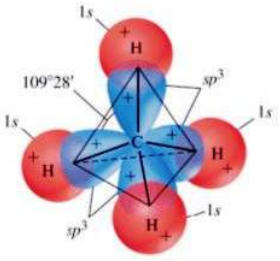

Figure 3.3: sp^3 orbitals-Example of metano molecule

3.2.2 sp^2 Hybridization

In the sp^2 hybridization the s,p_x and p_y orbitals combine and form three isoenergetic orbitals, called sp^2.
Three of the four valence electrons of carbon occupy the 3 hybrid orbitals and the other electron occupy the non-hybrid orbital (p_z)(Figure 3.4).

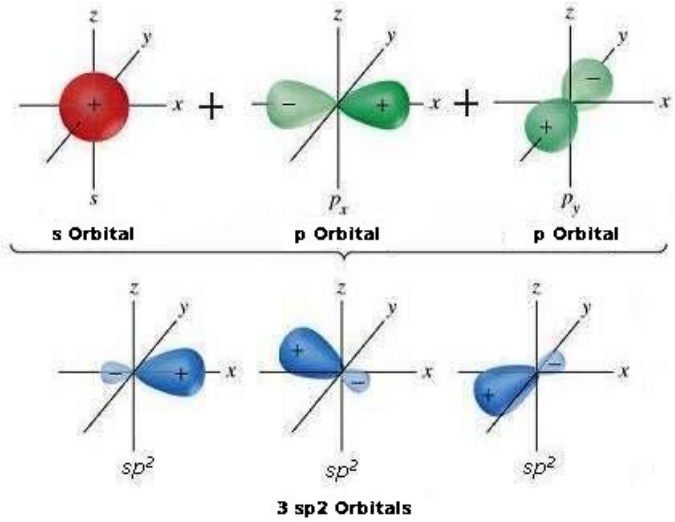

Figure 3.4: sp^2 orbitals

This type of hybridization is typical of compounds that form double bond. The three hybrid orbitals are on the same plane and the bond angle between them is 120 degrees. The unmixed pure p orbital will be perpendicular the plane formed by hybrid orbitals (Figure 3.5).

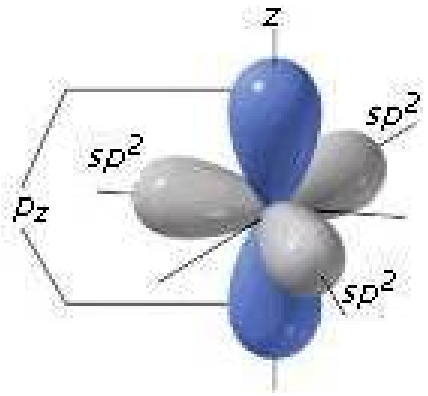

Figure 3.5: p_z orbital in sp^2 hybridization

The three hybrid orbitals form σ bonds. The non-hybrid p_z orbital form a bond with the p_z orbital of another atom with the creation of a couple of molecular orbitals called π and π^*. The π-π^* orbitals are less energetic than the σ-σ^* orbitals and both are less energetic than the starting bonds; the combination of π and σ bonds create a double bond C=C.
The double bond C=C is fundamental for the organic electronic because from it depend all the electrical characteristics of the organic semiconductors. Some example of double bond are etilene (Figure 3.6)and benzene (Figure 3.7).

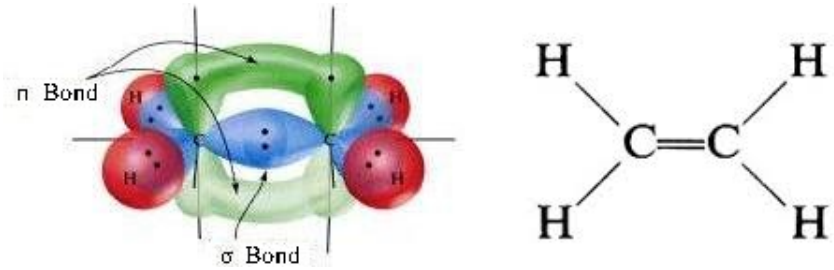

Figure 3.6: sp^2 orbitals-Example of etilene molecule

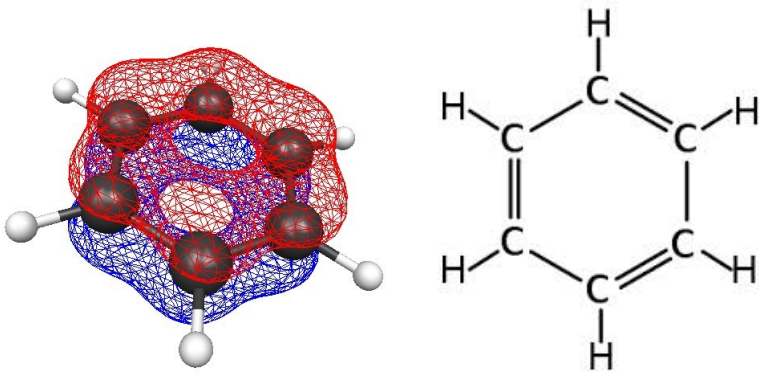

Figure 3.7: sp^2 orbitals-Example of Benzene molecule

3.2.3 sp Hybridization

In the sp hybridization the s and p_x orbitals combine and form two isoenergetic orbitals called sp.
The two sp hybrid orbitals arrange themselves in three dimensional space to get as far apart as possible. The geometry which achieves is linear geometry

with a bond angle of 180 degrees (Figure 3.8).

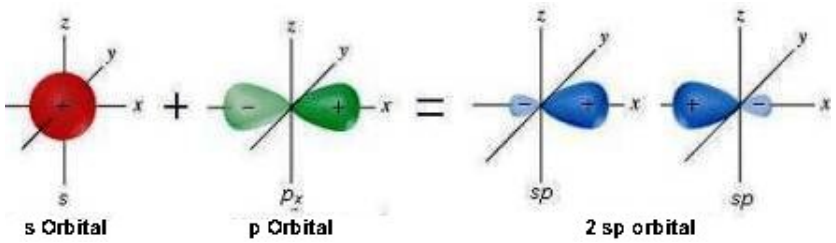

Figure 3.8: sp orbitals

The two pure p orbitals which were not mixed are perpendicular to each other (Figure 3.9).

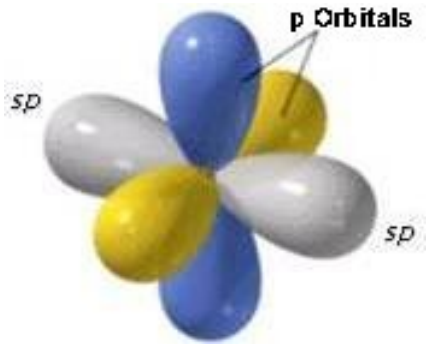

Figure 3.9: p orbitals in sp hybridization

Two atom of carbon in a sp hybrid configuration can form a triple bond. The σ bond is formed by the two sp orbital along the bond axis; the two π bonds are formed by the couple of pure parallel p orbital (Figure 3.10).

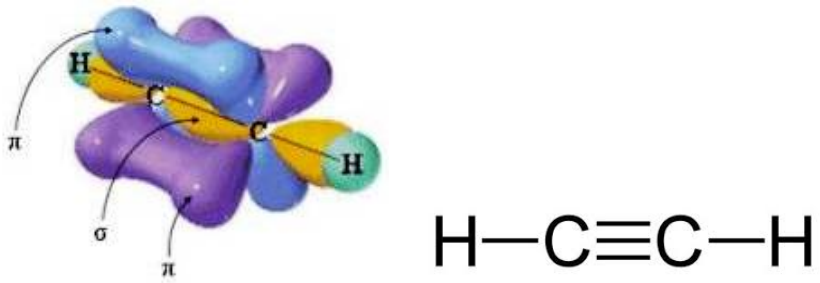

Figure 3.10: sp orbitals-Example of ethyne molecule

3.3 Molecular Orbitals of Conjugated Systems

A conjugated system is a combination of connected p-orbitals with delocalized electrons in compounds with alternating single and multiple bonds with chain or cyclic structure (Figure 3.11).

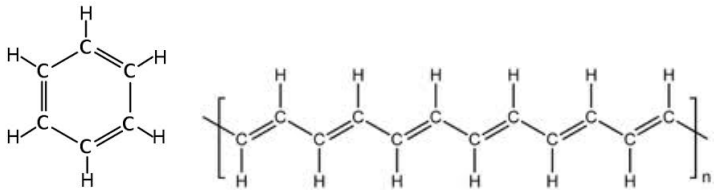

Figure 3.11: Example of cyclic and chain structures

A conjugated system has a region of overlapping p-orbitals, bridging the interjacent single bonds. They allow a delocalization of electrons across all the adjacent aligned p-orbitals. The electrons do not belong to a single bond or atom, but rather to a group of atoms.
This type of molecules are called resonance hybrids (Figure 3.12).

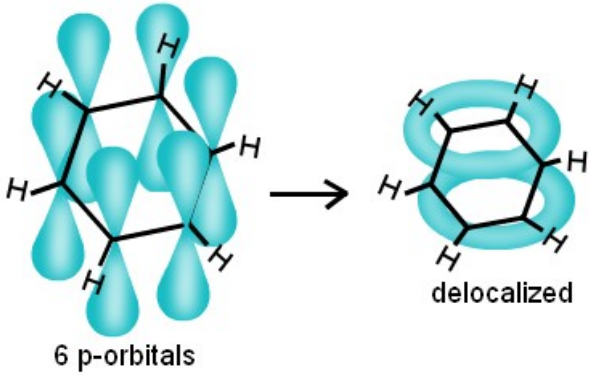

Figure 3.12: Electrons delocalization in a graphene molecule

If we consider a conjugated system with 2N atom of carbon with a cyclic or chain structure, the carbon atom form N single-bonds and N double-bonds. For each single-bond there are two σ and σ^* orbitals localized between the atom involved; both electrons occupy the low-energy σ level.
The remaining 2N p-orbitals form N π and N π^* orbitals (Figure).

Thus in the molecule there are two separated group of orbitals, each containing N energy levels. Two of these energy levels are really important for organic electronics:

HOMO Highest Occupied Molecular Orbital: The highest energy level that contain at least one electron at 0 K.

LUMO Lowest Unoccupied Molecular Orbital: The lowest energy level that doest't contain electrons at 0 K.

Comparing the molecule to the silicon lattice, HOMO and LUMO are respectively the valence and the conductive band and the difference between LUMO and HOMO levels can be compared to the Energy Gap in inorganic semiconductors.

3.4 InterMolecular Orbitals

When two conjugated molecules are close the molecular orbitals partly orverlap. The resulting orbital is called Intermolecular Orbital.
In a lattice of molecules the π and π^* orbitals divide into a lot of close different energy levels; if there are an high numbers of molecules each molecular orbitals form an energy band (Figure 3.13).

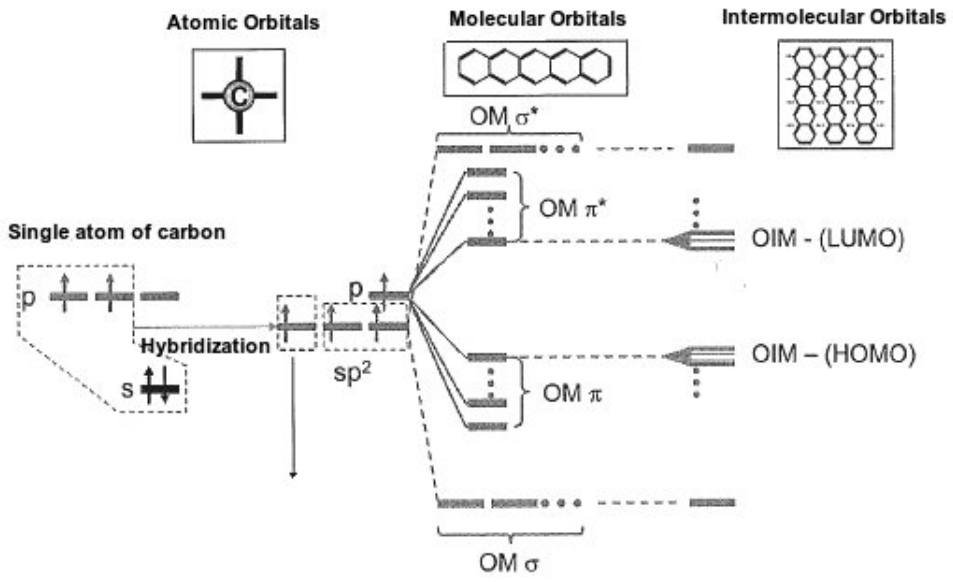

Figure 3.13: Formation of HOMO and LUMO bands

The Band originated by LUMO is called Electrons Transport Band.
The Band originated by HOMO is called Hole Transport Band.

It's interesting to analyze the difference between the inorganic and organic semiconductors

Electrons Delocalization The intermolecular forces that hold the molecules together are due to Van der Waals forces or dipole-dipole interaction and they are less strong than the covalent bond.
The overlap between molecular orbitals is lower than the covalent bond and the electrons are less delocalized in the group of molecules.

Width of the Bands Because of the limited delocalization of electrons, the separation between the energy levels on the molecular orbitals is low. Usually the width HOMO and LUMO bands is less than 1 eV, really low if compared with the 20 eV of the inorganic semiconductors bands.

Anisotropy of the Intermolecular Bond In the silicon the energy of the bond doesn't depend on the direction; the energy of the intermolecular bonds depend on the mutual position of the molecules: the force of the bond is higher when is higher the overlap between orbitals.

3.5 Generation and Recombination

The electrons of a molecule can occupy only particular energy levels.
When the molecule is in equilibrium condition, the electrons occupy the lowest energy levels respecting the Exclusion Principle.
The organic material can interact with photon and phonon and thus a molecule in the equilibrium condition can absorb a photon and perform a transition in a excited state.
In a molecule the energy levels are due to a combination of two contribution (Figure 3.14).

Molecular Orbital Energy Define the electronic states

Vibrational State Energy Define the vibrational state

There are two type of transition between energy levels

Electronic Transition Transition between two different electronic states; the starting and final vibrational states can be different.

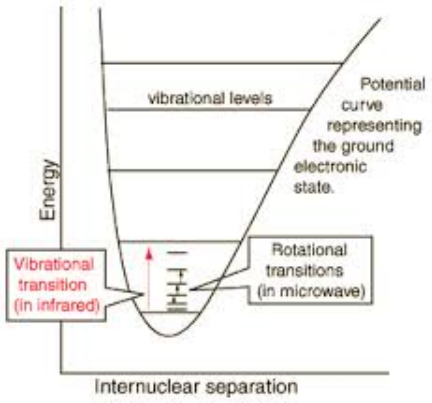

Figure 3.14: Energy levels on a molecule

Vibrational Transition Transition between two vibrational states into the same electronic state.

3.5.1 Exciton

Consider a molecule in the ground state: all the electrons of the π orbitals are in the HOMO band and the LUMO band is empty.
If the molecule moves to an excited state, for example because of the absorption of an photon, an electron moves from the HOMO to the LUMO (π^* orbitals).
In this situation the double bond is broken and the electrons can easily moves from the π^* orbital of the starting atom to the π^* orbital of a close atom; the starting atom is now positively charged with an hole on the π orbital.
The electron and the hole can now easily moves between different bonds in the molecule; the molecule is broadly neutral but contain electrically charged region.
This induce a deformation in the molecule structure and this deformation can extend in the close molecules.
An exciton is a bound state of an electron and an electron hole which are attracted to each other by the electrostatic Coulomb force. It is an electrically neutral quasiparticle that exists in insulators, semiconductors and in some liquids. The exciton is regarded as an elementary excitation of condensed matter that can transport energy without transporting net electric charge.
The difference between inorganic and organic semiconductor depend on the

energy of the excitons

Wannier-Mott Exciton They are low energy excitons. They are typical of materials with large dielectric constant and carriers concentration (inorganic semiconductors or conductors).
When the atom moves from a ground state to an excited state the charge redistribution produce an electric field screening that decrease the Coulomb interaction between the electron and the hole newly formed.
The bond energy of the exciton is small and the generated charges are "free to move " in the semiconductor lattice.

Frenkel Exciton They are high energy excitons. They are typical of material with small dielectric constant and carriers concentration (organic semiconductors and insulators).
The electric field screening, after the formation of the exciton, is low; the bond between electron and hole has high energy and is difficult to break it.
At room temperature the electrons and the hole that form the exciton tend to recombine.

3.5.2 Charge Transfer

In the inorganic semiconductors the generated charges can easily move in the lattice because the energy of the exciton is small. In the organic semiconductors the bond between electron and hole in the exciton is strong and the excited molecule can interact with the close molecules yielding energy to them.
Thus the exction can moves from a molecule to another, but there is not a transfer of charge but only a transfer of energy.

The exciton can trasfer its energy in two way

Energy Transfer with Dipole-Dipole Resonance The energy transfer for resoncance is base on the interaction between two molecules and occur without emission of light.
The donor molecule decays trafering all the excess energy to the acceptor molecule (Figure 3.17a).

This transfer occurs thanks to the long-range dipole-dipole interaction and is also necessary that the absorption spectrum of the acceptor molecule overlap the emission spectrum of the donor molecule (Figure 3.15). The efficency of this process is appreciable for distance below 10 nm.

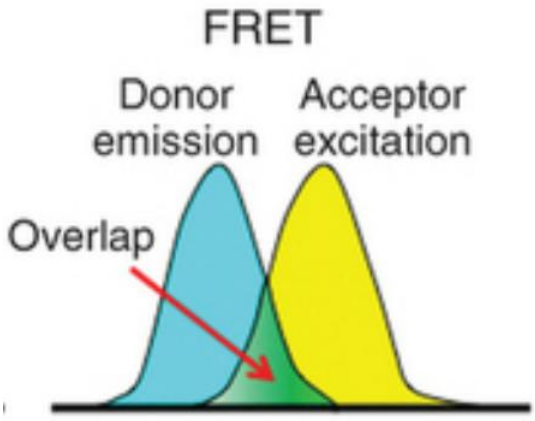

Figure 3.15: Foster transfer and spectrum overlap in foster transfer

Energy Transfer for resonance Exchange If the Donor and the Acceptor molecules are close, the orbitals (both excited and ground orbitals) are partially overlapping.

It's possible that an electron moves from the excited state of the donor molecule to the excited state of the acceptor molecule; at the same time an electron of the ground state of the acceptor molecule can move to the ground state of the donor molecule (Figure 3.17b-c). The efficency of this process is appreciable for distance below 1-2 nm.

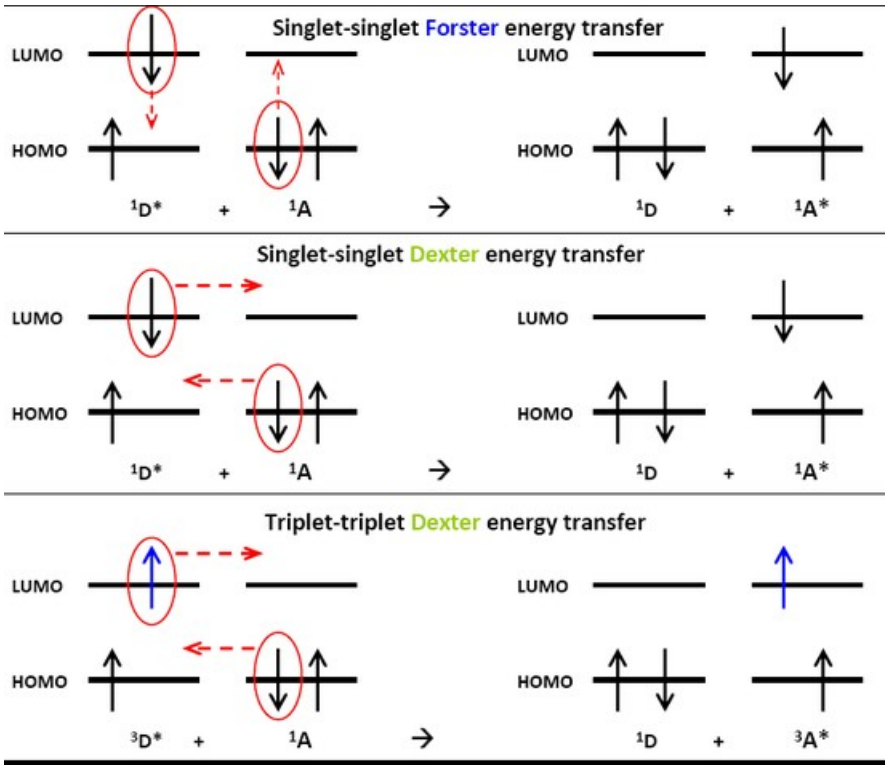

Figure 3.16: Foster and Dexter transfer

3.5.3 Polaron

When a molecule gains or loses an electron, the charge of the molecule produce a perturbation on the potential energy of the lattice and deform the orbitals in order to minimize the energy of the system.
The electric charge and the deformation induced in the molecular lattice form a excited electrically charged state (exited exciton) called polaron.
The dimension and the energy of the polaron depend on the type and the magnitude of the induced lattice deformation.

The deformation of the molecular lattice take place in three stepes (in this example we consider a molecule A that loses an electron)

1. **Electron Polaron**:Initially the electron clouds are polarized because of the electric field generated by the positive charge of molecule A.
   . The electronic polaron has two contribution: the free carrier and the electronic clouds deformation.

The electron clouds take 0.1-1 fs to polarize.

2. **Molecular Polaron**:There is a charge redistribution of the covalent bonds in order to stabilize the molecule A.
   Distance and angle of the bonds change, adapting to the charged molecule. The relaxation time is of 1-10 fs.

3. **Lattice Polaron**:The interaction of the charge of the molecule A with the close molecules induce a lattice deformation.
   The duration of this process is 100 fs - 1 ps.

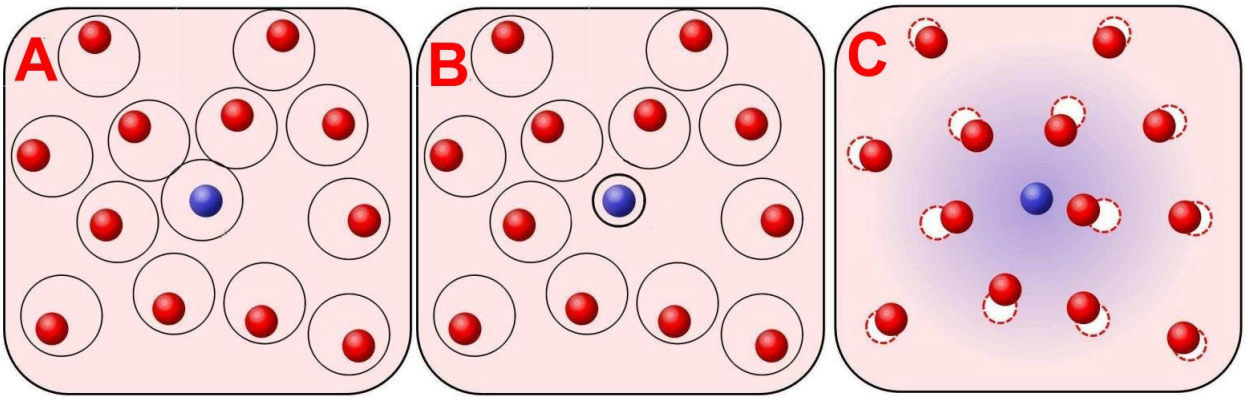

Figure 3.17: a)Electron Polaron b)Molecular Polaron c)Lattice Polaron

3.6 Charge Transport

The charge transport is based on two phenomena

Intramolecular Transport Carrier transport into the molecule

Intermolecular Transport Carrier transport between different molecule

3.6.1 Intramolecular Transport

The electron structure of a molecule can be consider like a small lattic and the electron is free to move in the molecular orbital; in a "molecular lattice" the electron can move only in one direction and the without collision because of the anisotropy and the small dimension of the molecule.
Thus the molecule can be considered like a one-dimensional potential well

with discrete energy levels; without external stressed, the electron can remain in the potential well mainteining energy and momentum and without collision.
The charge transport through a one-dimensional system like a molecule is described by the **Landauer Model**:
The quantic resistance of a one-dimensional lattice connected between two metallic electrode on which is applied a voltage is, in theory, constant and independent from the conductor lenght.

3.6.2 Intermolecular Transport

The intermolecular transport is a process that allows electrons to move through different molecules thanks to the orbitals overlapping.
The classic theory say that the current in a semicondutor on which is applied an electric field depends on the concentration and the velocity of the free charges in the material;the mobility depend on doping, temperature and defects concentration.
The situation in a organic semiconductor is completely different:

Big Lattice Usually the organic materials that form the lattice are molecules, polymers and group of moleculs, thus they are big.

Weak Bond The Van Der Waals bonds between molecules have short-range interaction

Polaron The charge trasport is based on polaron and the charge is localized in one molecule; the polaron induced a deformation of the lattice of the molecule thus the energy necessary to move the polaron is related both to elastic lattice deformation and electrostatic energy of the carrier

Small Mobility The mobility of the organic semiconductor is really small

The model that can explain better the organic semiconductor conductivity is the VHR (Variable Range hopping) model.
In this model the carriers are localized in discrete energy levels but they can move in close energy levels. This levels are divided by a potential barrier and the carrier can "jump" from one localized level to another thanks to three mechanism:

Tunnel Effect The tunneling probability decrease exponentially with the barrier width; the energy state can't be too far.

Temperature The phonons give the necessary energy to offset the difference between energy levels.

External Electric Field The Electric field bends the energy band of the lattice and the carriers can move easily to the other energy level.

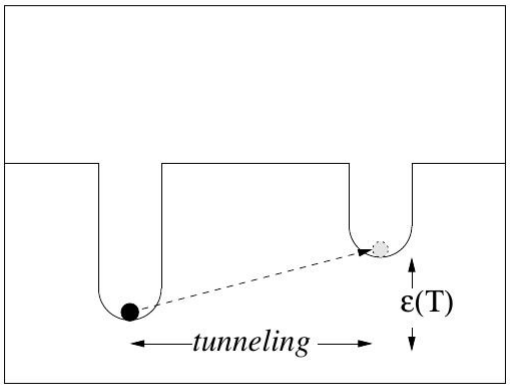

Figure 3.18: An electron can move to another impurity with help from quantum mechanical tunneling and thermal energy.

In the VHR model the motion of an electron is described using a percolative path (Figure 3.19): the electron jump in close energy states to minimize the tunnel distance but if the energy of the closest state is too big the electron prefers to do a "longest jump" in a state with lower energy.
Using the VHR model we can obtain the current relation in an organic semiconductor

$$j(E) = \frac{q^2 R^2 \omega_0 F}{kT} f(E) e^{-(\frac{T_0(E)}{T})^{\frac{1}{4}}}$$

The classic current relation for inorganic semiconductor is

$$j = qnF\mu$$

Thus we can define the mobility in organic material

$$\mu = \frac{q^2 R^2 \omega_0 F}{kT} e^{-H(E,T)}$$

In this way we obtain a relation where the mobility of the material depend on Temperature (higher temperature means higher mobility) and Energy (with the increase of energy there are more available states).
The mobility doesn't depends on Electric Field; this is true for small value of Electric Field but for big value of Electric Field the approximations done on VHR model are not correct.
Without approximations the relation between mobility and electric field is

$$\mu \sim e^{\beta\sqrt{E}}$$

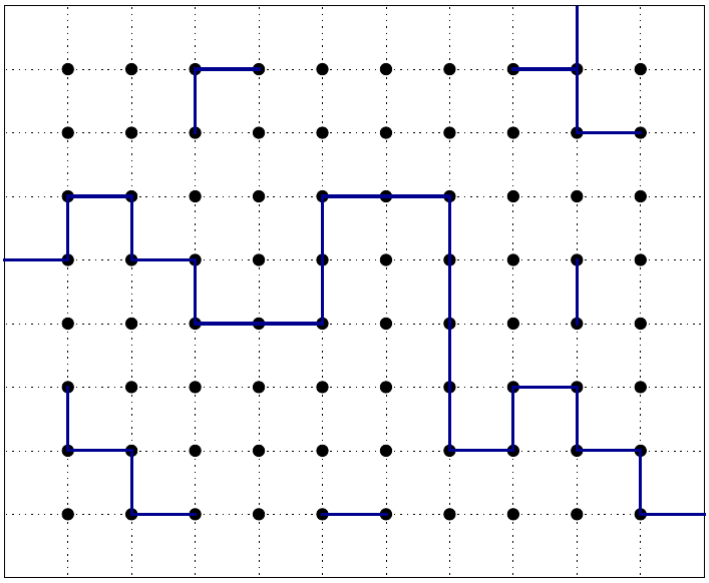

Figure 3.19: Illustration of the percolation bond problem where an infinite cluster takes form on a square lattice at the percolation threshold

The mobility depends also on

Morphology The morphology of the organic film affect the molecular orbitals overlapping and thus the charge transport on the material.

Orientation of the Molecules In the inorganic semiconductor the basic unit is the atom.
In the organic semiconductors the molecules are the basic units; they usually have a flat structure where one side is longer than others.
We can define three axes:

- **Conjugation Axis**: In this axis are located the double bonds
- **Axis of the Substituents**: Orthogonal to the Conjugation axis
- **Bonds Axis**: Ortogonal to the molecular plan; it's the direction of the P_z no-hybridized orbitals

The relationship between conductivity and molecular morphology is:

- The conductibility of the single polymer is maximum along the conjugation axis because the carriers can move easily in the molecular orbitals. However the conductivity between molecules aligned along the conjugation axis is low because of the poor overlap of the molecular orbitals
- The conductibility between molecules aligned along the $\pi - pi$ axis is better than the previous case due to the better overlap of the molecular orbitals; the hopping transport limits the mobility between the molecules
- The conductibility along the substituents axes depends on the presence of substituents groups

3.7 Band Diagram

Comparing inorganic and organic material we said that:

- The HOMO level in organic material is like the valence band in inorganic semiconductors
- The LUMO level in organic material is like the conductive band in inorganic semiconductors
- The LUMO-HOMO difference is the bandgap

This is not completely true due to some difference between inorganic and organic semiconductors:

Charge Transport The transport energy level is associable to the polaron energy level

Allowed Energy Levels The molecules interact through the weak Van Der Waals bonds ; the tail of the energy levels can extend also in the gap and so there isn't a clear separation between LUMO and HOMO levels

States Mobility Near the LUMO and HOMO levels thare is an high density of energy levels and so the polaron can easily move through them because of the high tunneling probability and the small energy separation between state; these states are called *high mobility state*. In the center of the gap the levels density decrease and polaron takes a long time to move through the states; these states are called *low mobility state*.

Thus we can define four states distribution (Figure 3.20):

- *Delocalized high energy levels*: High electrons mobility
- *Delocalized low energy levels*: High holes mobility
- *localized medium-high energy levels*: Electrons trap
- *localized medium-low energy levels*: Holes trap

The fact that there isn't a clear separation between LUMO and HOMO levels means that we can't define a bandgap like in the inorganic semiconductors.
In the organic semiconductor the bands are defined using a threshold mobility ; we can define the Conductive Band like the energy level that divide the high electrons mobility states and the low electorns mobility states(we can do the same with the Valence band considering holes mobility). Using this definition the conductive and valence band can be different from the LUMO and HOMO levels and we need to distinguish two type of bandgap:

Optic Gap It refers to the minimum energy needed to ionize an electron to the first free higher energy level. This level isn't necessarily a transport level (low carriers mobility).
In materials with a large exciton binding energy, it is possible for a photon to have just barely enough energy to create an exciton (bound electron-hole pair), but not enough energy to separate the electron and

hole (which are electrically attracted to each other).
The term "optic" is used because a photon with an energy equal to the optic gap can be absorbed by the material.

Mobility Gap It's the difference between the electrons-transport energy level and the holes-transport energy level; Ec and Ev are defined using the threshold mobility model.

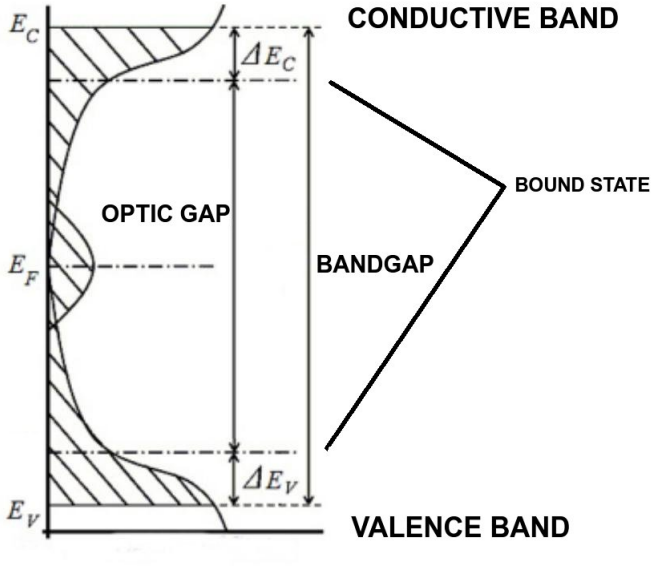

Figure 3.20: Band diagram of an organic semiconductor

3.8 Model of an Organic Semiconductor

In an organic semiconductor the energy states distribution has a Gaussian shape and its dispersion depends on the morphology of the material.
With VRH model we obtain a typical graph like the one in Figure 3.21. The graph shows also the Fermi-Dirac distribution f(E) and the product $n(E) = f(E)g(E)$ that means the carriers distribuition per unit of volume and energy.

Using some theoretical values we obtain

Mobility Threshold Considering a mobility threshold of 50% of the initial value we obtain a width of the LUMO band of 0.5-0.6 eV, very narrow if compared with typical inorganic semiconductor values.

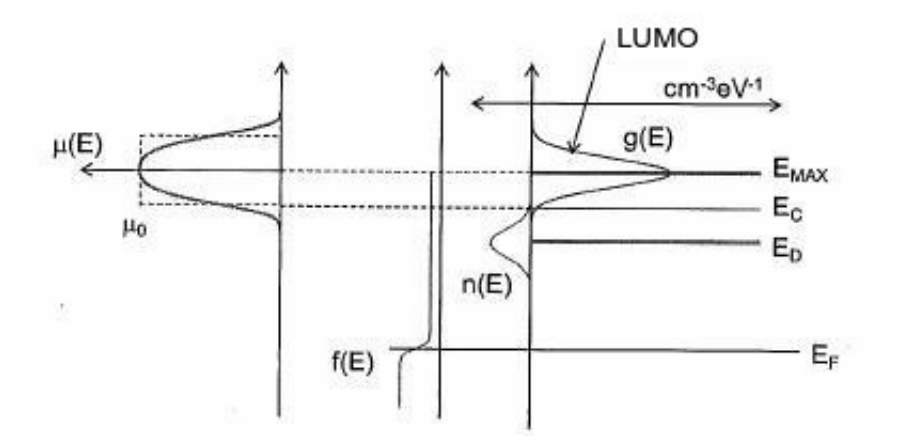

Figure 3.21: States density, mobility and carriers distribution

State Density The states density in the two bands can be calculated like

$$n = \int_{Ec}^{\infty} g(E) f(E)\, dE$$

The calculated value exceeds an order of magnitude of the typical value for silicon, due to high concentration of states in the HOMO and LUMO bands.

Carriers Distribution E_D is the energy level with the maximum probabililty to find carriers; it's outside the conduction band in a low-mobility energy zone.
This means that the largest number of carriers are below the conduction band with a low mobility; this states are traps for electroncs (below Ec) and holes (above Ev).

3.8.1 Defects model

A defect is an energetically and spatially localized state that can trap or release a carrier.
A defect can be classified in term of:

Condition A defect is *Free* if it doesn't hold a carrier or *Occupied* if it holds a carrier; its state depend on the position of the Fermi level: with a temperature of 0 K a defect below the Fermi level is occupied otherwise is free.

Charge The charge of a defect can be positive, negative or neutral. This depend on the position of its energy level and on the type of intrinsic charge. There are two tyoe of defect:

- **Donor**:The charge of the defect is neutral if occupied by an electron or positive if unoccupied
- **Acceptor**:The charge of the defect is neutral if unoccupied or negatie if occupied by an electron

Deep The deep of a defect is the difference between the energy of the defect and the energy of the level which with it interact (for an electron this means that the deep of the defect is the difference between the energy of the conductive band and the energy of the defect) A defect can be defined as

- **Shallow Trap**: Defect with an energy close to the energy of its band
- **Deep Trap**: Defect that is close to the middle of the gap

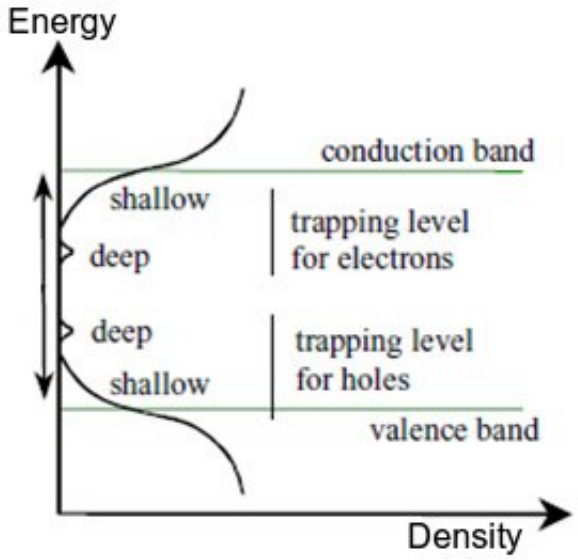

Figure 3.22: Shallow and Deep Trap

3.8.2 Free Carriers and Fermi Level

In this section we'll talk about the possibility to induce free carriers in an organic semiconductor. In the last section we said that the largest number of carriers are below/above the conduction/valence band and this state act like trap for electrons/holes because of the low mobility.
It's clear that the behavior of an organic semiconductor is defined by the presence of defects.This is true if the Fermi level is far from the conductive/valence band. Now we want to understand what happen when the Fermi level is close to the valence or to the conductive band.
There are two different situation:

Free Carriers Induced by Doping

Consider an organic semiconductor with the Fermi level $E_F = E_i$; we assume that all the defects below the Fermi level are occupied and all the defects above the Fermi level are unoccupied (this is true only with a temperature of 0 K).
The defect below the Fermi level result in a negative charge.
The defect above the Fermi level result in a positive charge.
In the equilibrium condition the total charge must be zero and so solving

$$Q = Q_p + Q_n = 0$$

we obtain the position of the Fermi level.
If the density and the distribution of the acceptor and the donors states are the same, without a doping, the Fermi level is exactly in the middle of the gap.
If the density of the donor/acceptor states is higher than the density of the acceptor/donor states the Fermi level is above/below the middle of the gap.
Now we introduce a doping in the semiconductor with a concentration N_A of acceptor states above the valence band and a concentration N_D of donor states below the conductive band. In this way all the dopants are active.
The electric charge in the semiconductor is now

$$Q(E_F) = Q_p + Q_n - qN_A + qN_D$$

The first and the second terms are related to the charge due to the

occupied defects.
The third and the fourth term are related to the charge due to the dopants. Thus the position of the Fermi level depends on the doping ; if the doping has a low value the Fermi levels is still in the middle of the gap and the charge on the semiconductor depends only on the presence of defects.
If we use an high doping value we can induce a high quantity of free carriers; the Fermi level in this condition is close to the valence/conductive band and the free carriers start to prevail on the trapped charge (Figure 3.23).

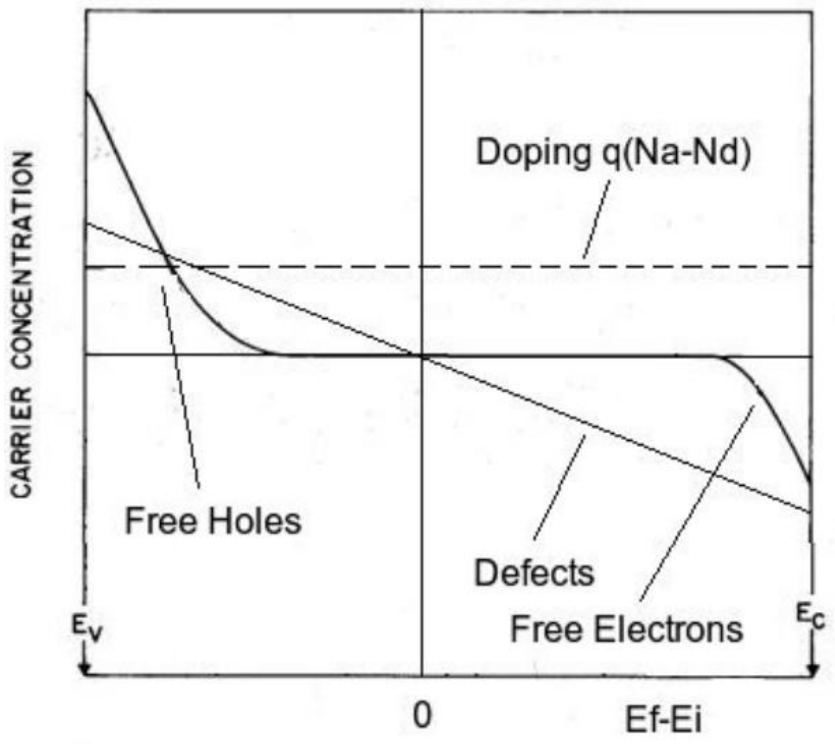

Figure 3.23: Electric Charge Vs Fermi level

Presence of a Metallic Electrode

Consider a juction formed by a metal electrode with a work function Φ_M and an organic semiconductor with a work fuction Φ_S; we assume that the Fermi level of the metal electrode is in the middle of the organic semiconductor gap and that the semiconductor has an infinite lenght. Figure 3.24 shows the band diagram in two different situation: $\Phi_M > \Phi_S$ and $\Phi_M < \Phi_S$.

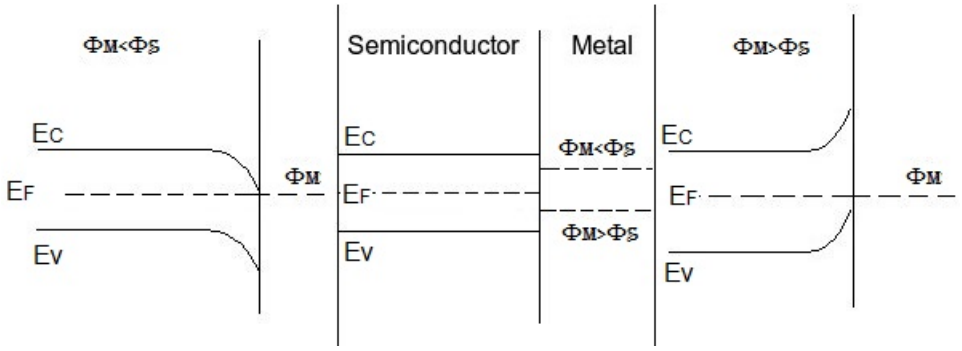

Figure 3.24: Band diagram with $\Phi_M > \Phi_S$ and $\Phi_M < \Phi_S$

The Fermi level is far from the transport bands and thus the charge in the semiconductor depends on the charged defects.
Using the Poisson equation we can find the bands bending in the semiconductor; the Fermi level is constant thus the charge of the defects depends on the new position of the bands compared with the Fermi level (Figure 3.25).

$E_F > E_I$ The acceptor states below E_F are charged; the total charge is negative

$E_F < E_I$ The donor states above E_F are free; the total charge is positive

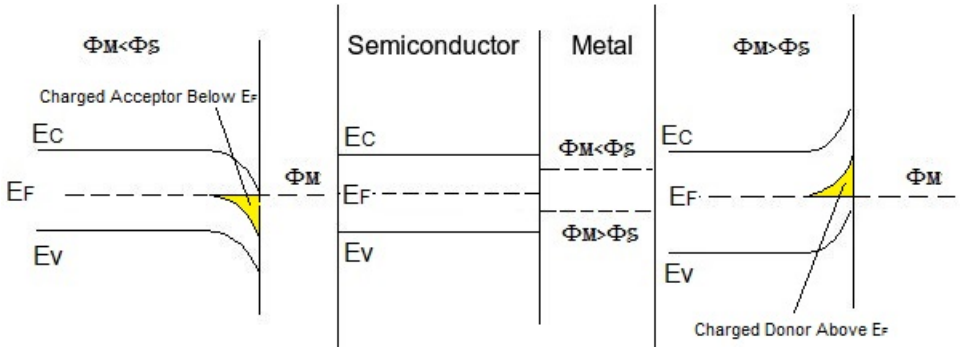

Figure 3.25: Defects charge with a positive (left) or negative (right) voltage

Considering the typical parameters of an organic semiconductor we can analyze the band bending obtaining that the damping constant is in the same order of magnitude of the organic film thickness; this means that when an organic film contact a metallic electrode, the metal affect the organic film in depth.

The consequence of this behaviour can be analyzed studyng the double junction metal-semiconductor-metal. We can calculate the bands bending in the organic semiconductor and using typical parameter we obtain that the presence of the metal electrodes affect also the center of the semiconductor and therefore the free carriers concentration in the organic film.
The presence of the electrode can increase the carriers concentration of several orders of magnitude, like the doping procedure in the inorganic semiconductor.

3.9 Injection and Conduction

In this section we will talk about the injection and the conduction process in an organic semiconductor focusing on the most important models.

3.9.1 Injecion of Carriers

Fowler-Nordheim Injection-Tunnel effect

Typically all the organic materials have not free carriers and so they behave like insulators.
To explain the injection of charge through an insulator we can use the tunnel effect.
Consider a metal-semiconductor junction; the work function of the metal is in the middle of the bandgap of the semiconductor.
If we apply a voltage (considering a constant electric field in the semiconductor) the bands bend forming a triangular potential barrier.
The electrons have to get over the barrier to enter in the semiconductor. If the barrier is too high the electrons have to pass through it with the tunnel effect (Figure 3.26a). The equation that we obtain for the Fowler-Nordheim current is:

$$J_{FN} = \frac{A}{L^2} V^2 \exp^{\frac{-BL}{V}}$$

where A and B are two constant related to the barrier's parameter and other physics constants.

Thermionic Effect

Considering a inorganic semiconductor the model used to describe the injection of carriers from the metal to the semiconductor is the thermionic emission (Figure 3.26b) according to which the current that pass through the junction is due to the electrons that have enough energy to get over the barrier.

But this theory assumes that:

- The barrier height is higher than kT
- The electrons don't hit nothing while passing through the barrier
- The drift current is negligible

The equation obtained for the current is

$$J = J_0(\exp^{\frac{qV}{kT}} - 1)$$

typical of the silicon diode

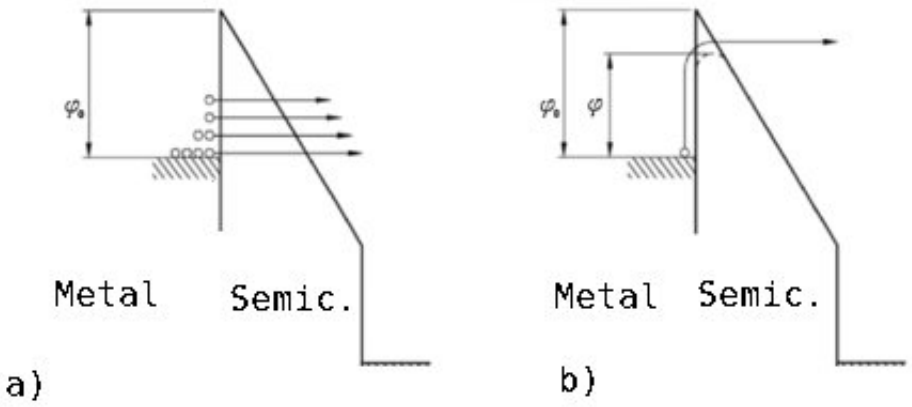

Figure 3.26: a)Tunnel effect b)Thermionic effect

Tail states effect and Scott Model

One of the hypothesis on the thermionic model is that the electrons can overcome over the barrier without collision if their energy is high enough. This means that the mean free path of the electron must be higher than the

barrier width; but in an organic semiconductor there are a lot of localized energy levels also in the bandgap and thus is impossible for an electron to get over the barrier without collision.
We can't define the barrier height just like the difference between the LUMO band and the Fermi level of the metal because the electrons "see" a lot of free states distribuited in the bandgap.Thus the electrons can overcome ther barrier simply by moving on a localized state that belongs to the tail of states of the semiconductor. A model that can explain the injection process in an organic semiconductor is the *Scott Model*. After the injection the carriers are in the first molecular layers and they have not yet overcome the barrier. Now there are two possibilities for the charge: diffuse in the organic film or return to the electrode due to the opposite electric field.

Diffusion in the organic film The diffusion works thanks to the concentration gradient due to injention.
The electrons move in states near to the trasport band untill they reach it.
The equation of the diffusion current is

$$J_{DIFF} = C \exp^{-\frac{\Phi_B^{eff}}{kT}} \quad with \quad \Phi_B^{eff} = \Phi_B - q\sqrt{\frac{qE}{4\pi\varepsilon}}$$

Φ_B is the potential barrier, Φ_B^{eff} is the potential barrier with te correction due to the image charge and C is a constant

$$C = qN_0\mu\frac{q}{16\pi\epsilon x_c^2}$$

Return to the electrode Part of the carriers can return to the interface due to the attractive force due to the image charge.
In his Model, Scott uses the ricombination hyphotesis of Langevin: the electron return to the interface if the attractive force is greater than kT (thermal energy).
The equation of the drift current is

$$J_{DRIFT} = qN_0 \exp^{-\frac{\phi_B^{eff}}{kT}} \mu(-E + \frac{q}{16\phi\epsilon x_c^2})$$

The total current injected in the semiconductor is

$$J_{INJ} = J_{DIFF} - J_{DRIFT} = qN_0\mu E \exp^{-\frac{\phi_B^{eff}}{kT}}$$

Compared with thermionic model the current depends on semiconductor proprierties (mobility and states density) and on the electric field.

3.9.2 Conduction in an Organic Semiconductor

The transport of charge in a semiconductor is devided in two phases:injenction of carriers and movement of the charge from one electrode to the other.
the total time taken for the charge to pass through the semiconductor is given by the sum of the transport and injection time. If the injection time is higher than the transport time the *conduction is limited by injection*; otherwise the *conduction is limited by the semiconductor film* If the conduction is limited by injection the equation for the current is given by the Scott Model. If the conduction is limited by the semiconductor there are two models depending on the semiconductor proprierties:

Ohmic Model The injected charge is negligible if compared with the intrinsic free carriers of the semiconductor

Space Charge Limited Model The intrinsic free carriers of the semiconductor is negligible if compared with the charge injected in the semiconductor

Ohmic Model

The Ohmic model is used for the inorganic semiconductor: the number of injected carriers is lower than the instrinsic majority carriers of the semiconductor.
The equation we obtain in this situation is the classic ohm equation:

$$J = qN_D\mu\frac{V}{L}$$

Space Charge Limited Model (SCL)

Consider an organic semiconductor connect between two electrode.
We use these hypothesis:

- Electrodes ohmic contact
- Film without free carriers
- Film without doping
- Absence of defects on the semiconductor
- Constant mobility along the film
- One type of carriers

The current equation obtained in this situation is

$$J = \frac{9}{8}\mu\varepsilon\frac{V_D^2}{L^3}$$

The current equation shows a parabolic trend, not linear as for the ohmic model. We can associate to the film an equivalent resistance given by

$$R_D = \frac{V}{J} = \frac{8L^3}{9\mu\varepsilon V_D}$$

This resistance is also non-linear. In the same way we can consider a capacity associated to the semiconductor film

$$C_D = \frac{3}{2}\frac{\varepsilon}{L}$$

Thus the Metal-Semiconductor-Metal system can be approximated like a non-linear resistor in parallel with a capacity.

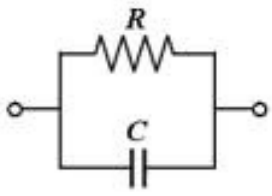

Figure 3.27: RC organic semiconductor model

It can be shown that if we also consider the deep and superficial defects, the equation is modified by defining an effective mobility that depends on the distribution of defects in the semiconductor (now we consider only one type of carriers)

$$\mu_{eff} = \frac{\mu n_C}{n_C + n_D + n_T}$$

with n_C the charge in the transport band, n_D the number of superficial defects occupied, n_T the number of deep defects occupied and μ the mobility of one of the carriers types.

3.10 Thin Film Processing

In this section we present some of the techniques used for the manufacture of organic devices. Many of these techniques are similar to those used in the electronics inorganic but many more are being developed for organic devices to lower times and costs of production.

3.10.1 Spin Coating

Spin-coating is exploited extensively by the microelectronics industry for depositing layers of photoresist films, generally polymers such as polyimides, on silicon wafers.
The various steps involved are illustrated in Figure ˙
A quantity of a polymer solution is first placed on the semiconductor wafer, which is then rotated at a fixed speed of several thousand revolutions per minute (or the solution can be applied while the wafer is slowly rotating). The resist solution flows radially outwards, reducing the fluid layer thickness. Evaporation of the solvent results in a film of uniform thickness.

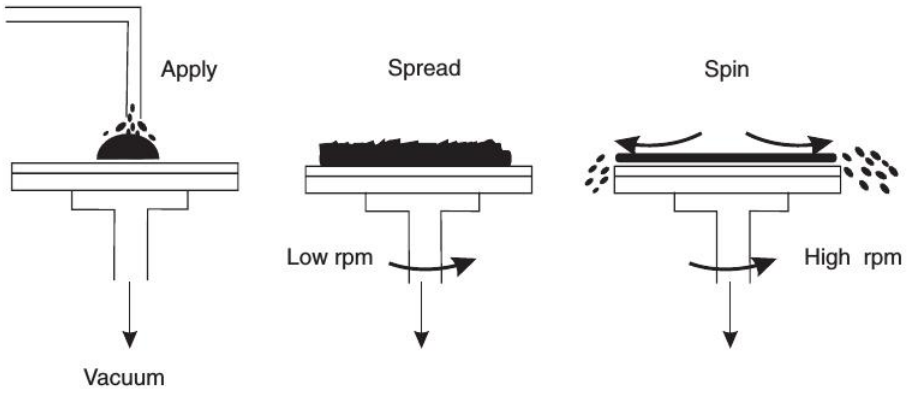

Figure 3.28: Schematic diagram of spin-coating

A quantity of solution is first applied to the substrate surface; this may be pretreated with an adhesion promoter to improve wetting. The initial volume of fluid dispensed on the rotating disk and the rate of fluid delivery have a negligible effect on the final film thickness.
In contrast, the resist viscosity (dependent on the concentration of the starting solution) and final film speed are both important process parameters. An increase in angular velocity decreases the film thickness. The thickness of the film can be calculated using this equation

$$h = \sqrt{\frac{\eta}{4\phi\rho\omega^2 t}}$$

with η viscosity coefficient, ρ solution density, ω the angular velocity of the spinning, t spinning time.

3.10.2 Vacuum Thermal Evaporation

Solid materials vaporize when heated to sufficiently high temperatures and this process may proceed through the liquid phase. A thin film is then obtained by the condensation of the vapour on a colder substrate. This method has traditionally been used for the deposition of films of inorganic materials, such as metals and their alloys. However, the technique is now being exploited for the formation of layers of low molecular weight organic compounds.
The rate of evaporation $[m^{-2}s^{-1}]$from a surface is given by

$$F = \frac{P}{\sqrt{2\phi k_B T m}}$$

with P vapour pressure, T temperature of evaporation, m the molecular mass of the single molecule and K_B the Boltzam constant. Because of collisions with ambient gas atoms, a fraction of the vapour atoms will be scattered. For a straight-line path between the evaporating material (source) and the substrate, it is necessary to use low pressures , where the mean free path of the gas atoms λ is much greater than the source-substrate distance.
From kinetic theory, λ is given by

$$\lambda = \frac{K_B T}{\sqrt{2} p \phi d^2}$$

with d diameter of the molecule. It is possible to suppose that the fraction of molecules that reach the substrate depend exponentially from the mean free path and thus the fraction can be calculated in this way

$$\exp^{-\frac{a}{\lambda}}$$

with a distance between substrate and source. Obviously not all the particle can reach the substrate and condense on it; the efficency of the process depends on the reaction speed between the molecules and the substrate and it is controll setting up the temperature of the substrate.
This method allows to obtain high quality film with homogeneous and controlled thickness but the deposition/evaparotion rate is really low, it's not suitable for large area deposition and the speed of the process is quite low. Figure 3.30 shows the typical stages of growth of a thin film.

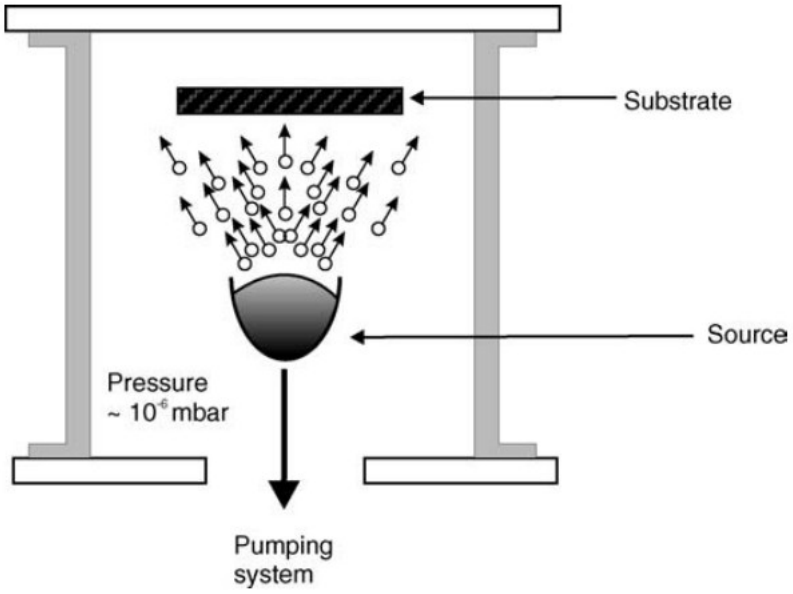

Figure 3.29: Vacuum evaporation system. Evaporating atoms or molecules traverse the space between the source and the substrate at reduced pressure

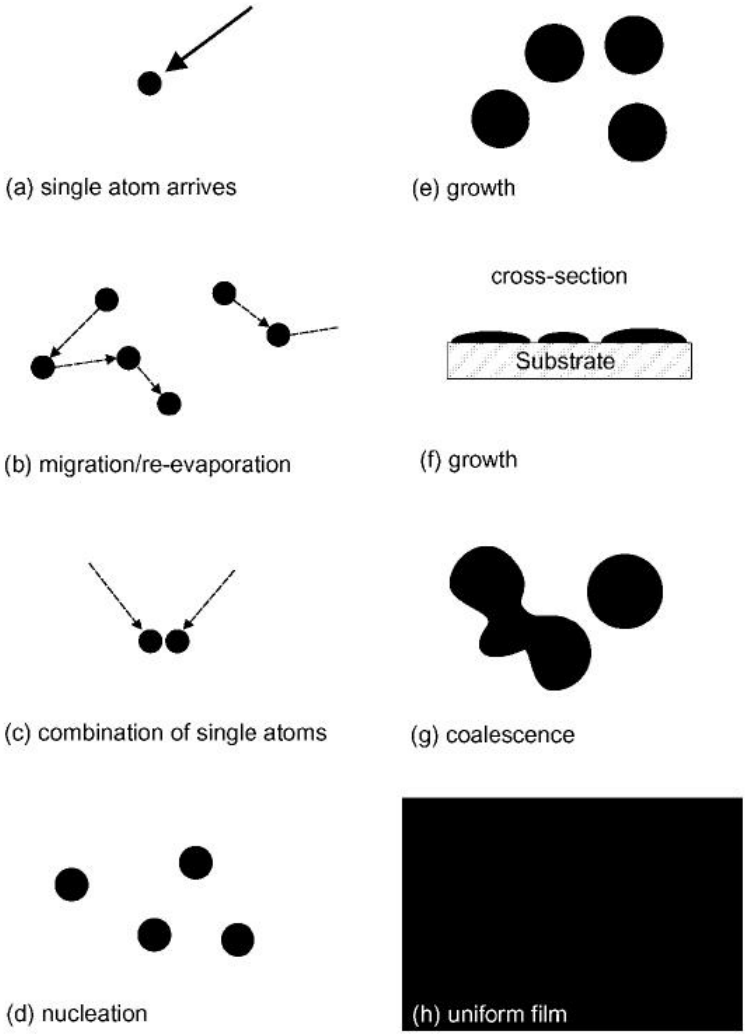

Figure 3.30: Stages of growth of an evaporated thin film

3.10.3 Organic Molecular Beam Deposition

The OMBD (Organic Molecular Beam Deposition) is an evaporation technique which consists in directing a beam of molecules to a heated substrate. The OMBD uses lower pressure and have a lower deposition speed than the VTE.
The source of the beam is called "cella di Knudsen".
The Knudsen cell has a small evaportion chamber that contain the organic material; a coil heats the cell at the decomposition temperature of the or-

ganic material. In the opposite side there is a really small hole and the distance between the evaporation chamber and the hole is lower than the mean free path thus only the molecules with a momentum orthogonal to the substrate can exit.
This tecnique allow to have a collimated beam and a perfect controll on the thickness and on the concentration of the material during the deposition on the substrate.
The typical growth speed of this tecniquw is of 1-2 nm/minuto.

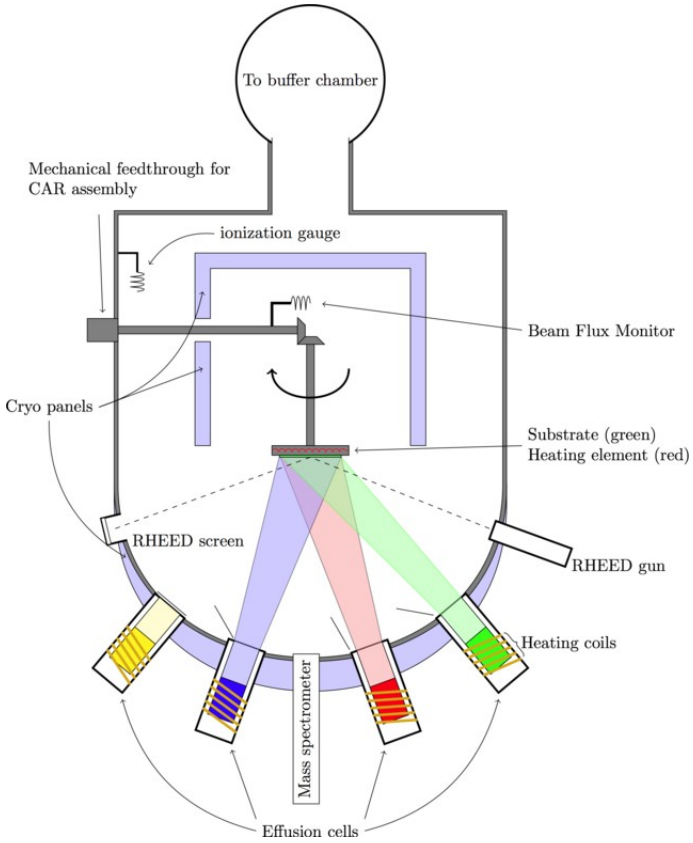

Figure 3.31: Diagram of an OMBD diagram

3.10.4 Organic Vapor Phase Deposition

The control of film thickness uniformity and dopant concentrations over large areas needed for many applications can be difficult when using vacuum evaporation.
In addition, a considerable fraction of the evaporant coats the cold walls

of the deposition chamer; over time, inefficient materials use results in a a thick coating which can flake off, leading to particulate contamination of the system and substrate.
The potential throughput for vacuum evaporated organic thin film devices is low, resulting in high production costs.
Low pressure organic vaport phase deposition (OVPD) has been demostrated as an alternative technique that signigicantly improves control over doping and is adaptable to rapid, particle-free, uniform deposition of organics on large-area substrates.
In OVPD, the organic compound is thermally evaporated into a diluting, non-reactive gas stream and then traposrted in a hot-walled reactor toward a cooled substrate where condensation occurs (Figure 3.32).

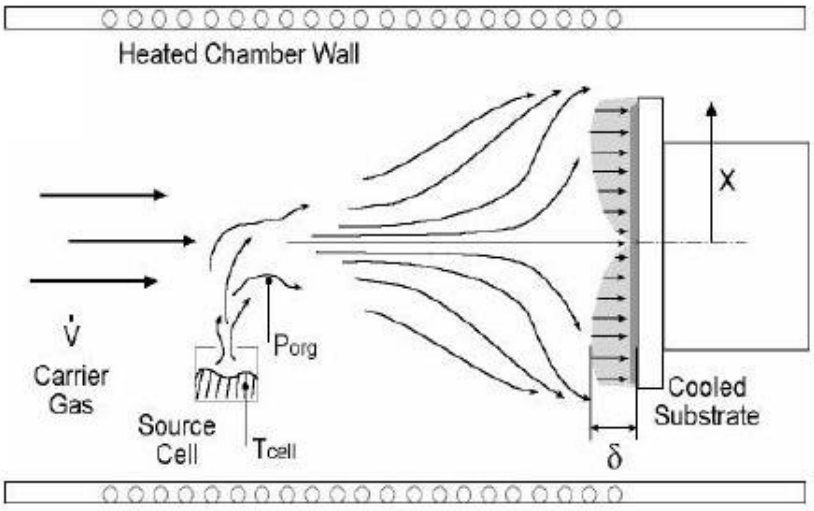

Figure 3.32: Schematic of the OVPD process

Flow patterns may be engineered to achieve a substrate-selective, uniform distribution of organic vapors, resulting in a very uniform coating thickness and minimized materials waste.
All the organic materials used in thin film devices have sufficiently high vaport pressures to be evaporated at temperatures below 400 degress and then trasported in the vapor phase by an inert carrier gas such as nitrogen.
To grow doped films with uniform composition across the entire substrate area the component streams must be mixed prior to deposition. By carrying

out the process at reduced pressure, gas diffusivity is increased improving rated of mass transfer between component streams and to the substrate, which promotes thickness uniformity of the deposited films.
When the mixture of vapor reach the substrate they condense; the process is optimized keeping the substrate at a temperature lower then the condensation chamber.
the advantages of using this technique are:

- The condensation chamber, the evaporation chamber and the pipelines are heated thus the vaport condenses only on the substrate improving the deposition efficency.
- Low pressure
- The possibility to mix different vapor is usefull to grow up dopped film
- Large area deposition

3.10.5 Roll-to-Roll

The roll-to-roll technique ensures low costs, speed, large area, flexible substrate and deposition in the air.
The deposition is performed continuously on long sheets or other flexible polymeric support (Figure 3.33).
Many deposition techniques solution can be adapted to be used in a roll-to-roll. In the Following I will present some tecnique combined with this type of deposition.

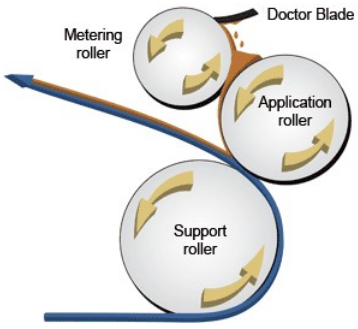

Figure 3.33: Roll-to-Roll tecnique apply with the doctor-blading deposition

Inkjet Printing

The need to combine large area coatings with device patterning has resulted in the development of direct-write fabrication methods, such as inkjet printing.

Inkjet deposition is based on inducing an electric charge in the liquid by ejecting a jet of ink from an orifice through a region with an external electric field. The drops can then be deflected to a substrate or to a reservoir for recycling. In the case of drop-on-demand printers, droplet ejection can be achieved with thermal (bubble-jet) and piezoelectric modes of operation, both shown schematically in Figure 3.34 . The combination of solution-processable emissive polymers with inkjet printing offers some promise in the development of low-cost, high-resolution displays. The technique has also been applied to the manufacture of all-polymer transistor circuits.

The resolution of the inkjet printing process can be improved by using various surface pattering techniques. The substrate surface is pretreated to form hydrophilic and hydrophobic regions. This can be accomplished with a variety of methods, including laser printing, deposition of self-assembled monolayers using a rubber stamp or ultraviolet light exposure. Water-based ink droplets are then confined to the hydrophilic pattern by the surrounding hydrophobic regions.

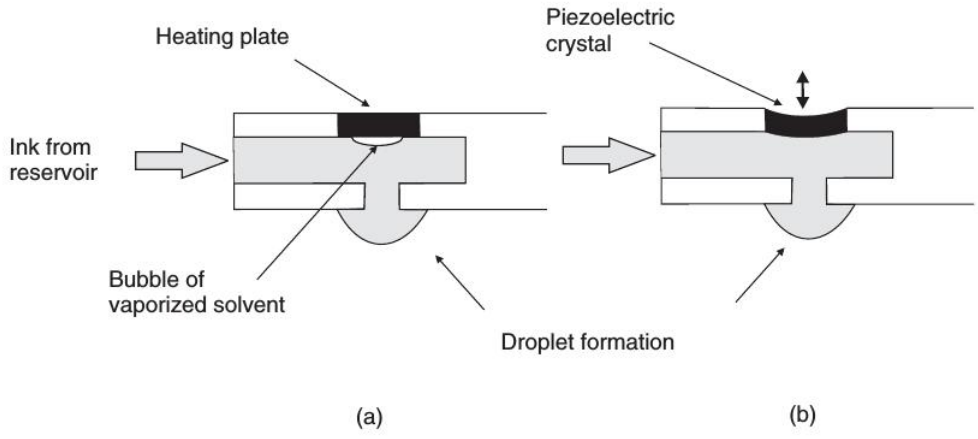

Figure 3.34: Inkjet print heads: (a) thermal (bubble-jet) operation; (b) piezoelectric operation

Flexographic Printing

The Flexographic printig is a rotative printing method that uses the relief patterns on a master stamp to form patterns of ink on the surface of a substrate through conformal contact.
The organic ink is in a tank and it is picked up by a "inking roller". Then the solution go in the "anilox cylinder" where a blade remove the excess solution. The solution is trasfered at the "plate cylinder" where there are the relief patterns and then the plate cylinder transfer the ink to the substrate (Figure 3.35).

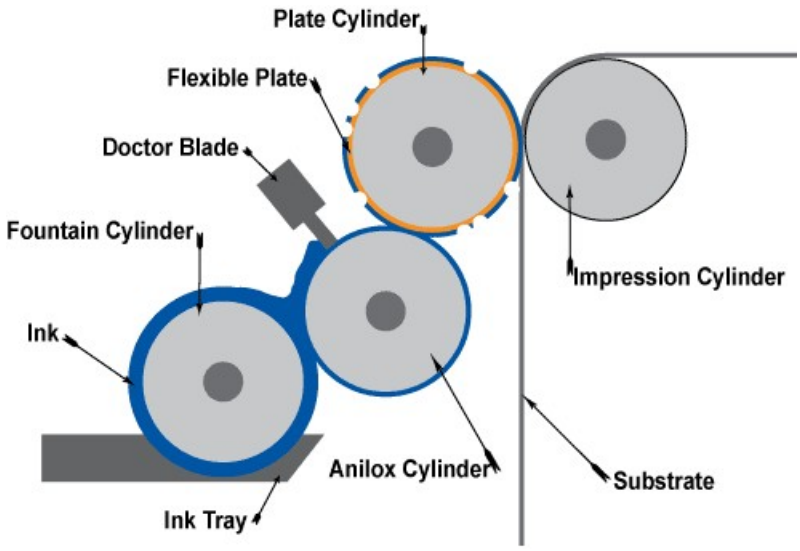

Figure 3.35: Flexographic Printing

Spray Coating

It's similar to the inkjet printing but with this tecnique the organic material is sprayed on the substrate.
The polimeric solution is usually contained in a tank and is first nebulized using an inert gas (like nitrogen) and then sprayed through a small hole.
If the flow of the nebulizer and the velocity of the substrate is constant it is possible to obtain a film with a constant thickness.

Organic Vapour-Jet Printing

OVJP (Organic Vapor Jet Printing) is a natural extension of OVPD deposition through shadow mask apertures, where organic patterns are individually deposited through a small orifice onto a substrate located directly beneath a nozzle.
The nozzle itself is fed by a vapor of organics and a carrier gas, thereby transporting a small amount of material in a spatially confined area.
similar to ink jet printing, the deposition of individual pixels on extender plastic substrates continuously deplyed in close proximity to the localized jet of gas can be achieved. It differs substantially from solution-based ink jet printing of polymers, however, in that the solvent in OVJP is a gas. Hence, it is easily volatilized during growth to leave a uniform film of the desired organic.
This process has the possibility of revolutionizing the growth of small molecule organic thin films by rapidly and simply depositiong ultrasmall patterns of organic thin film materials or precursors.
Like OVPD the process works by passing a molecular species carrying it through a valved nozzle to a cooled, horizontally traslating substrate where the material deposits.
The praticl limits to these dimensions are 500nm, using an orifice with micropores. Below this diameter the gas viscosity wil limit the transport of material through the orifice.

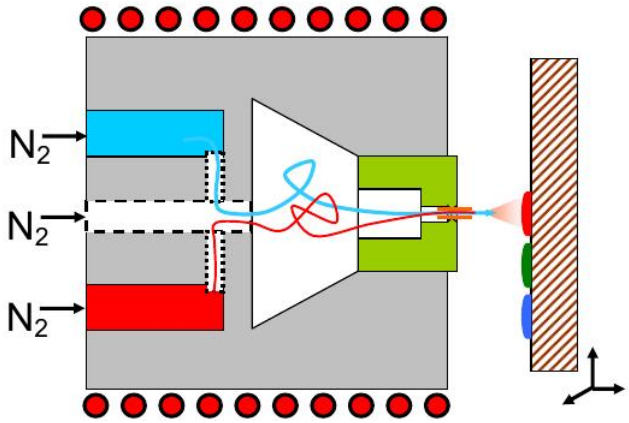

Figure 3.36: Schematic of the OVJP process.

Doctor Blading

Blade coating, also known as knife coating or doctor blading, is a processing method for the fabrication of large area films on rigid or flexible substrates. The well-defined thickness is mainly controlled by the gap size of the blade to the surface. For lab-scale processing the blade is moved over a flat surface. For large-scale roll-to-roll processes the blade is fixed over the moving substrate. The ink is placed in front of the fixed blade whereby the substrate moves relatively to the blade as shown in in Figure. Adjustable gap widths allow the deposition of variable wet layer thicknesses. The final wet layer thickness is roughly half of the gap width depending on the coating speed and flow behavior. Further coating parameters that influence the film formation are surface energy of the substrate, surface tension of the fluid, coating speed, viscosity, and surface temperatures. The deposition speed of this tecniqe is misured in meters of material deposited per minute. The deposition speed range of this tecnique goes from 0.1 to 200 m/min; however the maximux speed is limited by the drying time.

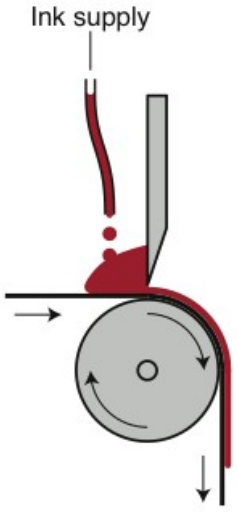

Figure 3.37: Principle of R2R knife coating or doctor blading.

Chapter 4

Organic Photovoltaic Devices

The solar cells are devices that transform the light energy in electric energy. The typicall inorganic-semiconductor solar cells are composed by an p-n junction between two metallic electrodes. Illuminating the p-n junction, the radiation generates electron-hole pairs which are then separated by the electric field in the p-n junction; Connecting a load to the cell it generates a flow of electrons from the n-layer to the p-layer.
In the following i will present some example of basic structure of organic-semiconductor solar cell focusing on the junction behavior and on the electric characteristics.

4.1 Single Layer Cell

Single layer organic photovoltaic cells are the simplest form. These cells are made by sandwiching a layer of organic electronic materials between two metallic conductors, typically a layer of indium tin oxide (ITO) with high work function and a layer of low work function metal such as Aluminum, Magnesium or Calcium. The basic structure of such a cell is illustrated in Figure 4.1a .

When the cell is in equilibrium condition the difference between the work function generate an electric filed throught the organic layer. The cathode is the electrode with the lowest work function and thus the electric field is directed from the cathode to the anode.
When a photon is assorbed by the cell it generates an exciton; the exciton moves in the cell for diffusion and, if the electric field throught the active

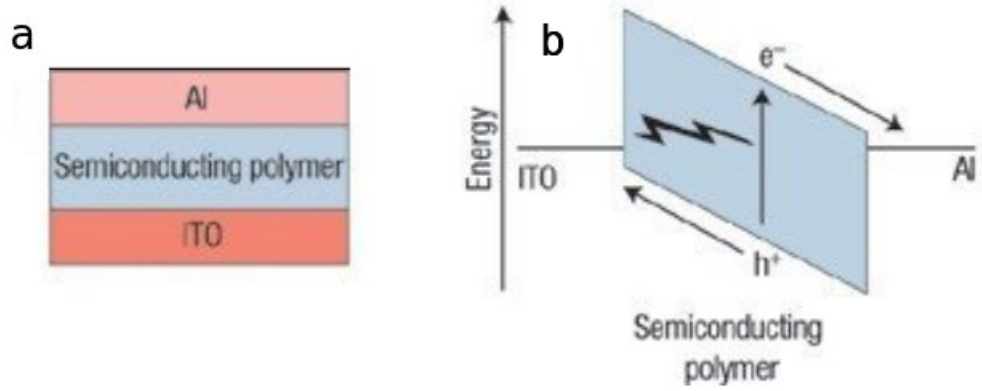

Figure 4.1: a)Sketch of a single layer organic photovoltaic cell b)Photon conversion process

layer is strong enough, it can separate the exciton forming two polaron. When the electron-hole pair is formed the electric field drive the hole to the anode and the electron to the cathode (Figure 4.1b).

Photon Absorption

A photon with an energy equal or higher than the band gap can escite the electron to an excited state. The minimum energy necessary to form the exciton in an organic material is the difference between the HOMO and LUMO levels.
The number of excitons generated S is directly proportional to the light intensity but if the intensity is too high the annihilation of excitons reduce the number of exciton and S depends on the square root of the intensity.

$$S = \frac{\sqrt{1 + 4\tau^2 K_{ANN} G_0} - 1}{2\tau K_{ANN}}$$

with K_{ANN} annihilation speed, τ excitons life time and G_0 is the generation ratio.

Exciton Diffusion

The typical diffusion lenght of an exciton is about 10nm; the exciton must be divided before that it travels this distance or the exciton annihilates.

Exciton Separation

In a single layer solar cell the exciton can be separated only by the electric field internal to the cell or by the thermal energy.
The typical value of electric field necessary to separate the exciton is 4.8 MV/cm.
The internal electric field of the cell depends on the difference between the work function of the electrodes; we can assume an average values of electric field of 100 KV/cm.
We can conclude that the bond energy is higher that the thermal energy (enviroment temperature is not enough to separate the exciton) and than the energy of the internal electric field (the electric field can't separate the exciton).

Charge Transport

The number of carriers collected at the electrode dependes on:

- Number of dissociated excitons
- Carriers recombination
- Number of carriers that can reach the opposite electrode
- The series resistance of the semiconductor that reduce the electric field

To improve the cell characteristic (primarily the exciton separation) a double-layer structure is preferable.

4.2 Double-Layer Cell

Bilayer cells contain two layers in between the conductive electrodes. The two layers have different electron affinity and ionization energies, therefore electrostatic forces are generated at the interface between the two layers. The materials are chosen to make the differences large enough that these local electric fields are strong, which splits excitons much more efficiently than single layer photovoltaic cells. The layer with higher electron affinity and ionization potential is the electron acceptor, and the other layer is

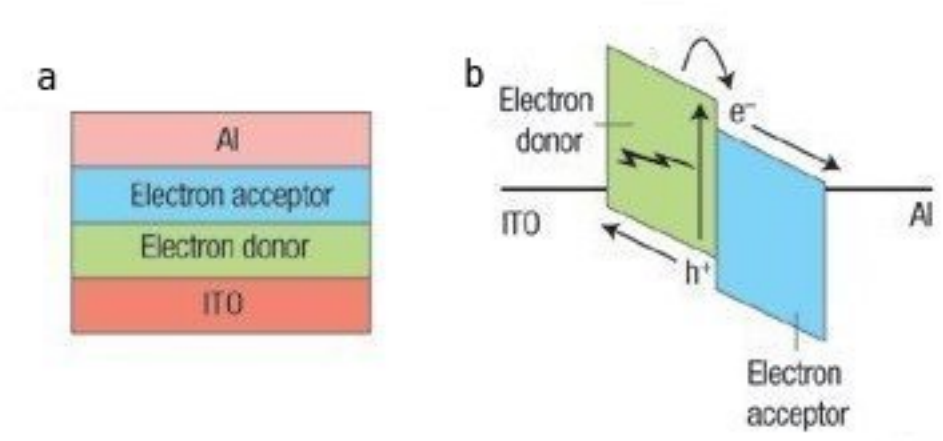

Figure 4.2: a)Sketch of a double-layer organic photovoltaic cell b)Photon conversion process

the electron donor. This structure is also called a planar donor-acceptor heterojunction (Figure 4.2a).

However only the electrons generated close of the separation surface between the two organic films are effectively dissociated; if an exciton is generated far from the interface it could recombine (the typical diffusion lenght is 10 nm as seen before).
In order to increase the surface of the active region it's possible to use an interdigitated structure (Figure 4.3b). In this way the volume of the active region may also be increased by 10 times.
The realization of an interdigitated structure is complex and requires an high precision during the deposition. The blended heterojunction allow to obtain the same result but with lower cost.
In a blended heterojunction the organic film is composed by two materials (aceptor and donor) mixed togheter.
If there is a path between one of the regions of the film and the corresponding electrode it's possible to generate electron-hole pairs in almost all the volume (Figure 4.3c).
Isolated region on the film do not contribute to the generation of free carriers.

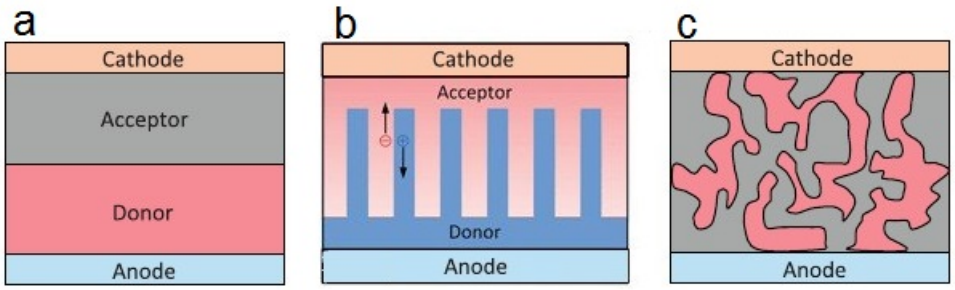

Figure 4.3: a)Normal structure b) Interdigitated structure c)Blended heterojunction structure

4.3 Characterization and Electric Model

4.3.1 Band Diagram

Considering a blended heterojunction, that is composed by a mix of an acceptor and a donor compounds, the regions are equally distributed in the active layer; this means that in the same point we thare are two band of semi-delocalized states: one for the acceptor and the other for the donor (Figure 4.4).

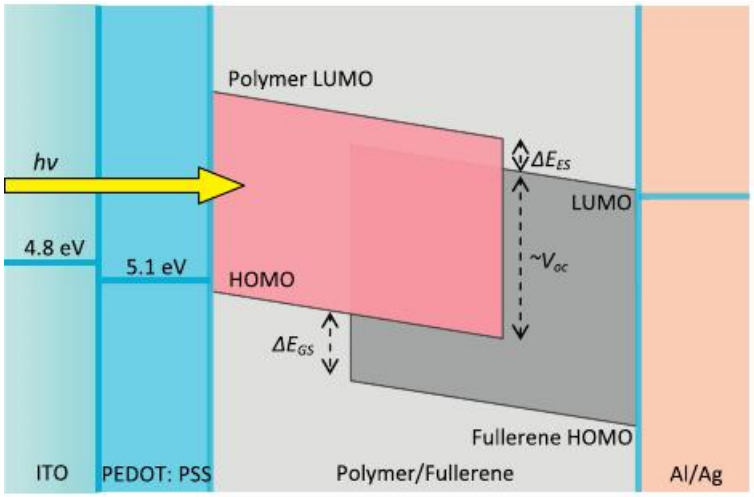

Figure 4.4: Energy band diagram of donor-acceptor materials in bulk-heterojunction organic solar cells

The electrons are transported in the LUMO band of the acceptor material and the holes are transported in the HOMO band of the donor material.

Thus we can say that the blended heterojunction can be described like a single material where the HOMO is the HOMO of the donor material, the LUMO is the LUMO of the acceptor material and the absorption spectrum is given by the overlapping of the spectrum of the material that form the band.

4.3.2 Voltage-Current Equation

To obtain a simplified electric-model of a blended heterojunction solar cell we assume that the net charge in the film is small thus we can consider the electric field constant; when the cell is exposed to light the photo-current generation process is divided in three steps

Generation and Diffusion of the Excitons

We assume a constant generation throughout the film and that the excitons don't recomine at the electrodes.
The resulting excitons concentration is

$$S = \frac{\sqrt{1 + 4\tau^2 K_{ANN} G_0} - 1}{2\tau K_{ANN}}$$

Excitons Separation

Considering the Braun-Onsager model, after the separation of an exciton we obtain a pair of polaron strongly bound (with G_X polaron pairs generated). After the generation of the polaron pair there are three possible phenomena

- *Recombination* It depende on the carriers concentrations as $R = \delta np$
- *Decay to the Ground State* The ionized donor-acceptor pair has a limited life time; the recombination time is $1/K_{REC}$
- *Separation* Generation of the hole-electron pair; the separation time is $1/K_{SEP}$

Neglecting the recombination and considering a constant generation rate throughout the film ($G_X = K_D S$), the electron-hole pairs generation rate is

$$G = PG_X = G_X \frac{K_S EP}{K_S EP + K_R EC} = K_D \frac{K_S EP}{K_S EP + K_R EC} S$$

Carriers Extraction

The model we use to calculate the number of pair extracted is the Sokel-Hughes model, used for the photo-current in the insulator materials.
The carriers concentration can be calculated using the continuity equation for electrons and holes

$$\frac{1}{q}\frac{dJ_p}{dx} = \mu_p E\frac{dp}{dx} - \mu_p\frac{KT}{q}\frac{d^2p}{dx^2} = G$$

$$\frac{1}{q}\frac{dJ_n}{dx} = \mu_n E\frac{dn}{dx} - \mu_n\frac{KT}{q}\frac{d^2n}{dx^2} = G$$

and applying the boundary condiction

$$n(x) = p(x) = 0 \quad at \quad the \quad electrodes$$

we obtain this solution for the continuity equation

$$p(x) = \frac{Gd}{\mu_p E}\left[\frac{x}{d} - \frac{\exp(-\frac{qEx}{KT}) - 1}{\exp(-\frac{qEd}{KT}) - 1}\right]$$

$$n(x) = \frac{Gd}{\mu_n E}\left[\frac{\exp(-\frac{qEx}{KT}) - 1}{\exp(-\frac{qEd}{KT}) - 1} - \frac{x}{d}\right]$$

We can calculate the current throughout the film using the previous boundary condition where $n(0) = p(0) = 0$

$$J = qGd\left[\frac{exp(\frac{qEd}{KT}) + 1}{exp(\frac{qEd}{KT}) - 1} - \frac{2kT}{qEd}\right] = qGd\left[\frac{exp(\frac{V_{bi}-V}{V_T}) + 1}{exp(\frac{V_{bi}-V}{V_T}) - 1} - \frac{2V_T}{V_{bi} - V}\right]$$

with $V_T = \frac{KT}{q}$; the photo-current does not depend on mobility but only generation rate, the internal voltage V_{bi} and the voltage apply to the cell.

4.3.3 Figures of Merit

Short-Circuit Current Density

The short circuit current density (Jsc) is the maximum photo-current density which can be extracted from the device at short circuit condition.

$$J_{CC} = qGd\left[\frac{exp(\frac{V_{bi}}{V_T})+1}{exp(\frac{V_{bi}}{V_T})-1} - \frac{2V_T}{V_{bi}}\right] \simeq qGd\left[1 - \frac{2V_T}{V_{bi}}\right]$$

Open-Circuit Voltage

Open circuit voltage (Voc) is the difference of electrical potential between two terminals when a device is disconnected from any circuit. If $V = V_{bi}, E = 0$ and $J = 0$ so $V_{oc} = V_{bi}$.

Fill Factor

The Fill Factor (FF) is the ratio between the maximum output power and the product $J_{sc}V_{oc}$.

$$FF = \frac{P_{max}}{V_{oc}J_{sc}} = \frac{V_M J_M}{V_{OC}J_{SC}}$$

with V_M voltage of the maximum power point and J_M current of the maximum power point. Combining all the previous result

$$FF = \frac{1 - \sqrt{\frac{2V_T}{V_{bi}}}}{1 + \sqrt{\frac{2V_T}{V_{bi}}}}$$

Efficency

The definition of the efficency of the cell depends on what process of the cell we are focusing on:

External Quantum Efficiency Ratio between the number of electron-hole pairs extracted and the number of incident photons

Internal Quantum Efficiency Ratio between the electron-hole pairs extracted and number of photons absorbed in the active layer

Electrical Efficiency Ratio between the maximum produced power and the incident solar power.

4.3.4 Calculation of the Quantum Efficiency

The quantum efficency depends on a lot of processes that affect its final value

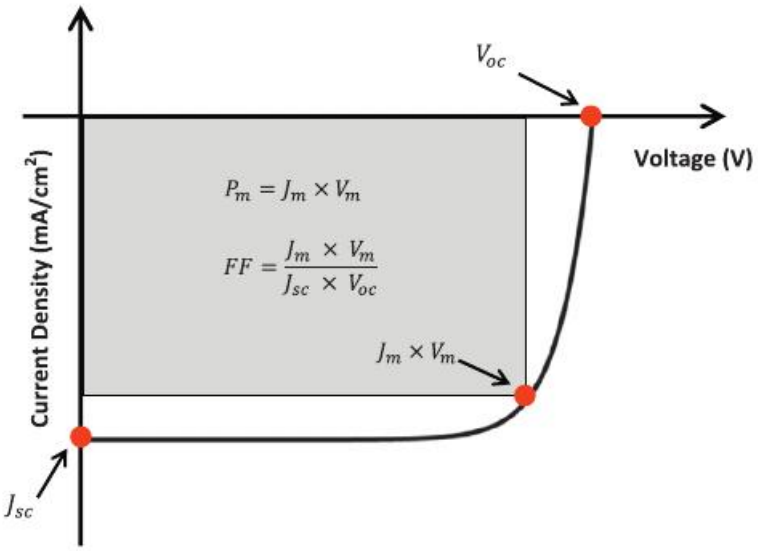

Figure 4.5: Solar cell characterization

Absorption

Not all the incident light is converted in carriers because of

- *Reflection outwards*
- *Absorption of light* in no-active regions of the cell
- *Absorption Spectrum* of the active layer
- *High energy photons*; the excess energy is dissipated as heat

The absorption coefficient η_A is the ratio between the absorbed photons and the incident photons.

$$\eta_A = \frac{number \quad of \quad excitons \quad generated/sec}{number \quad of \quad incident \quad photons/sec}$$

Diffusion and Dissociation

Some of the generated excitons can recombine or reach the electrode without generating the polaronic pair.
The diffusione efficency η_D is the ratio between the number of excitons dissociated and the number of excitons generated.

$$\eta_A = \frac{number \quad of \quad excitons \quad dissociated/sec}{number \quad of \quad excitons \quad generated/sec}$$

Separation

Not all the polaronic pairs are separated; some of them recombine. The separation efficency η_S is the ratio between the number of polaronic pairs separated and the number of exctions dissociated.

$$\eta_A = \frac{number \quad of \quad polaron \quad separated/sec}{number \quad of \quad excitons \quad dissociated/sec}$$

Extraction

After the separation the electron-hole pairs have to reach the electrodes without recombination. Some of the electron-hole pair recombine in the cell generating an internal current called *Recombination current*. The Extraction efficency η_E is the ratio between the number of carriers extracted and the number of polaron pairs separated.

$$\eta_A = \frac{number \quad of \quad carriers/sec}{number \quad of \quad polaron \quad dissociated/sec}$$

The external quantum efficency is given by

$$EQE = \eta_E \eta_S \eta_D \eta_A$$

and the internal quantum efficeny is given by

$$IQE = \eta_E \eta_S \eta_D$$

4.3.5 Limiting factors

Series and Shunt Resistance

The series resistance is related to the electrodes resistance and to the film region close to the electrode where there is no charge generation (Figure 4.6a). The shunt resistance is related to the conductive path between the anode and the cathode (Figure 4.6b).

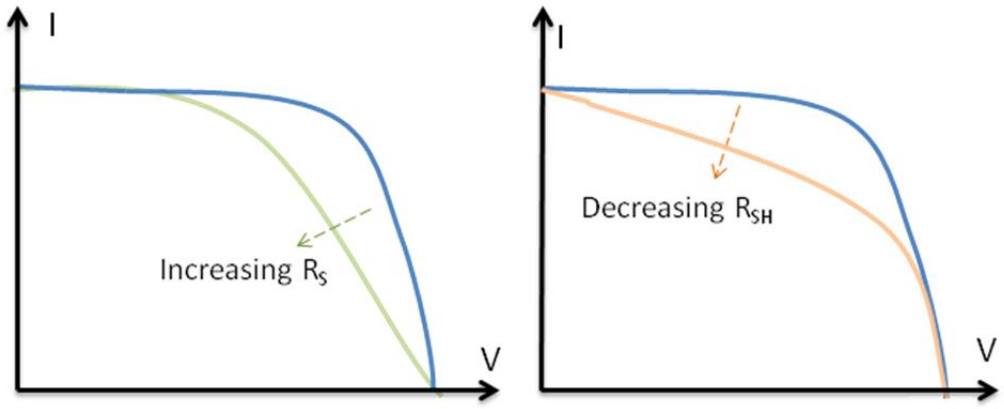

Figure 4.6: Effect of series and shunt resistance on fill factor

Recombination

Using the Sokel model, the recombination introduce a reverse current that is subtracted to the photo-current.

$$J_{REC} = \frac{qG_0 d^3}{2\langle \mu_{eff} \rangle (V_{bi} - V}$$

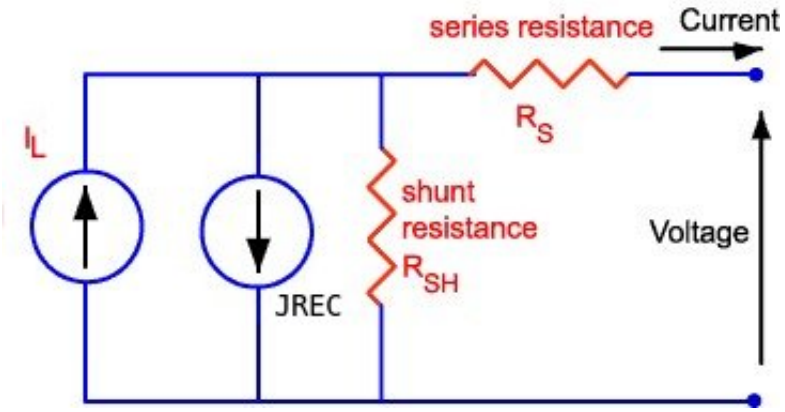

Figure 4.7: Electric model of an organic solar cell

Chapter 5

Measurement Techniques

In this chapter i will describe the typical procedure for a complete characterization of the cell i have tested, focusing on the instrument used. The cells are produced by the Polymeric solar cells group of the Department of Energy Conversion and Storage of DTU (Technical University of Denmark) where i spent the last three month of my thesis period.
Figure 5.1 shows three examples of samples i received from Denmark.
The detail about the internal structure of the devices will be presented in the following.

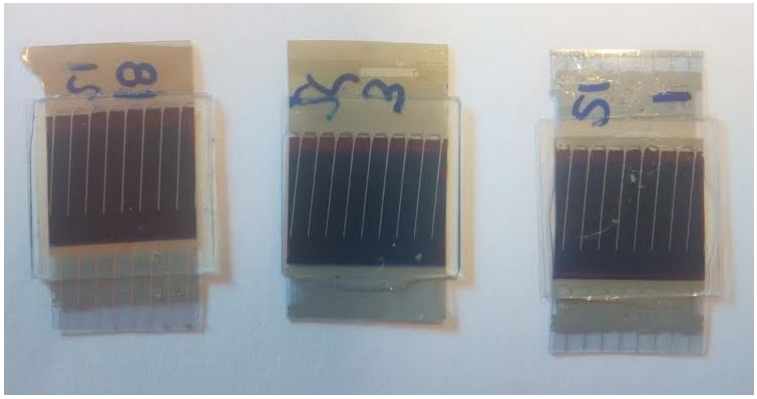

Figure 5.1: Organic solar cells samples from DTU

In the beginning the cells were connected to the instrument using crocodile clips; then to reduce the risk to damage the contact, i realize a simple PCB-connector which exploits the flat structure of the device to realize the electrical contact (Figure 5.2).

All the measure are made under illumination condition. I used two

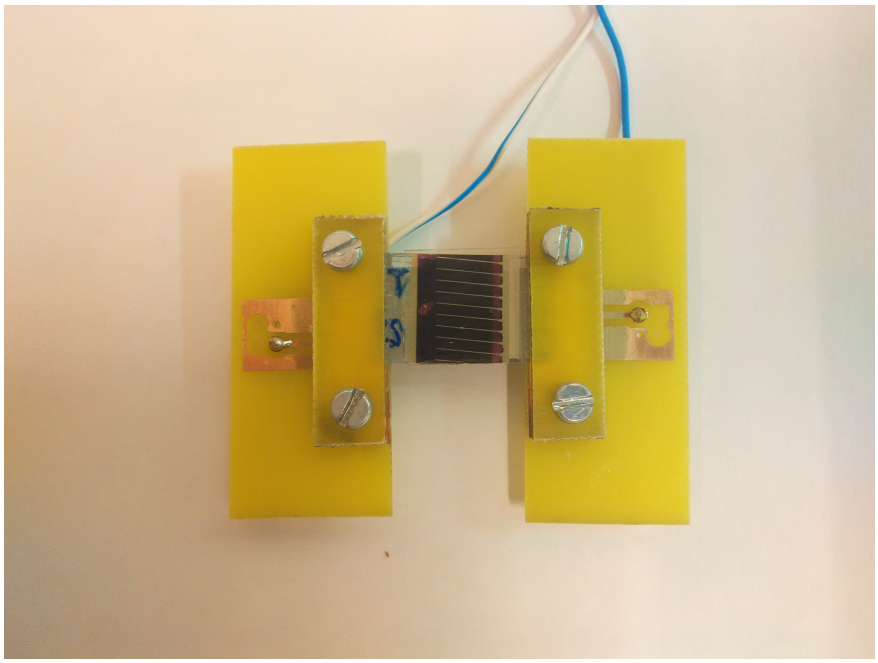

Figure 5.2: PCB-Connector for organic solar cells

different type of sources for my tests:

- The solar simulator for the initial IV characteristics and for the standard Impedance Spectroscopy measures
- A Power LED (100 W) for the tests which implied different illumination condition

To calibrate the solar simulator i used a reference solar cell (NEWPORT 91150 V Figure 5.3).

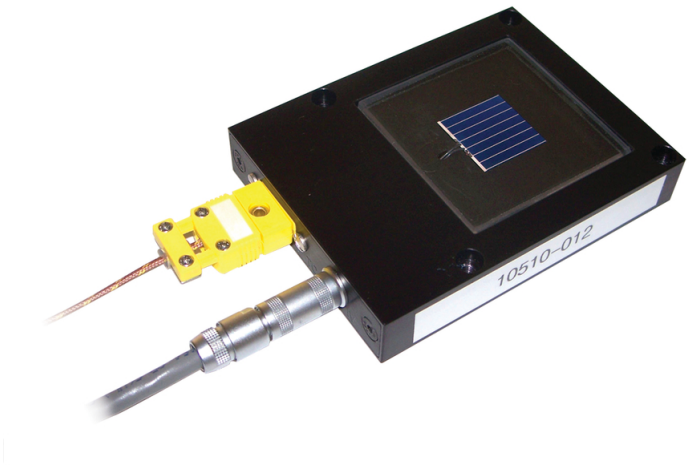

Figure 5.3: Reference cell NEWPORT 91150 V

5.1 IV Characteristic

The first measure i did on all the devices is the IV characteristic. It allow to verify the cell condition (sometimes the cell is too degrade to be useful for other test) and to determine the standard figures of merit for a solar cell:

- Open Voltage Circuit (V_{OC})
- Short Circuit Voltage (J_{SC})
- Fill Factor (FF)
- Efficiency

The IV characteristic is performed applying to the cell a DC voltage between -1 and 0.7 V (with steps of 0.1 V) while the cell is exposed to a light beam with an intensity of 1 SUN.
Usually the IV measure is executed twice: the first time (forward) the voltage goes from negative to positive values; the second time (back) the voltage goes from positive to negative values. This allow to identify any phenomena of hysteresis in the device. Usually the IV characteristic is converted on the JV characteristic to compare the result of device with different areas. The samples i analyzed had an area of 1 cm^2 thus basically the conversion was not necessary.

The instrument i used for the IV Characteristic is AGILENT E5263 (Figure 5.4).

Figure 5.4: Parameter AGILENT E5263

5.2 Impedance Spectroscopy

Impedance spectroscopy (IS) is a widely used method in the study of the operational mechanisms of different types of solar cells: dye-sensitized solar cells (DSC), organic solar cells, and also in silicon solar cell devices. Impedance Spectroscopy is made applying an AC voltage signal to a device and measuring the current through it. In solar cells the impedance is normally measured using a small AC excitation signal (this is done so that the device's response is pseudo-linear) and a DC polarization signal to force the operating point of the cell (we did all the test using a DC polarization equal to the Voc of the cell) (Figure 5.5).

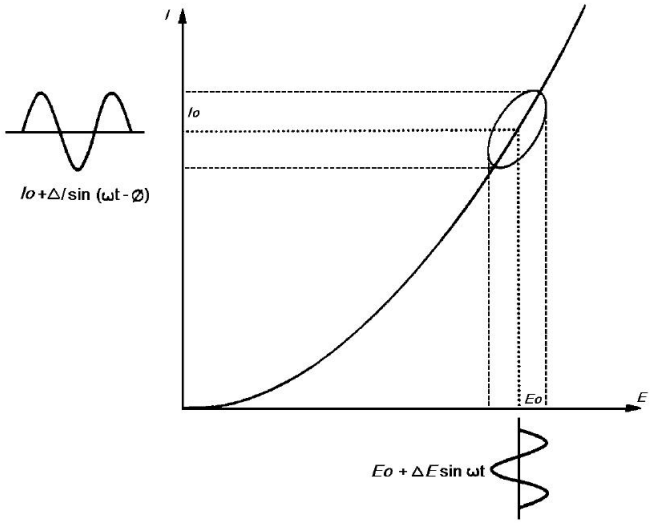

Figure 5.5: AC and DC signal in a impedance spectroscopy measure

Using the value of the voltage apply to the device and the measured current we can obtain the impedance of the system as

$$Z(\omega) = \frac{E}{I} = Z_0 \exp(j\phi) = Z_0(cos\phi + jsin\phi)$$

The expression for Z(ω) is composed of a real and an imaginary part. If the real part is plotted on the X-axis and the imaginary part is plotted on the Y-axis of a chart, we get a "Nyquist Plot". Usually, for readability, if the behavior of the device is purely resistive-capacitive the Y-axis shows the opposite of the imaginary part (Figure 5.6).

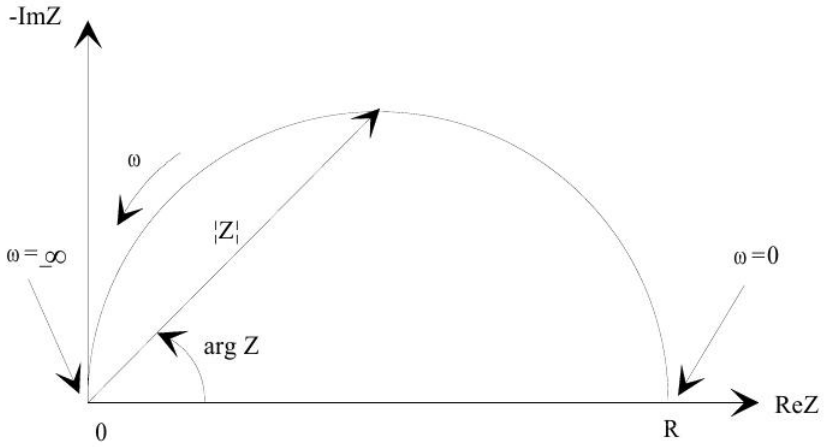

Figure 5.6: Example of Nyquist plot

From the impedance measure we can obtain an electric model of the device. For example for the Nyquist plot of figure 5.6 the model is a simple parallel RC circuit (Figure 5.7).

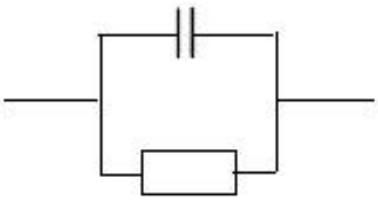

Figure 5.7: Parallel RC model

Using this simple circuit as an example, we can obtain all the paramenter using the impedance spectroscopy data.
From the Immaginary part characteristic we can obtain the ω reading the frequency of the peak (Figure 5.8).

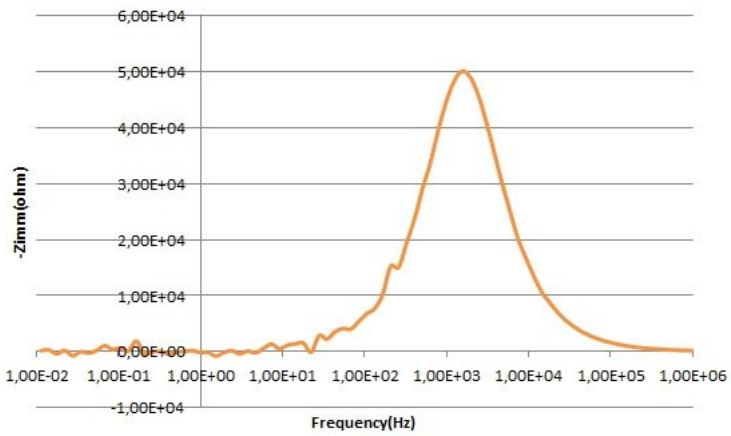

Figure 5.8: Immaginary part characteristic; the frequency of the peak is $\sim 1600Hz$

The diamenter of the nyquist plot is the value of the resistance R (Figure 5.9).

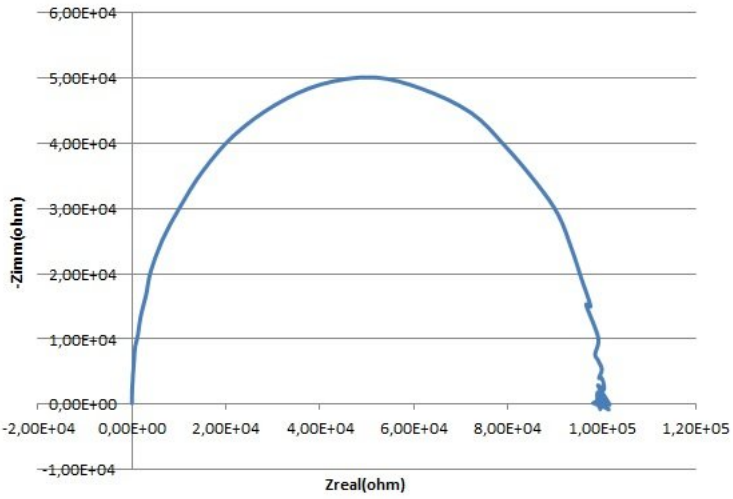

Figure 5.9: Nyquist plot; the value of the resistance is 100KΩ

Thus we can obtain the value of the capacitor C as $C = \frac{1}{R\omega}$ (the value of the capacitance in this test was 1 pF).
Obviously this is one of the simplest case but is a good way to understand the typical procedure to analyze the impedance data.
With more complex system the situation could be completely different.
For example figure 5.10 shows the nyquist plot of one of the device i studied.

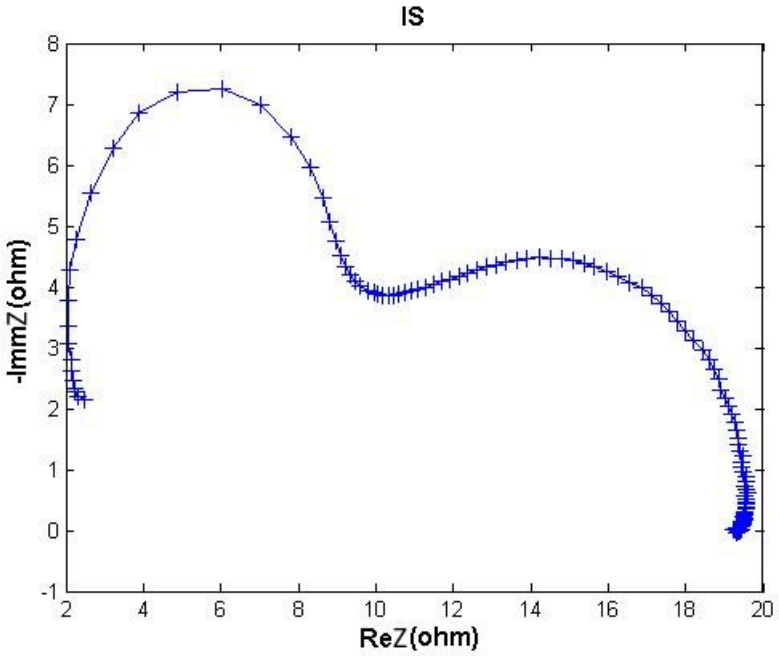

Figure 5.10: Example of Nyquist plot of an organic solar cell

The main difference between this plot and the previous one is the precence of a second lobe.
The reason of this behavior will be explained in the following.
Now i want only to remark that if we have more impedance contribuition they influence each other in the nyquist plot and thus is more difficult to extract the model parameters.

To obtain a good electrical model of a device it is necessary to understand all the phenomena that take place in it. The impedance spectroscopy is one of the most flexible tecnique to study the behavior of a device in different condition.
Varying the operation condition we can observe the variation on the impedance data and comparing them we can understand which phenomenon may have contributed.
For example one of the first test to do for a solar cell is to vary the illumination condition and observe which lobe on the nyquist plot is affected. In this way it is possible to identify which lobe is related to the active layer.
Impedance spectroscopy is also useful to study the reliability and stability of

the devices. In fact, once identified which part of the cell is responsible for each contribution of impedance (and therefore of each lobe in the Nyquist plot) is possible to determine which part of the device is degrading.

Usually for the devices based on electrochemical process is necessary to use instrument with wide frequency range (from μHz to MHz).
The organic solar cells are based on faster phenomena so a simple LCR is enough.
The LCR i used is E4980 (Figure 5.11) with a range of frequency from 20 Hz to 2 MHz with the typical 4 cable configuration: two cable are for the anode connection and two cable for the cathode (on each side one is to force the voltage and the other to measure the current).

Figure 5.11: LCR E4980

Chapter 6

Tests on DTU samples

6.1 Switching Procedure

The basic structure of a DTU polymeric solar cell is shown in figure 6.1. The *Flextrode* is a semitransparent flexible thin-film electrode for use in printed optoelectronic devices such as displays, touch panels, solar cells, organic LEDs etc. *Flextrode* is developed as a substitute for the widely used but costly and environmentally unsound Indium Tin Oxide (ITO) electrode.
The *Flextrode* is basically composed by a PET substrate, a silver grid (print with an automated roll to roll tecnique), PEDOT:PSS layer and a ZnO layer both to obtain a good band alignment.

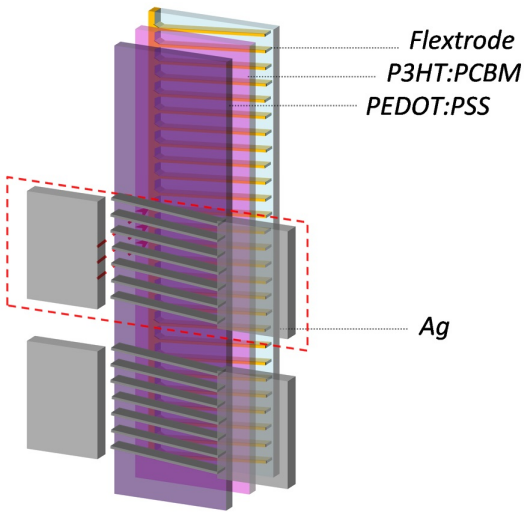

Figure 6.1: Basic Structure of a DTU polymeric solar cell

The *Flextrode* is manufactured in long foil; to realize the samples a piece of this foil is cut and used in a manual mini roll-to-roll machine.
The other layers are then deposited on the *Flextrode* substrate.
After the coating of the PEDOT:PSS layer, a silver grid is print with the "flexographic printic" technique using a silver paste deposited on a master stamp.
At the end of the coating process could happen that somewhere in the cell the PEDOT:PSS penetrate through the active layer creating a short circuit between the anode and the cathode of the device, thus is necessary to "activate" the cells using a technique called *Switching*. The procedure used by DTU is here reported

- Connect the positive pole of the power supply to the negative terminal of the solar cell via cord A.
- Connect cord B to the power supply's negative pole while leaving the other end of the cord free/unconnected.
- Connect cord C to the positive terminal of the solar cell while leaving the other end of the cord free/unconnected
- Set the power supply to the required switching power for you specific solar cell.
- Briefly connect the free end of cord B and C in an instant stroke and by this create a short electrical pulse through the solar cell.

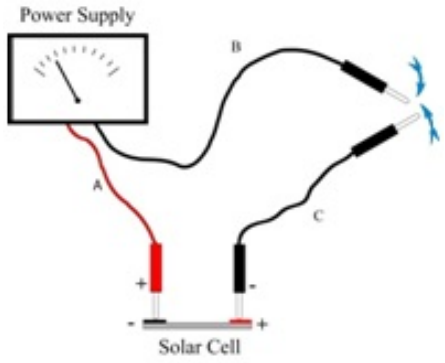

Figure 6.2: Switching Procedure

In this procedure the switch is made manually; we decide to inspect the correlation between the activation pulse width and the efficiency of the cell using an Impedance Spectroscopic analysis.
Initially we have try to activate the cell at different voltage value, evaluating the IV characteristics and the IS (impedance spectroscopy) curves. For the characterization we used a solar simulator with an intensity of 1 SUN. In the second part of the tests we have try to activate the cell with different pulse length.
To find a good start point for the pulse length we did some test evaluating the average length of a handmade switching. We found a range of 80-160 ms. Thus we have made a simple pulse circuit with a range from 100 ms to 100 μs. For the tests we have used a simple pulse generator that use a NE555 and a MOSFET switch to obtain pulse of different lengths; we have tested cell with pulse of 100 ms, 50ms and 1 ms (Figure 6.3).

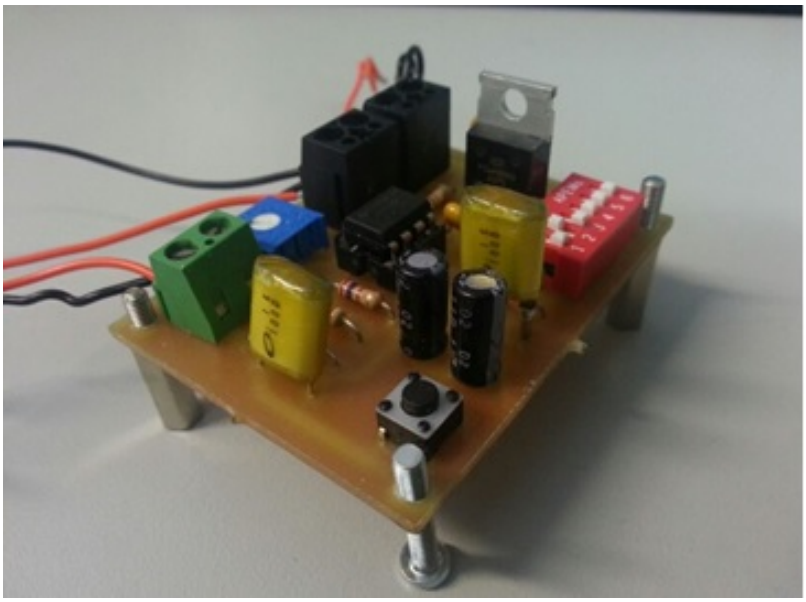

Figure 6.3: Pulse Generator

We have not used shorter pulses because we have verified that 1-ms pulse gives bad result.

6.1.1 Variable Voltage

*We used a current compliance of 500 mA for the voltage supply.
*We omitted all result about the cells before switching because they show all the same resistive behavior (Figure 6.4)

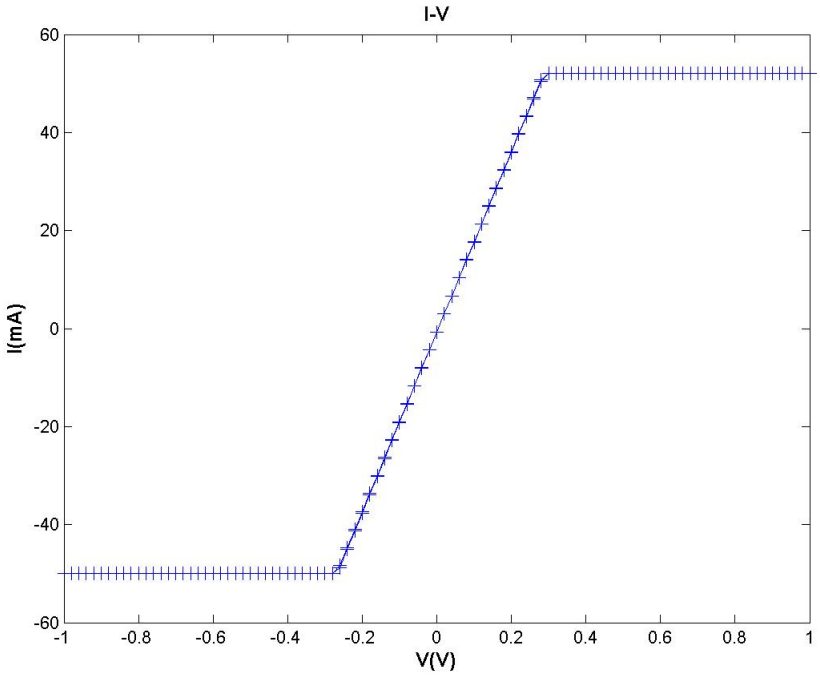

Figure 6.4: Example of IV curve before switch

In the First test we used a constant pulse length of 100 ms varying the pulse voltage:

PULSE VOLTAGE:20 V

The cell is activated with high Voc and Jsc (V_{OC}=0.51 V J_{SC}=3.6 mA). IS (Figure 6.6) shows large resistance and the presence of one well-defined lobe, and a tail of high frequency which can be likely related to a second small lobe.

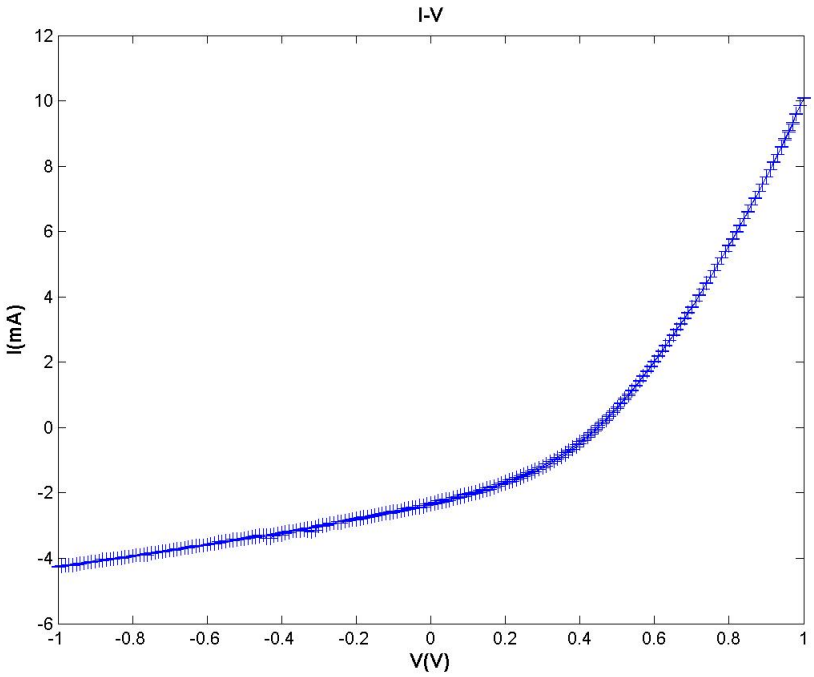

Figure 6.5: IV with a pulse of 20 V and 100 ms

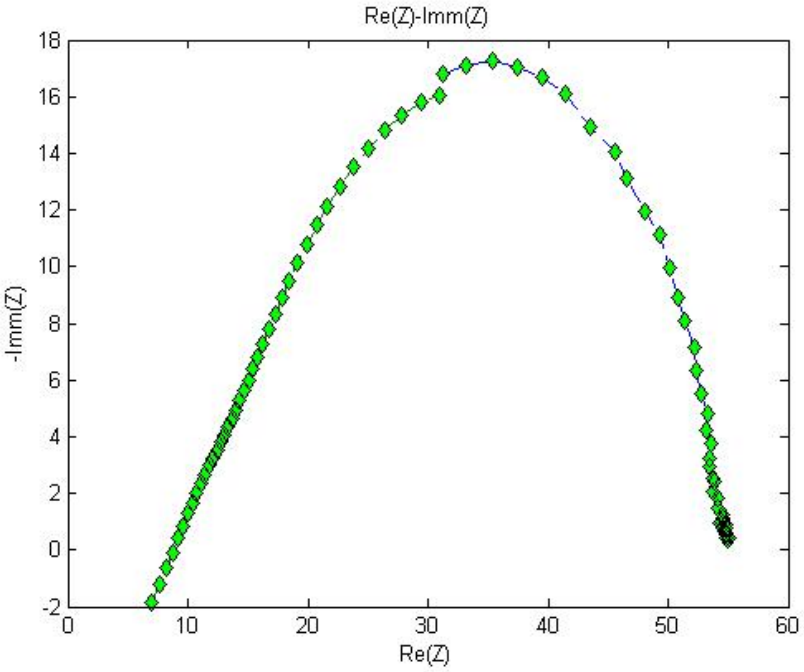

Figure 6.6: IS with a pulse of 20 V and 100 ms

PULSE VOLTAGE:10 V

With a lower voltage we observe a lower value of Voc (V_{OC}=0.4 V J_{SC}=2.84 mA).
This is probably due to the residual impurities of PEDOT:PSS on the active layer which involves the presence of conductive path in it and thus a small shunt resistance.
From the IS (Figure 6.8) results we observe a large LF-resistance value. It looks like the low Voltage apply to the cell has not destroy completely silver short cut and has probably damage the polymeric material due to high temperature related to the high current/voltage used for switching test.

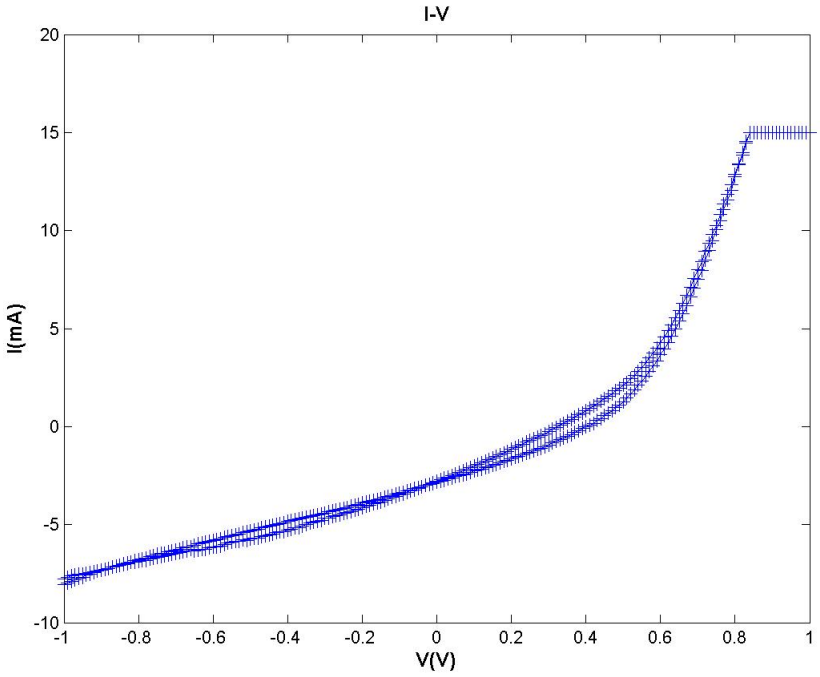

Figure 6.7: IV with a pulse of 10 V and 100 ms

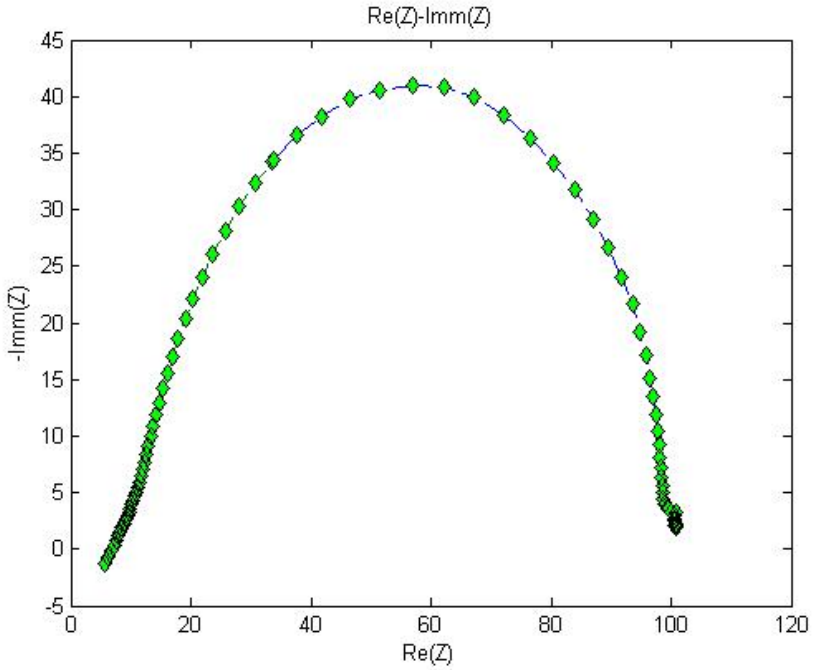

Figure 6.8: IS with a pulse of 10 V and 100 ms

MULTIPLE PULSES

In this test we applied a multiple pulses on a cell starting with a 5 V pulse. The aim was to verify the lower value at which the cell start to have a solar-cell behave and if was possible to activate the cell with multiple pulses without damaging the blend.
Figure 6.9 and 6.10 show a summary of the IV and IS curves obtained.
The cell in the beginning showed the typical resistive behaviour. We applied 2 pulses with a voltage of 5 Volt and a length of 100 mS but the cell didn't change its behaviour. This is probably due to the low power not sufficient to eliminate the PEDOT:PSS impurities. After 8-V pulse the cell show a resistive behavior but a positive Voc and Jsc. IS curves (Figure) show that after the 8 V switching the cell looks activated but the shunt resistance is still low.
After 10-V pulse the device shows cell like behavior, but with a low Voc and Jsc values. On the other end the low frequency resistance indicates that we are probably damaging the polymeric material. After 20-V pulse there is a high V_{OC} but a very low J_{SC}.

On the one hand this confirms that PEDOT:PSS impurities are being eliminated during pulses. On the other hand multiple pulses degrade the polymeric blend.
In fact we are applying multiple pulses and at every pulses the cell seam to increase its resistivity. So we are continuously eliminating part of the impurities of PEDOT:PSS in the active layer, but a fraction of the current is also flowing through polymeric blend damaging it. This can also be the reason of the high value of resistivity we have found in IS result also with 20-V pulse activation.

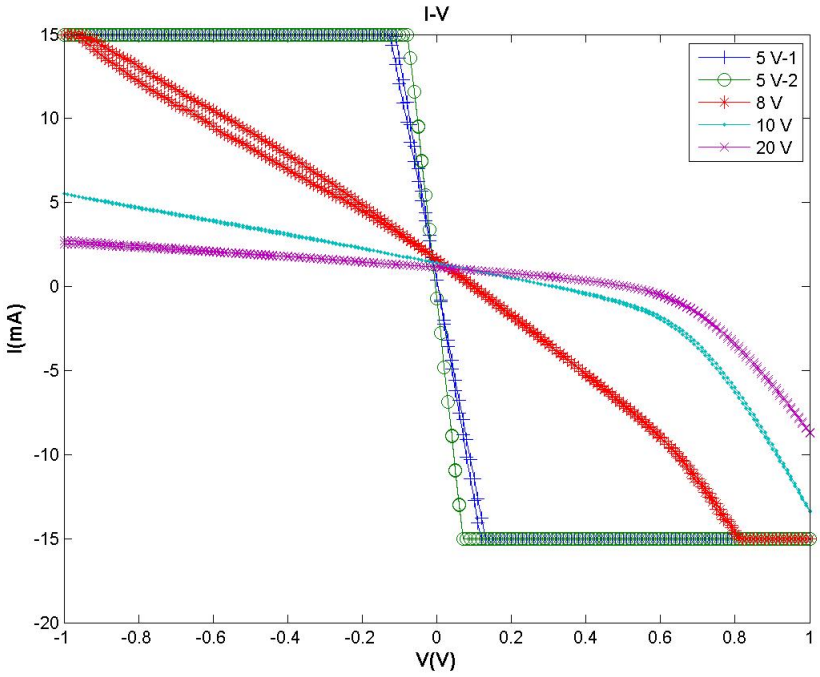

Figure 6.9: IV characteristics after each pulse

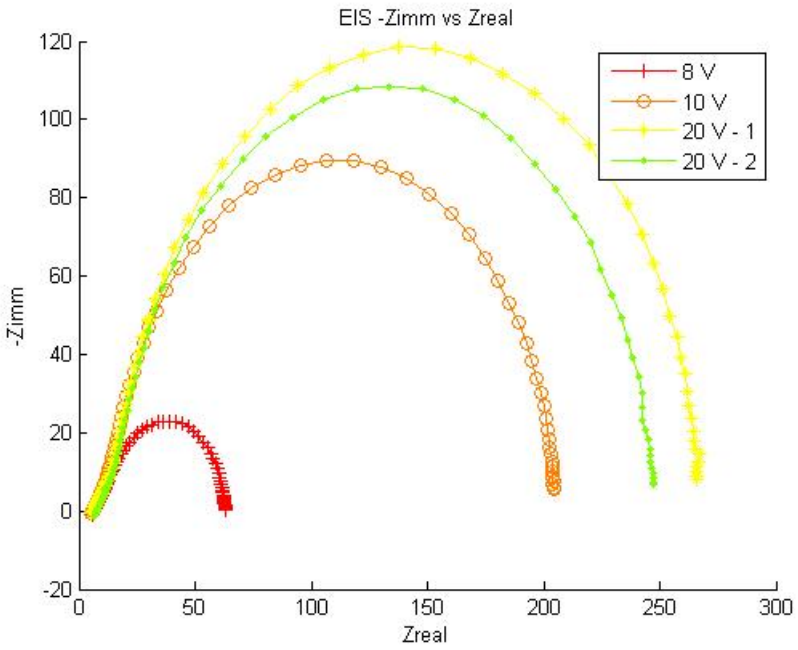

Figure 6.10: IS curves after each pulse

6.1.2 Variable Pulse Length

From the *variable voltage* test we found that the 20-V pulse was the best to switch the cell properly obtaining high V_{OC} and J_{SC}.
With this test we aim to verify the reproducibility of the switching procedure using different pulse length.
For this test we used 3 pulses length :100 ms, 50 ms and 1 ms.
Figure 6.11 and 6.12 show the IV characteristics after 100-ms pulse switching.
All the cells switching with the 100-ms pulse present low reproducibility. They have an high V_{OC} but the J_{SC} is low.
Figure 6.13 and 6.14 show the IV characteristics after 50-ms pulse switching. This set of cells show an high reproducibility

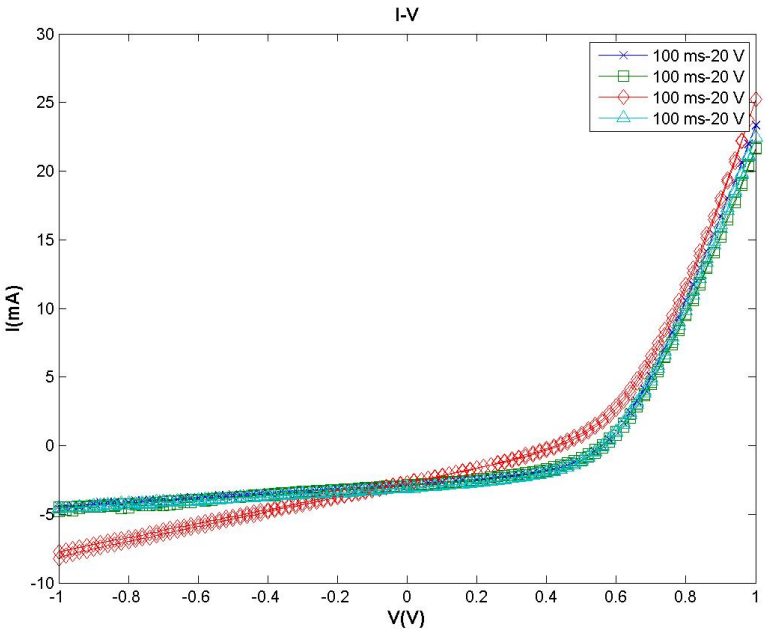

Figure 6.11: IV characteristics after 100-ms pulse switching

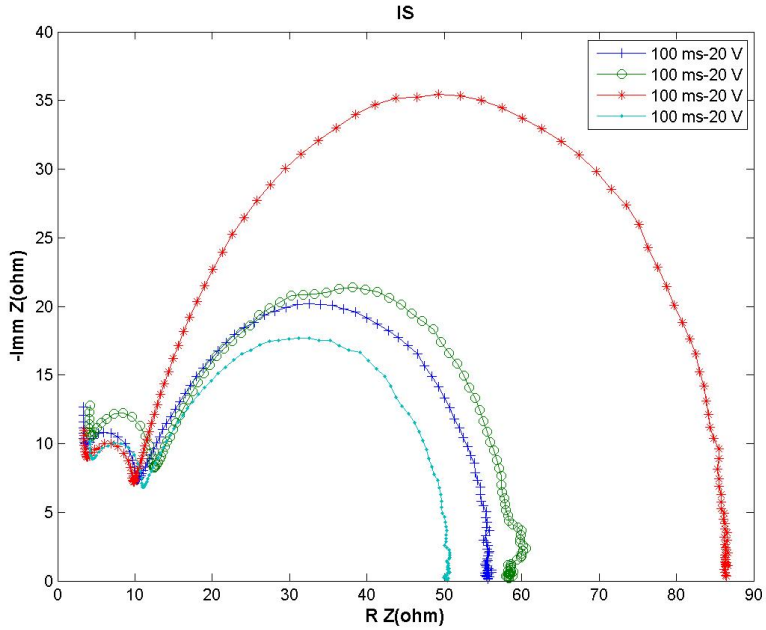

Figure 6.12: IS curves after 100-ms pulse switching

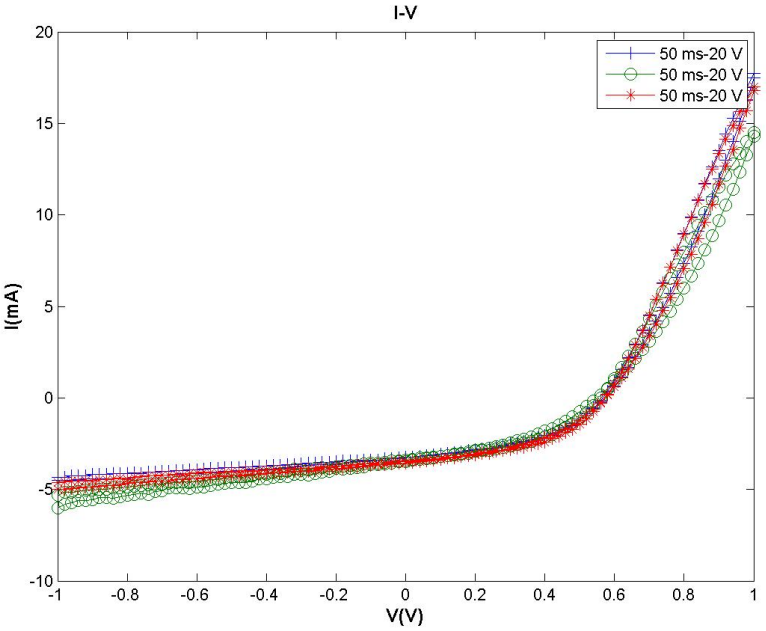

Figure 6.13: IV characteristics after 50-ms pulse switching

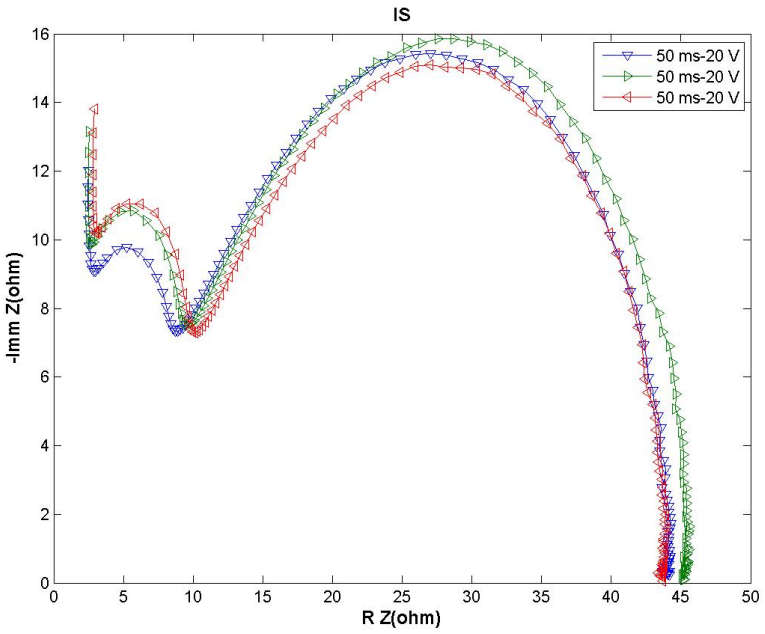

Figure 6.14: IS curves after 50-ms pulse switching

Table 6.15 shows also that the cells activated with the 50-ms pulse have an higher efficiency (the J_{SC} is higher than the cells activated with 100-ms pulse). The low frequency resistance is lower in the cell activated with the 50-ms pulse and this means that all the conductive paths have been destroyed after the pulse without damaging the polymeric material.

PULSE LENGHT	Voc(V)	Jsc(mA)	FF	η(%)
100 ms	0.56	2.85	46.4	0.74
100 ms	0.56	2.93	45.5	0.74
100 ms	0.56	3.12	46.2	0.80
50 ms	0.56	3.25	47.4	0.86
50 ms	0.56	3.45	44.1	0.85
50 ms	0.56	3.55	46.7	0.96

Figure 6.15: Summary of the result on variable pulse test

To verify if it was possible to activate the cells also with shorter pulse we tried to apply a 1-ms pulse to the cell.
The cell show a large instability (hysteresis phenomena on IV curve) and a lower Voc. It looks like activated but probably the pulse is too short to destroy all the conductive path and a small shunt resistance still remains, leading to the small Voc (Figure 6.16 and 6.17).

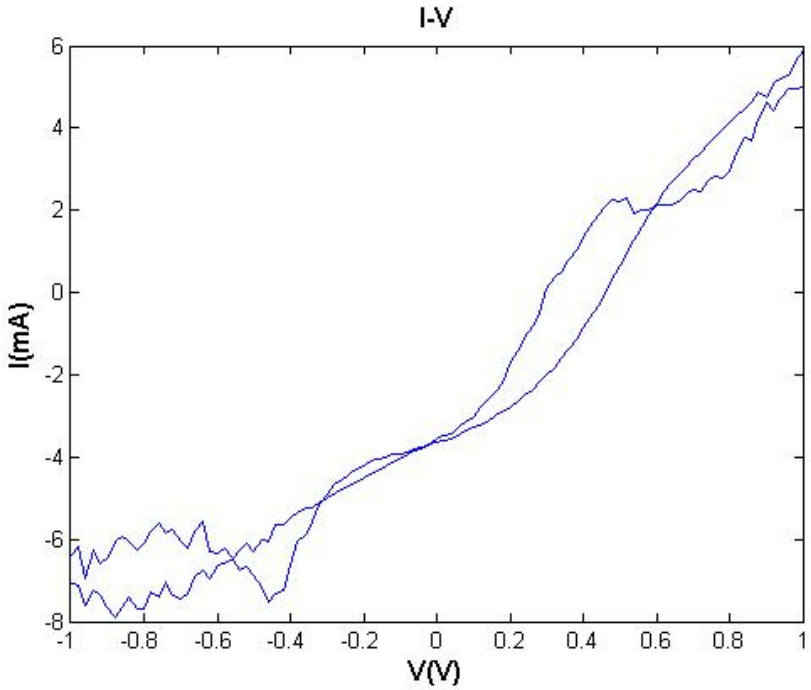

Figure 6.16: IV characteristics after 1-ms pulse switching

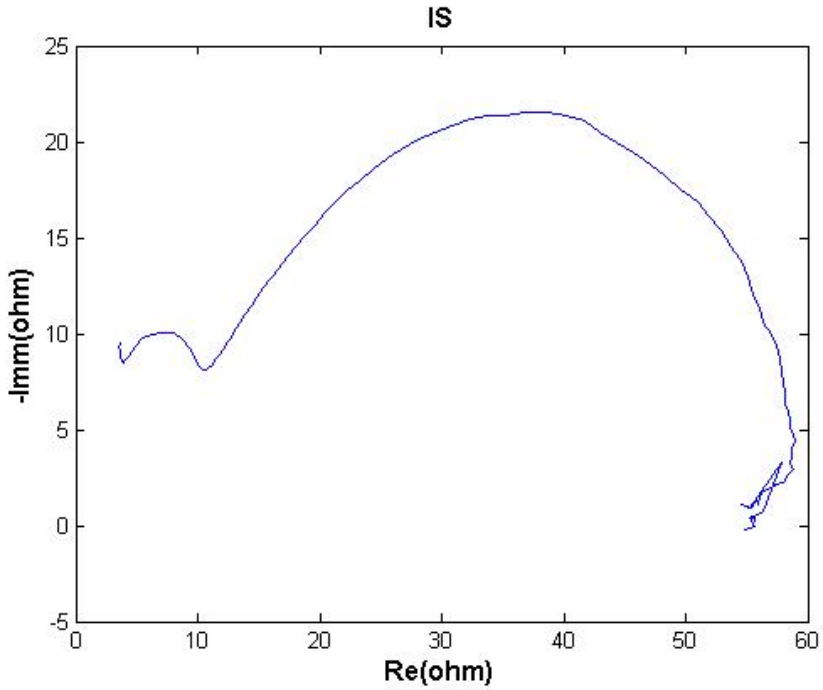

Figure 6.17: IS curves after 1-ms pulse switching

From these results, we conclude that:

- 100-ms pulse allows cells activation, but the pulse is too long and part of the current can flow through polymeric blend, damaging the organic materials.
- 50-ms pulse allows to activate the cells, but the current does not flow through polymers and thus the cells present similar characteristic with no degradation after switching.
- 1-ms pulse is too short to destroy all silver path and thus the cell present large hysteresis and low V_{OC} (low shunt resistance).

It is worth to remark that in most cases simple IV curves does not show appreciable and clear variations after activation with different conditions. However, by means of IS we see that the pulse length has a crucial role for reproducibility of the cell characteristics.

6.2 Interface Identification

6.2.1 Initial Characterization

The second set of samples we received was composed by two different type of cells:

- Cells realized on the flextrode substrate
- Cells realized on a silver substrate with a manual coat of the ZnO layer

We did a complete characterization of all the cell received using a solar simulator with a power density of 1 SUN.
Here i have omitted all the result about not working cells.

Cells with Flextrode Substrate

The cells realized on the flextrode substrate had three different thickness of the active layer (200, 500 and 600 nm).
Table 6.18 Shows the electrical characteristics of the cells tested.

Thickness(nm)	Voc(V)	Jsc(mA)	FF(%)	η (%)
200	0.53	-3.51	50.7	0.94
500	0.52	-5.01	54.3	1.41
600	0.51	-5.07	53.1	1.37

Figure 6.18: Electrical characteristic of the cells realized on the flextrode substrate

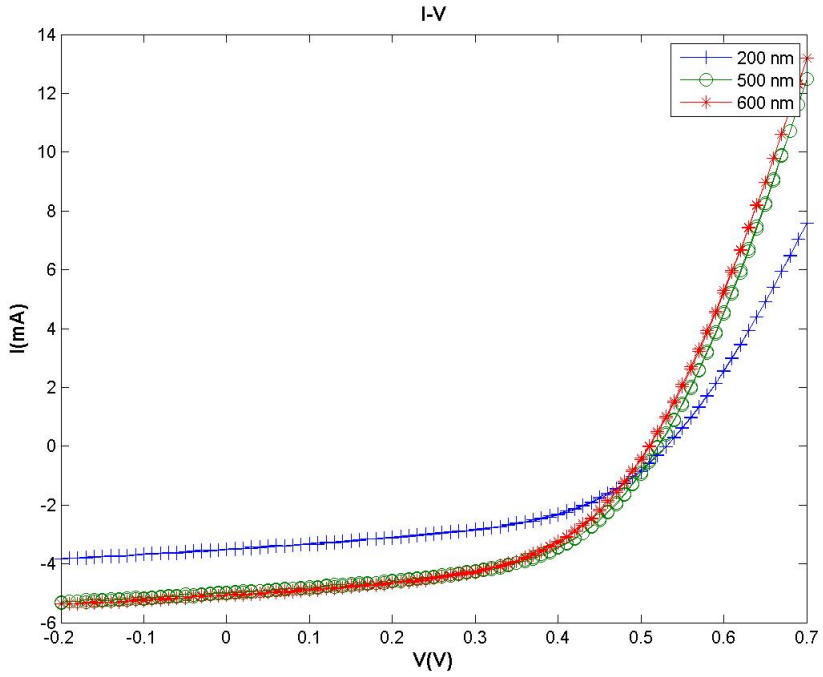

Figure 6.19: IV characteristics of the cells realized on the flextrode substrate

I-V characteristics (Figure 6.19) show a clear dependence between Jsc and thickness of the active layer. Cells with greatest thickness have a higher Jsc and this is due to increased absorption in the active layer. Cells with thickness of 500 nm and 600 nm show similar results.

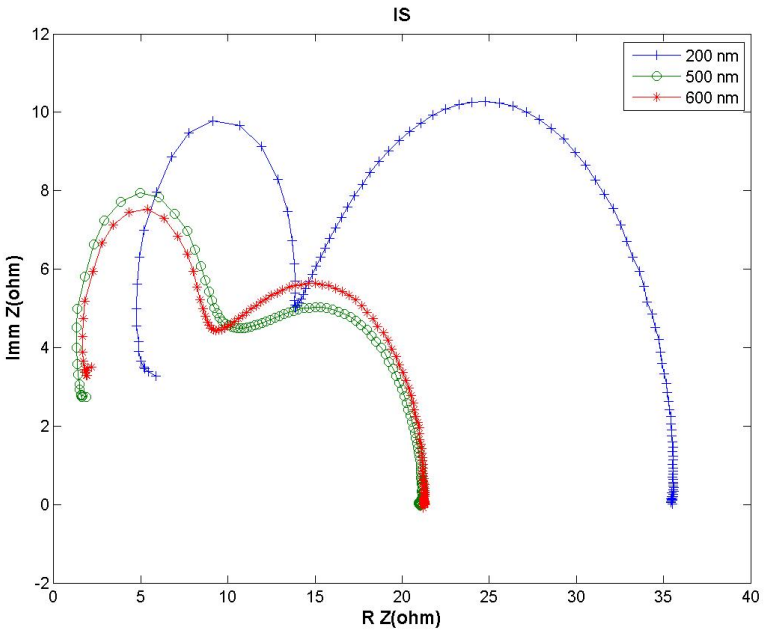

Figure 6.20: IS curves of the cells realized on the flextrode substrate

IS curves (Figure 6.20) show that the cell with 200-nm active layer has a higher resistive contribution. SCL (Space Charge Limited) model can explain this behavior:

- Greater thickness results in the generation of a greater number of excitons and therefore a greater number of carriers. This determines a decrease of the resistance in the active layer (See Figure 6.21).
- With more charge generated in the active layer the capacitance contribution increase (Figure 6.22).

From these results, it is clear that in order to obtain high efficiency an active-layer thickness of 500-600nm is the best choice.

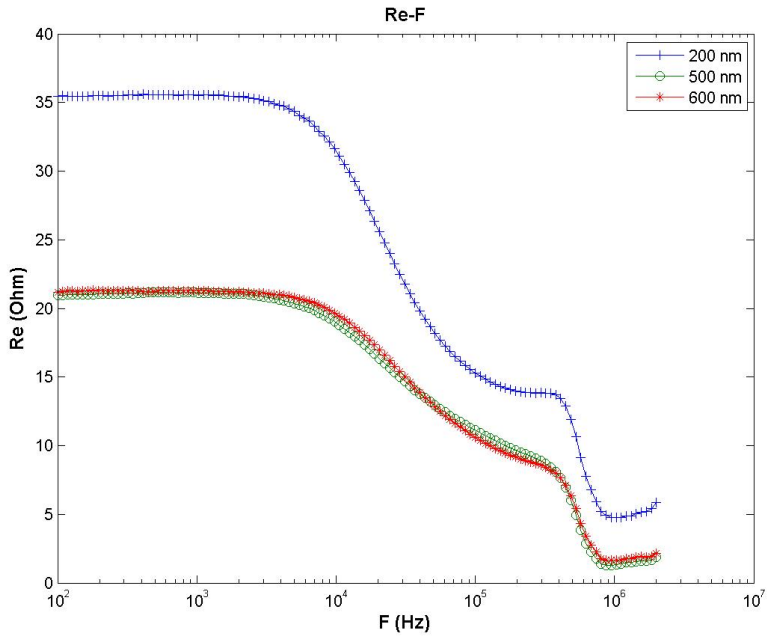

Figure 6.21: Real part characteristics of the cells realized on the flextrode substrate

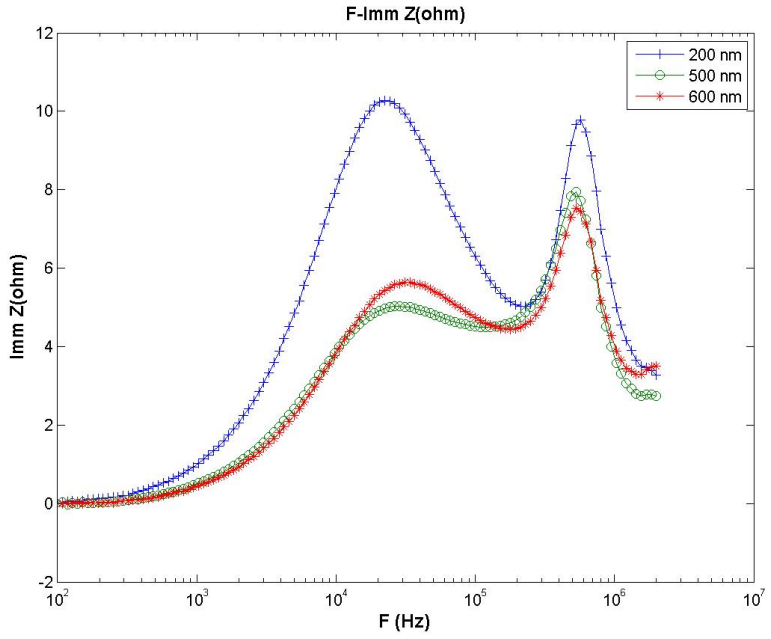

Figure 6.22: Imaginary part characteristics of the cells realized on the flextrode substrate

Cells Without Flextrode Substrate

The cells realized without the Flextrode substrate had two different thickness: 400 nm and 500 nm.
The table shows the electrical characteristic of the cell without the Flextrode substrate with a layer of 400 nm.

CELL	Voc(V)	Jsc(mA)	FF(%)	η (%)
1	0.50	-6.50	44.3	1.44
2	0.51	-6.77	51.6	1.78
4	0.52	-6.76	49.2	1.73

Figure 6.23: Electrical characteristic of the cells realized without flextrode substrate and an active layer of 400 nm

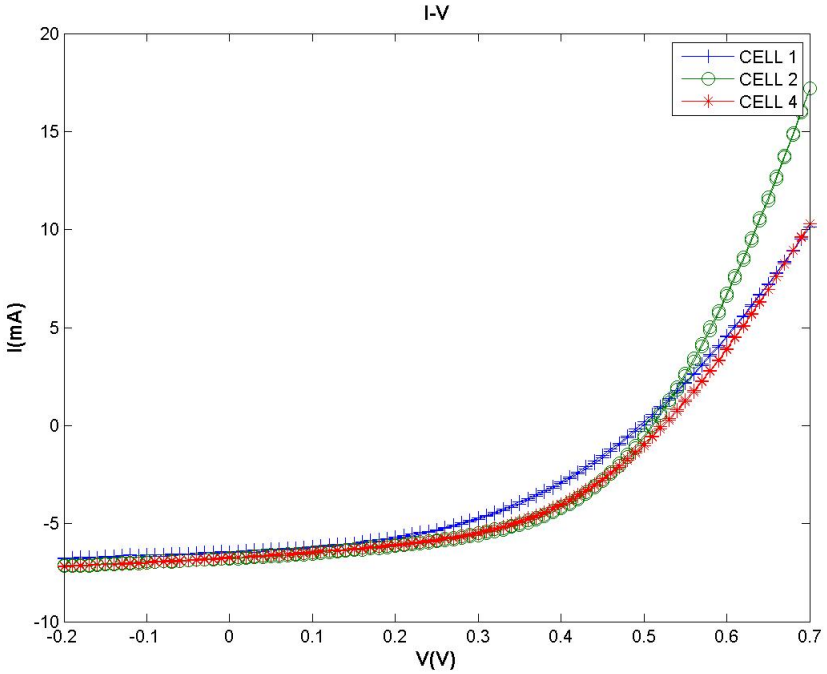

Figure 6.24: IV characteristics of the cells realized without flextrode substrate and an active layer of 400 nm

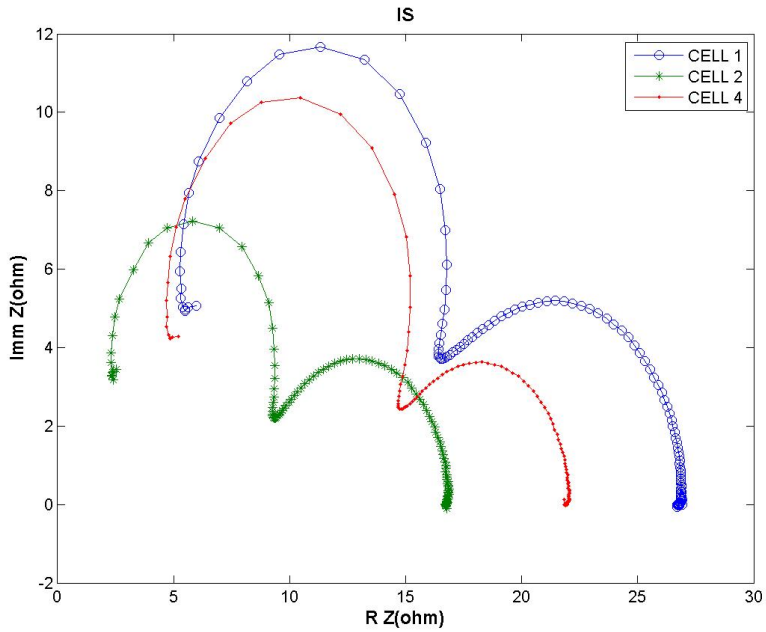

Figure 6.25: IS curves of the cells realized without flextrode substrate and an active layer of 400 nm

I-V characteristic (Figure 6.24) shows big difference between cells although they are all of the same type. Analysing IS curve (Figure 6.25) it is clear that there are no reproducibility between cell characteristics. Imaginary-part characteristics (Figure 6.27) show differences in both LF and HF peaks; also real-part characteristics (Figure 6.26) show that all the cells have a different behaviors. It is important to remark another big difference between the two types of cells (flextrode and no-flextrode cells): the substrate of the no flextrode-cells is made with silver and so it can reflect light and this can improve the absorption capability of the cells. This could be the reason of the higher Jsc of the cell. Thus, a comparison between the two types of cells is not possible. In order to explain the differences on IS curves, we have analysed some of them using an ESEM (Environmental Scanning Electron Microscope); what we found was an non-homogeneous coating of the ZnO layer that could affect both imaginary part and Real part characteristic on the impedance of the devices.

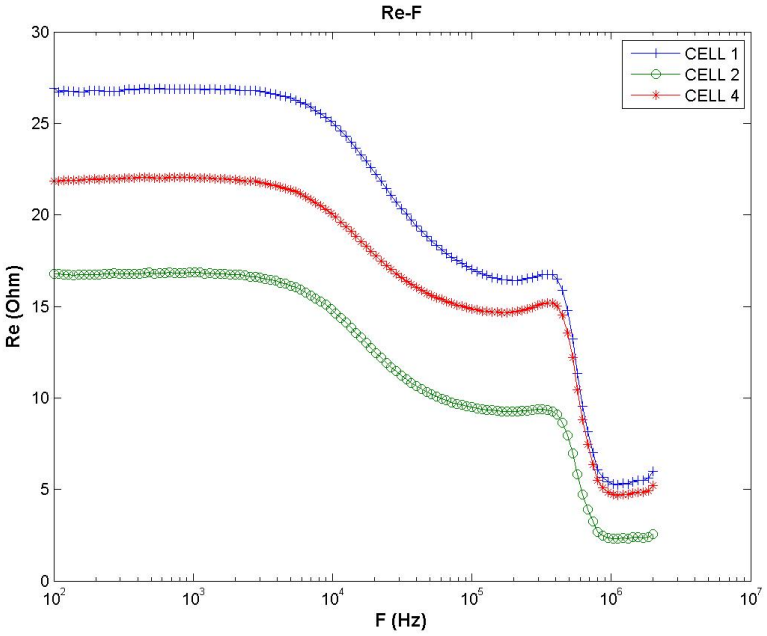

Figure 6.26: Real part characteristics of the cells realized without flextrode substrate and an active layer of 400 nm

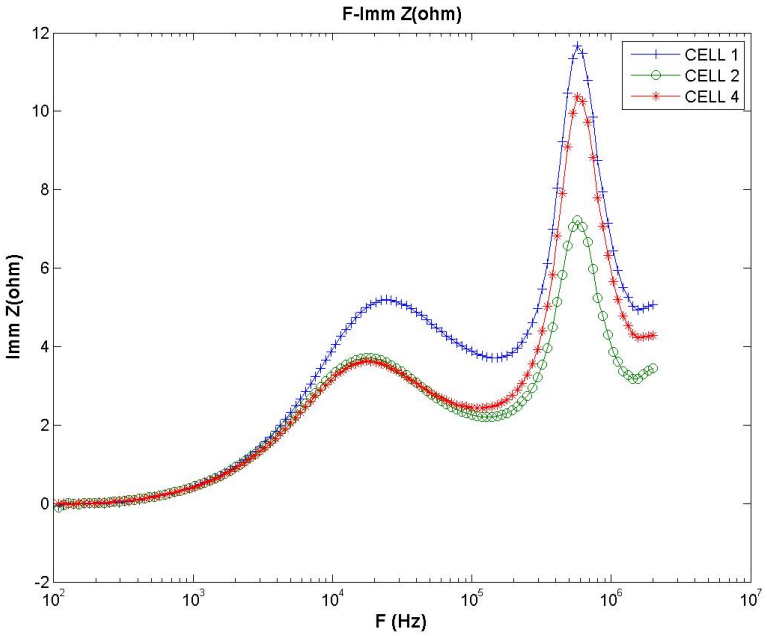

Figure 6.27: Imaginary part characteristics of the cells realized without flextrode substrate and an active layer of 400 nm

Analysing the cells realized without the flextrode substrate but with the 500-nm thickness we found another situation. The table shows the electrical characteristic of the cell without the Flextrode substrate with a layer of 500 nm.

CELL	Voc(V)	Jsc(mA)	FF(%)	η (%)
1	0.51	-6.00	49.22	1.50
2	0.49	-4.17	44.69	0.91
3	0.53	-6.11	44.50	1.44
4	0.51	-4.64	55.09	1.30
6	0.49	-4.79	49.51	1.16
7	0.51	-4.11	54.92	1.15
8	0.50	-4.41	42.39	0.93

Figure 6.28: Electrical characteristic of the cells realized without flextrode substrate and an active layer of 500 nm

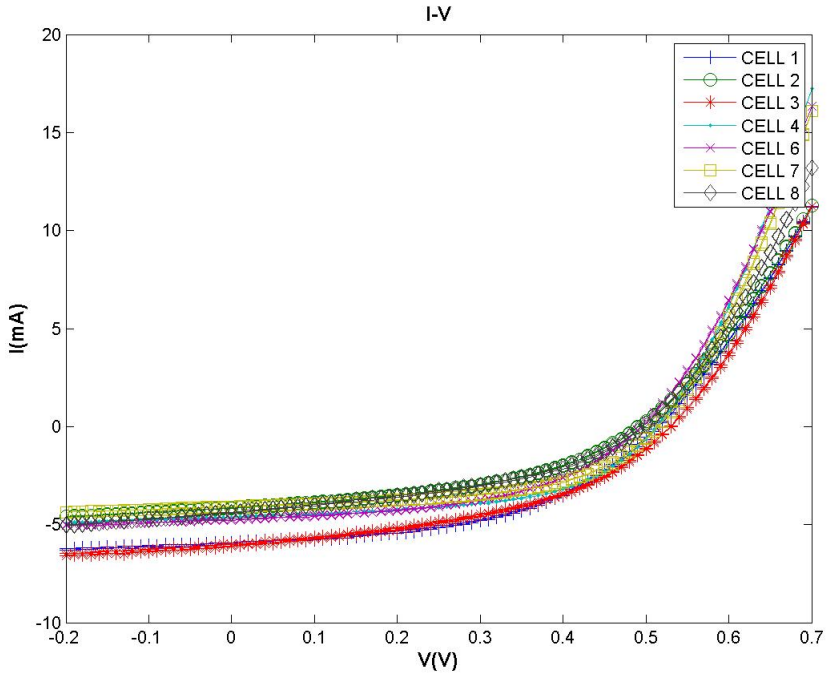

Figure 6.29: IV characteristics of the cells realized without flextrode substrate and an active layer of 500 nm

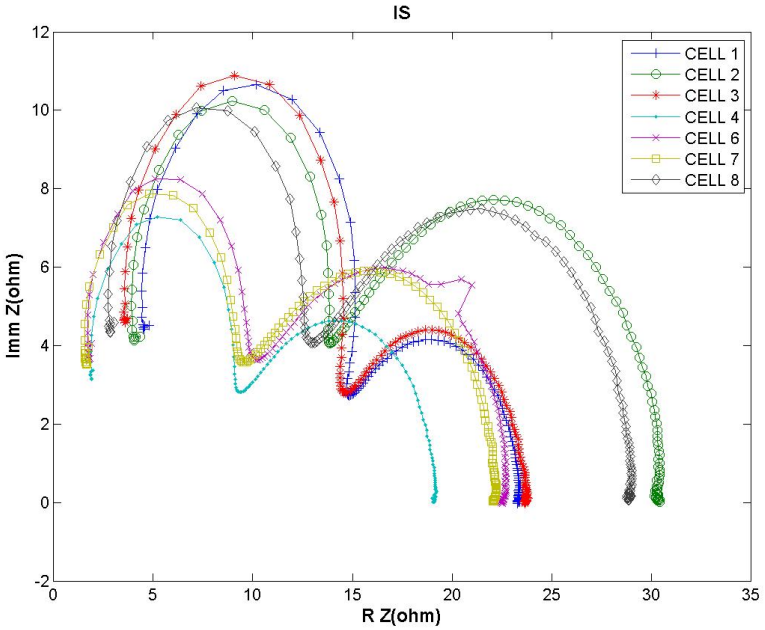

Figure 6.30: IS curves of the cells realized without flextrode substrate and an active layer of 500 nm

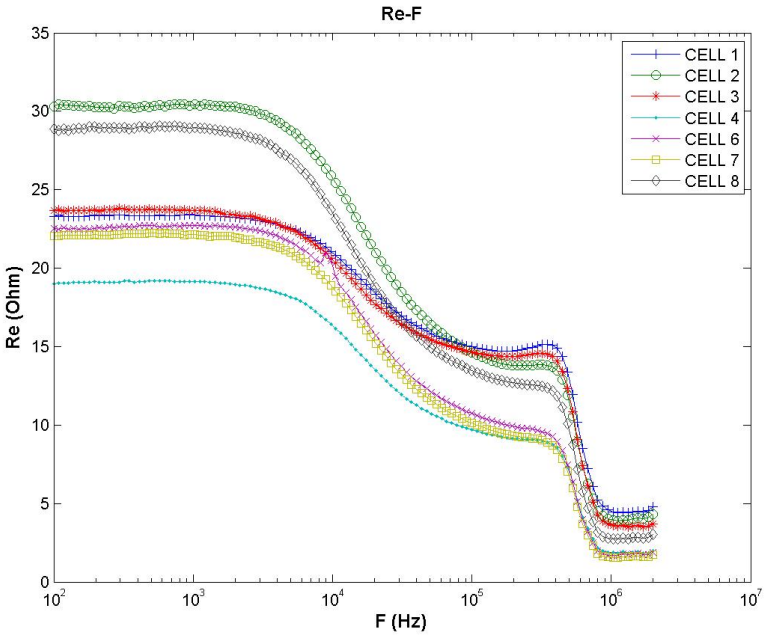

Figure 6.31: Real part characteristics of the cells realized without flextrode substrate and an active layer of 500 nm

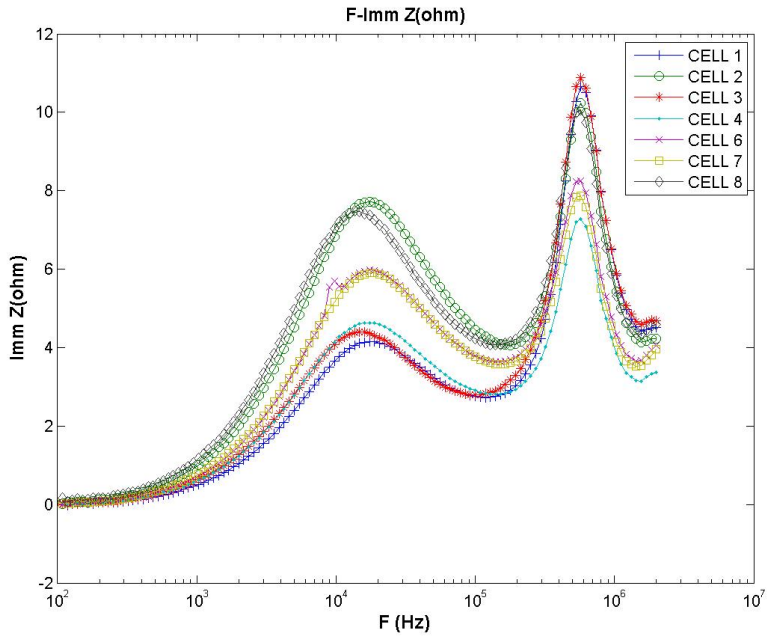

Figure 6.32: Imaginary part characteristics of the cells realized without flextrode substrate and an active layer of 500 nm

For these cells the IV characteristics (Figure 6.29) don't shown big differences but looking at IS curves (Figure 6.30) it's clear that there are no reproducibility on this type of devices.

External Quantum Efficiency Test

We did some preliminary also to evaluate the absorption of the two different types of cells.
The Flextrode and No-Flextrode cells was indeed illuminated on two different sides

- Flextrode Cells are illuminated on flextrode-substrate side
- No-Flextrode cells are illuminated on PEDOT:PSS side (due to the presence of the silver substrate that is not transparent)

We basically aim to verify how the different illumination condition affect the absorption spectrum of the devices.
We made all the analysis with the *Solar Cell Analysis system LOANA* by PV-tools (Figure)

Figure 6.33: Solar Cell Analysis system LOANA

Figure 6.34 and 6.35 show the EQE results of the two types of cells.

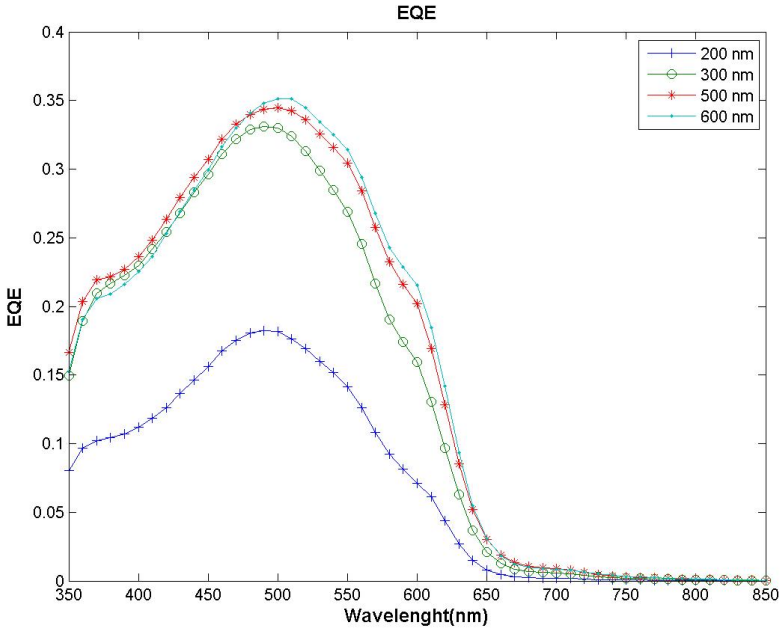

Figure 6.34: EQE of Flextrode cells

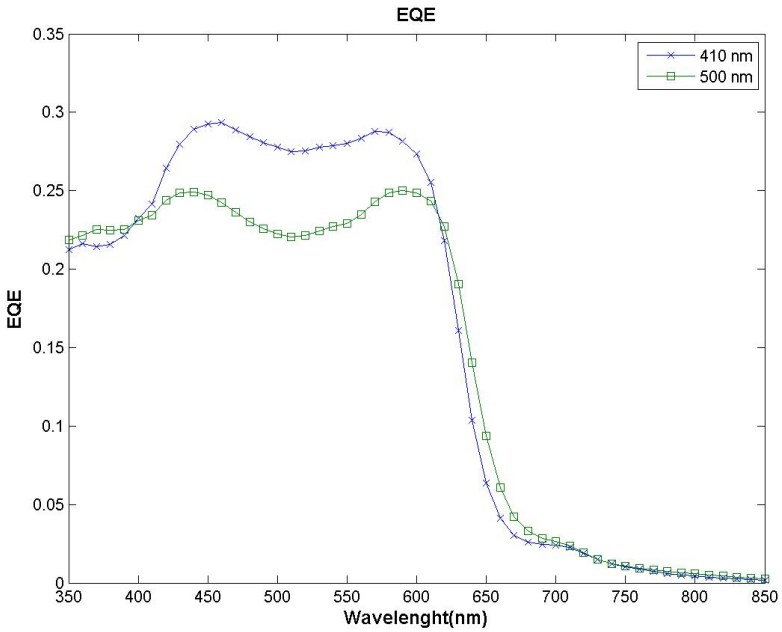

Figure 6.35: EQE of No-Flextrode cells

EQEs of Flextrode cells (Figure 6.34) show a clear trend: greater thickness means greater absorption and it was the hypothesis we have done to explain the increase of the Jsc current on cell with greater thickness. EQEs of No-Flextrode cells (Figure 6.35) show an opposite result: the cell with the greatest thickness is the cell with the lowest absorption. This result is completely discordant with that we have obtained on flextrode cell. An explanation for this behaviour is that we illuminate this type of cells from the PEDOT:PSS side, the hole transport layer. The P3HT Absorb the light in the first molecular layer and generate the charge, but it is not a good electron transport material and thus the charge recombine really fast without reaching the other electrode. With a thinner active layer the charge can reach the other electrode easily and this increase the cell efficiency.

Figure 6.36 show a comparison of the EQE of the same types of cells but with two different thickness:200 and 480 nm;the absorption in the thinner cell is better and also the hollow has disappeared due to an lower charge recombination in the P3HT.

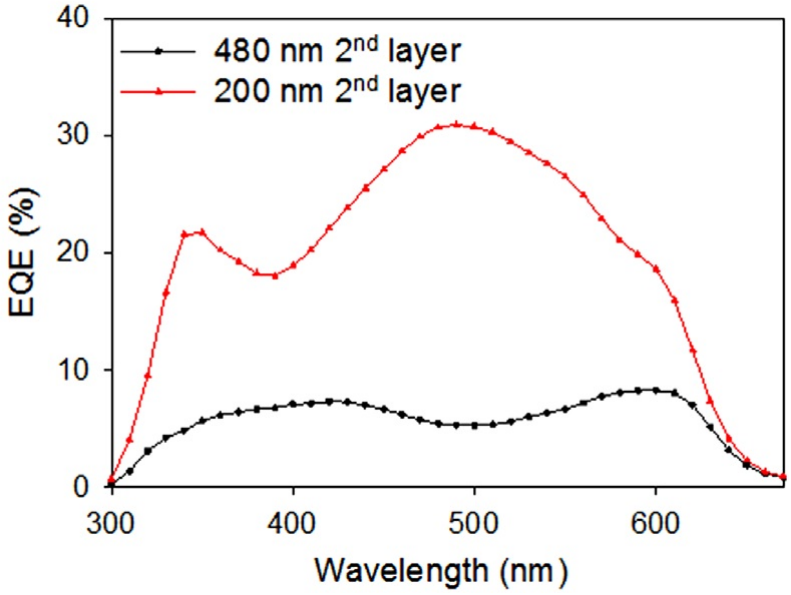

Figure 6.36: EQE on cell without flextrode with two different thickness

6.2.2 Interface Identification Tests

Figures 6.37 shows the typical curves we obtained on DTU device. In order to obtain an electrical model the solar cells we did some tests trying to identify what is the part of the solar cell responsible of each lobe. First hypothesis was that one lobe was due to the active layer (P3HT:PCBM interface) and the other to ZnO-Active-layer or PEDOT:Active-Layer interface. We start focusing on the active-layer interface doing some tests at different light intensity in order to identify variation on lobes on IS curve. For each lobe we did more tests thus i will divide them using this notation:

- Interface analysed
- Type of test

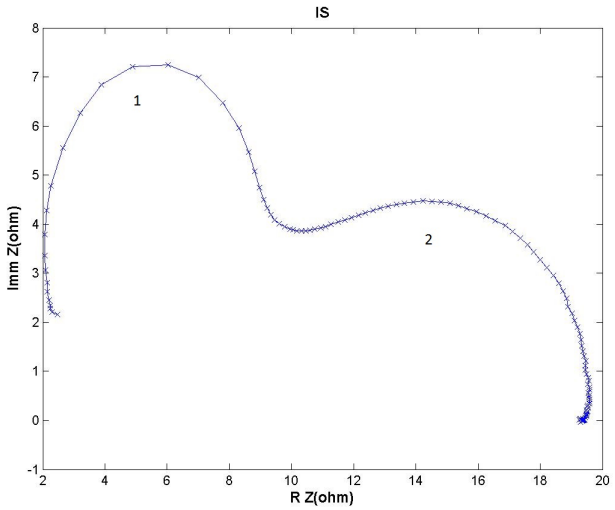

Figure 6.37: Example of IS obtained on DTU samples

Low Frequency Lobe-Light Intensity Variation

In the beginning we did some comparison between the results obtained with the Solar Simulator and a Power LED.
The LED allows to adjust easily the light intensity but affects the resistivity of the ZnO layer because it doesn't produce UV-radiation.
We started using the Solar Simulator obtaining a reference Jsc with a light intensity of 1 SUN. Then we illuminated the cells with the Power LED,

increasing the LED Current in order to reach the same Jsc obtained with the Solar Simulator.

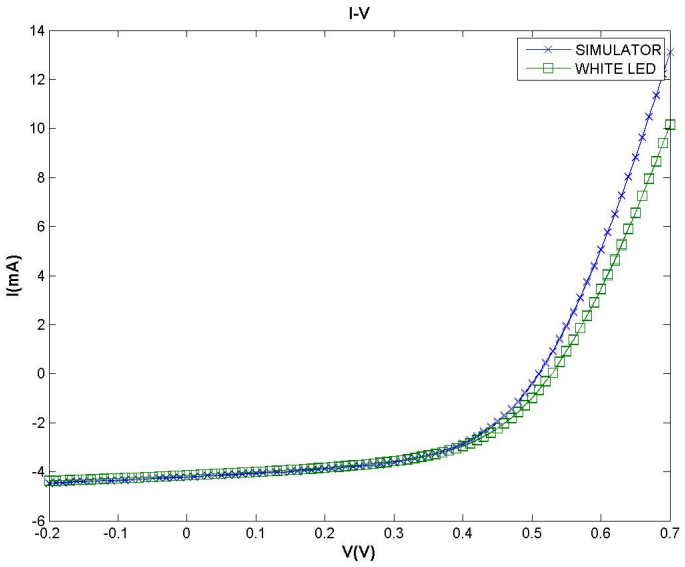

Figure 6.38: Comparison of the IV-Characteristics $Jsc = -4.2mA$

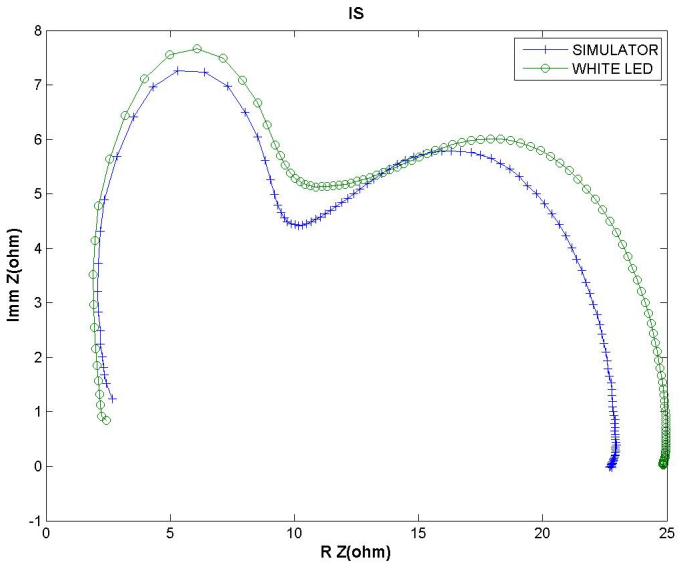

Figure 6.39: Comparison of the IS curves

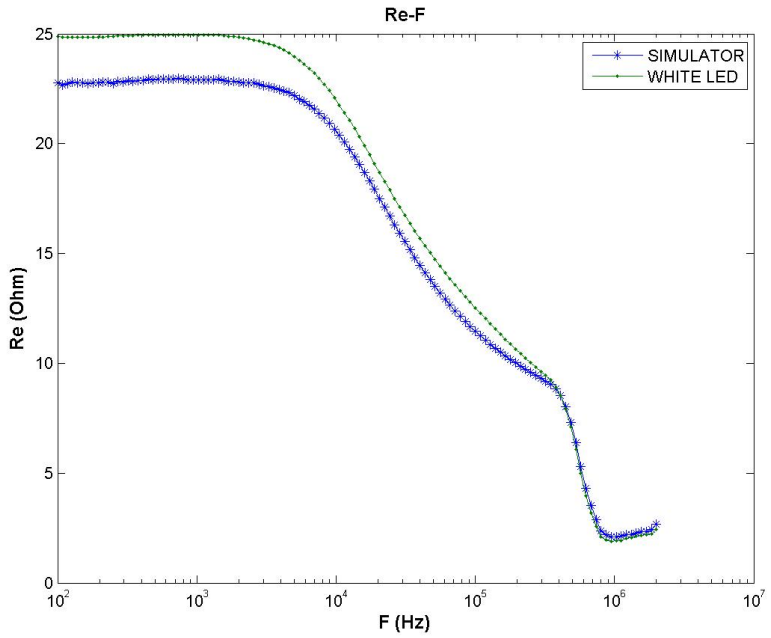

Figure 6.40: Comparison of the Imaginary part characteristics

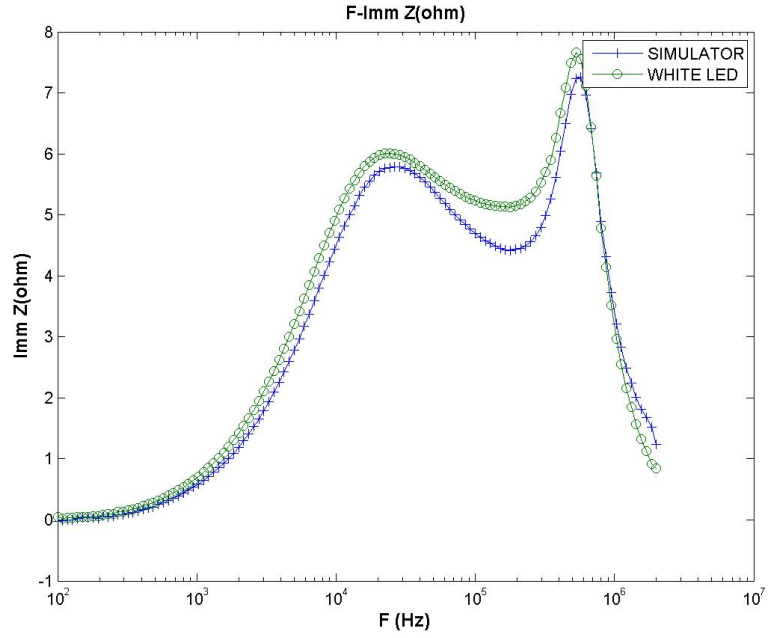

Figure 6.41: Comparison of the Real part characteristics

I-V characteristic shows that we have obtained the same Jsc in both situations.

On the one hand when illuminated with the SUN simulator the cell has a lower Voc (0.51 V) than when illuminated with the white LED (0.53 V); on the other hand when illuminated with the SUN simulator the cell has a higher FF (55.3%) than when illuminated with the white LED (54.2%). This can be due to the fact that the cell contains ZnO that can absorb UV radiation; using SUN simulator ZnO decrease its resistance due to the generation of carriers (ZnO can be modeled using SCL condition) and the effect is a decrease in the Series-resistance of the cell (Figure 6.40).

Variations on HF lobe may be due to the injection of charge from the Active Layer. All IS characteristics are made with a value of the DC polarization equal to the V_{OC} of the cell, measured for every current variation (this is important due to the fact that in this way the cell is always in the same work condition).

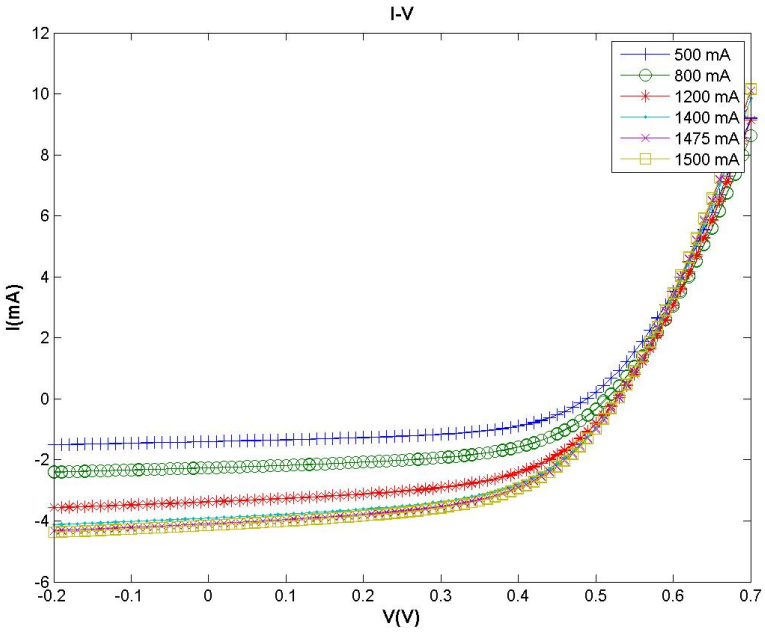

Figure 6.42: IV Characteristics with LED source

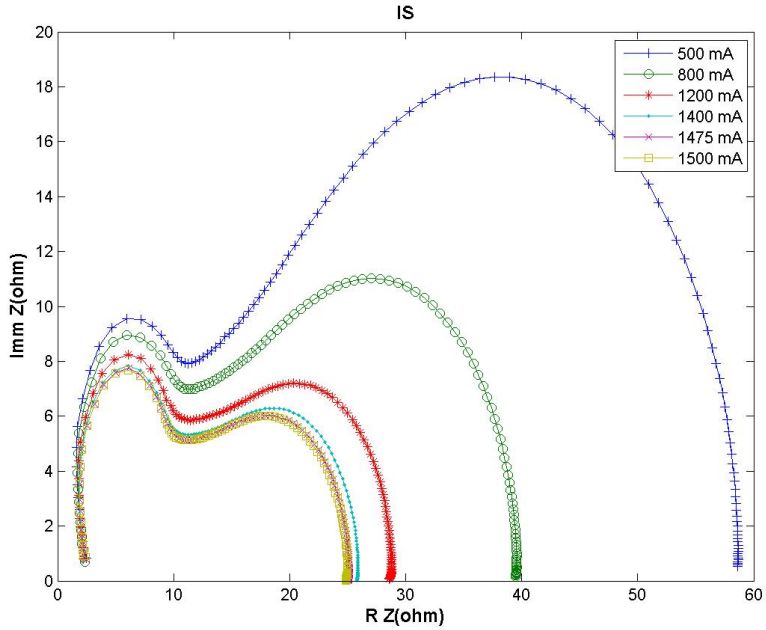

Figure 6.43: IS curves with LED source

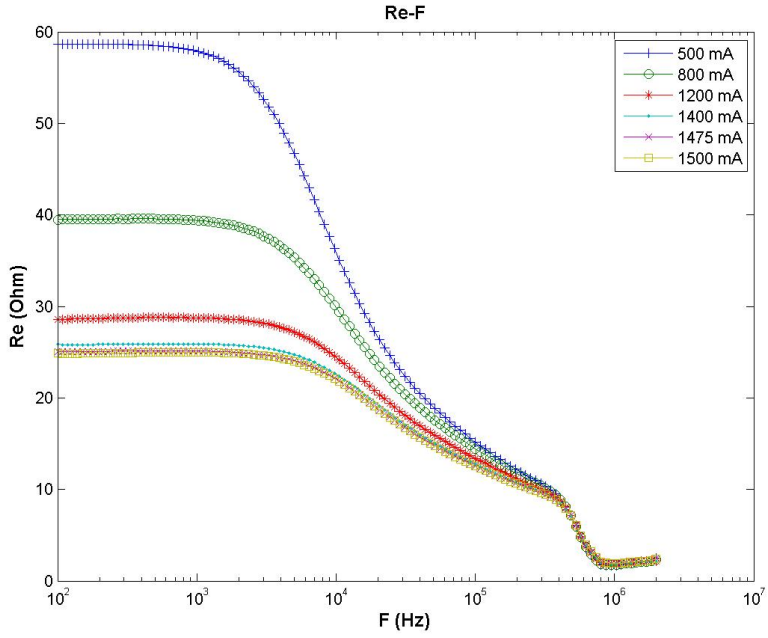

Figure 6.44: Real part characteristics with LED source

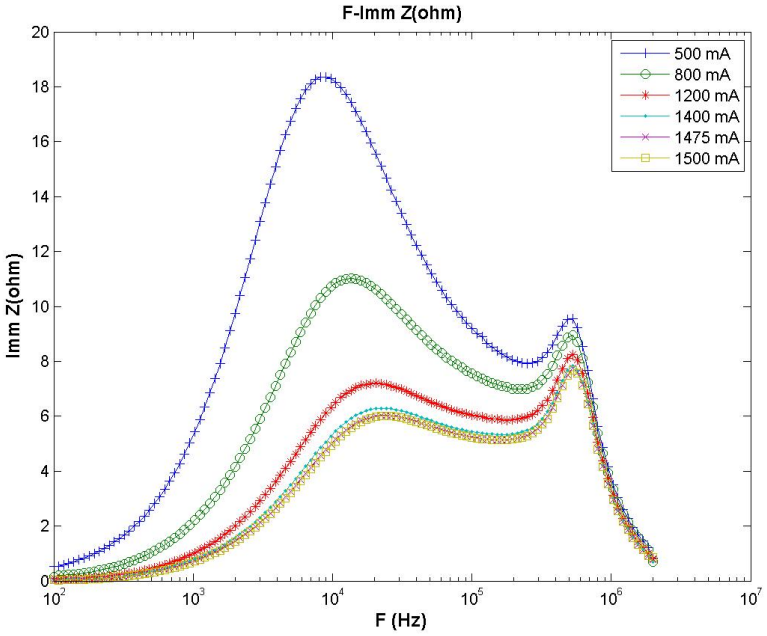

Figure 6.45: Imaginary part characteristics with LED source

IS curve (Figure 6.43) shows variations both in high and low frequency, but low frequency variations are dominants. Imaginary-part characteristics (Figure 6.45) show variations on both HF and LF lobe peak due to the carriers photo-generated in the active layer; the Variations on HF lobe may be due to the injection of charge from the Active Layer. Real-part characteristics (Figure 6.44) show a decrease of the resistance at low frequency and this can be explained using SCL model (high number of carrier induce a decrease on film resistance). This test confirm that the LF lobe is due to the active layer interface (P3HT:PCBM).

Low Frequency Lobe-Degradation

Another way to prove that the low frequency lobe is due to an organic material is to evaluate the IS curves after some degradation of the cells.
We performed D3 L2 and L3 tests (see Figure).
We monitored the efficiency of the cells during the tests; as the cells reached the 50% of the initially efficiency tests was stopped. Table 6.1 shows the parameter for the test performed.

TEST ID	LIGHT SOURCE	TEMPERATURE	HUMIDITY
D1	NO	ENVIRONMENTAL	ENVIRONMENTAL
D2	NO	65/85 °C	ENVIRONMENTAL
D3	NO	65/85 °C	85%
L2	1 SUN	65/85 °C	ENVIRONMENTAL
L3	1 SUN	ENVIRONMENTAL	50%

Table 6.1: Tests Parameters * The ambient conditions are defined as 231C-50 %RH in general, and 271C-65 %RH accepted in tropical countries according to ISO 291(2008) Plastics-Standard atmospheres for conditioning and testing

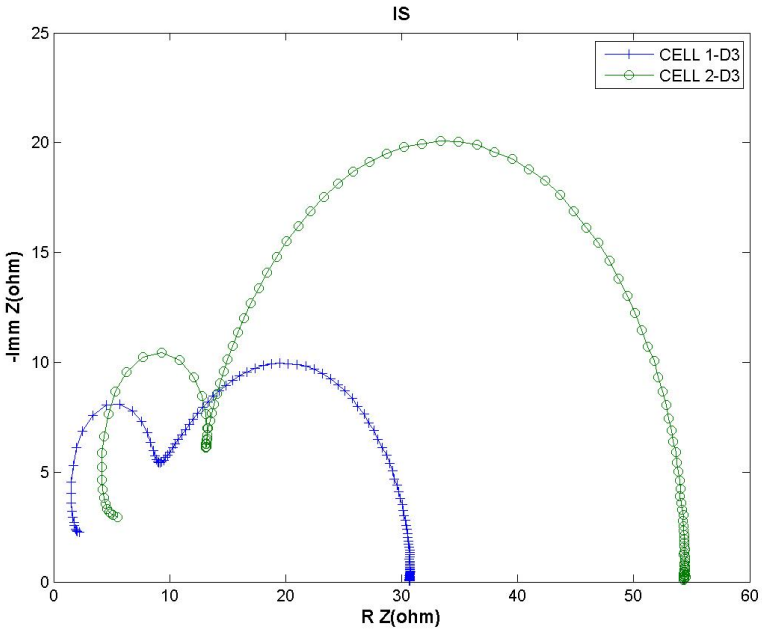

Figure 6.46: IS curves—TEST ID: D3

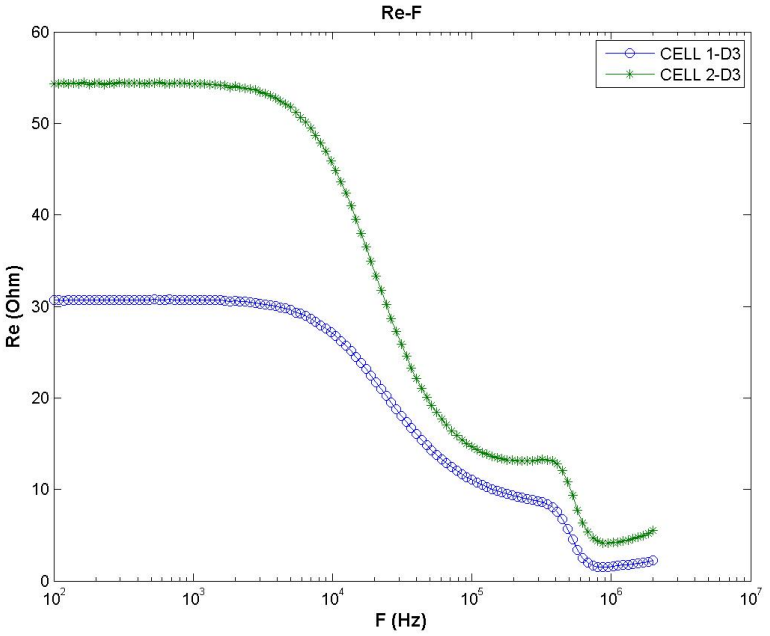

Figure 6.47: Re Z-Frequency Characteristics—TEST ID: D3

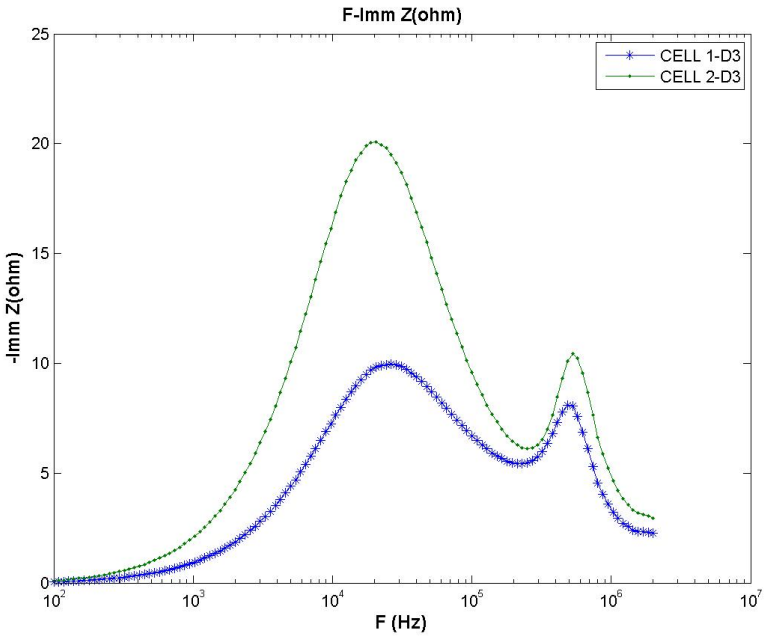

Figure 6.48: Imm Z-Frequency characteristics—TEST ID: D3

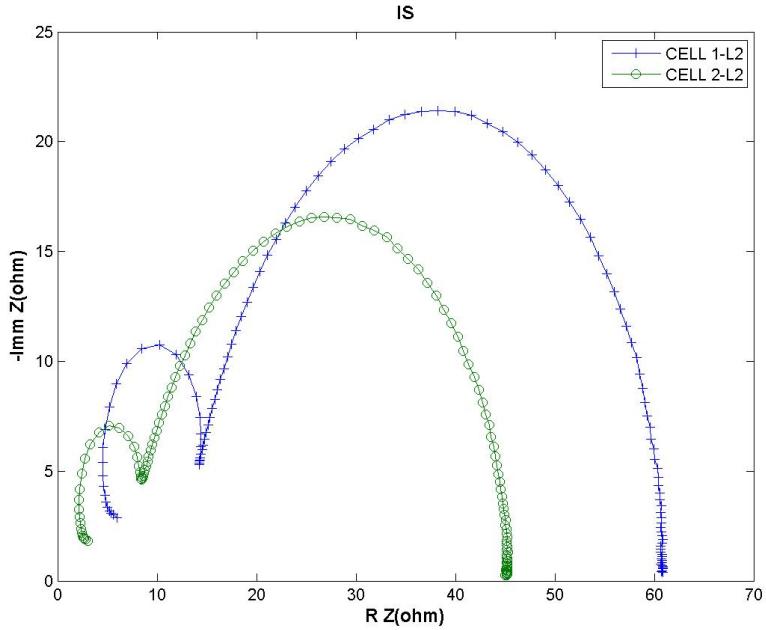

Figure 6.49: IS curves—TEST ID: L2

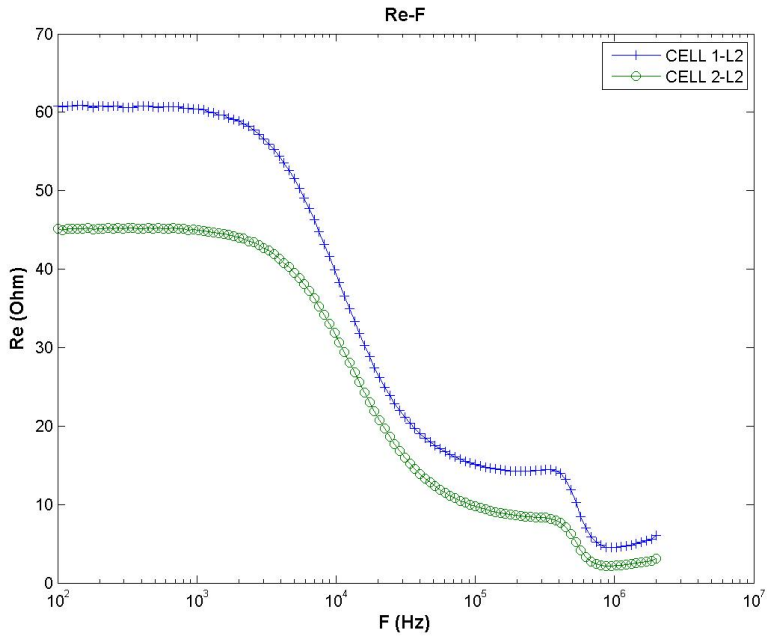

Figure 6.50: Re Z-Frequency Characteristics—TEST ID: L2

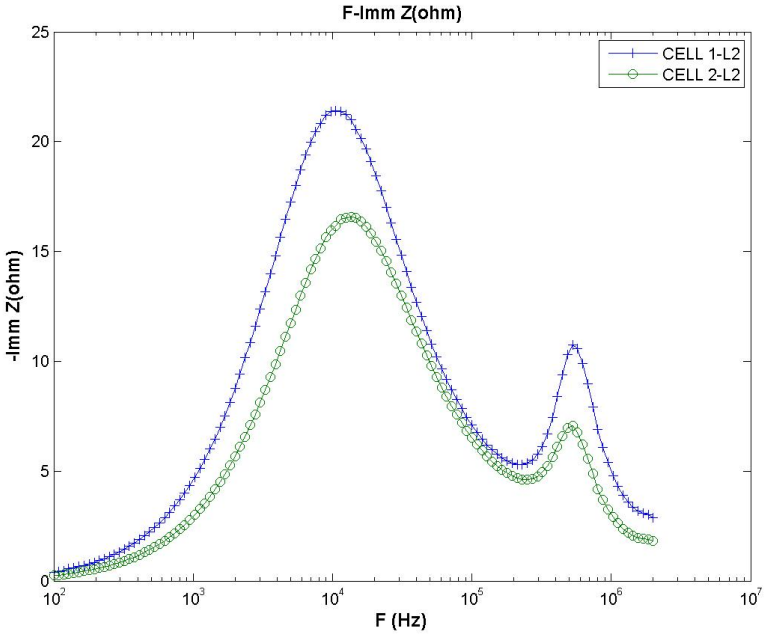

Figure 6.51: Imm Z-Frequency characteristics—TEST ID: L2

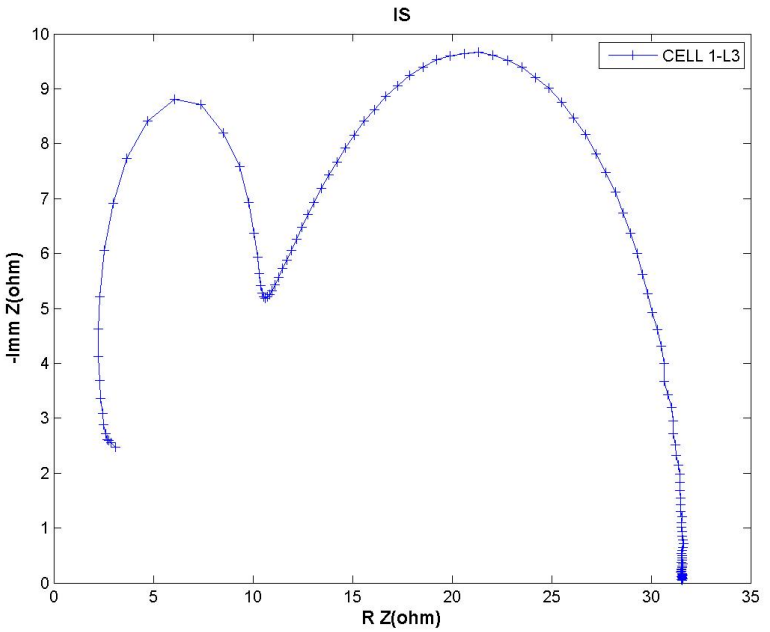

Figure 6.52: IS curves—TEST ID: L3

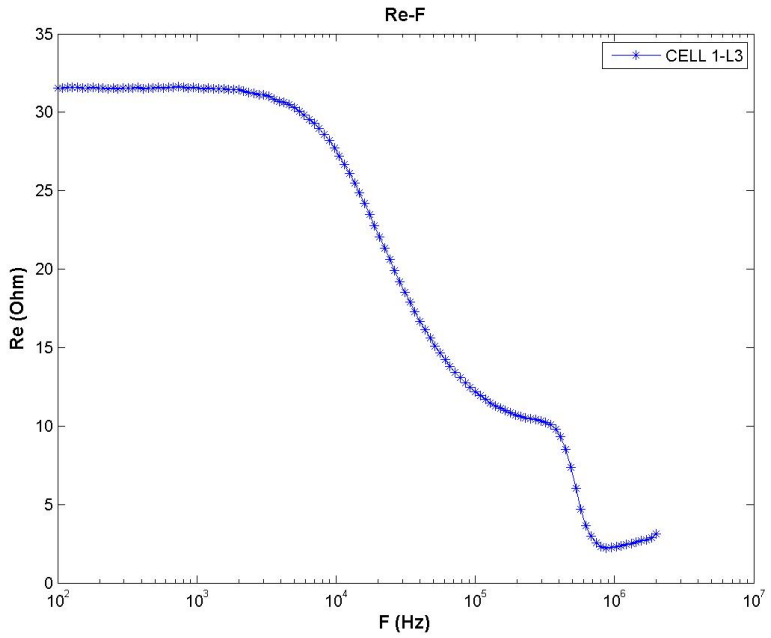

Figure 6.53: Re Z-Frequency Characteristics—TEST ID: L3

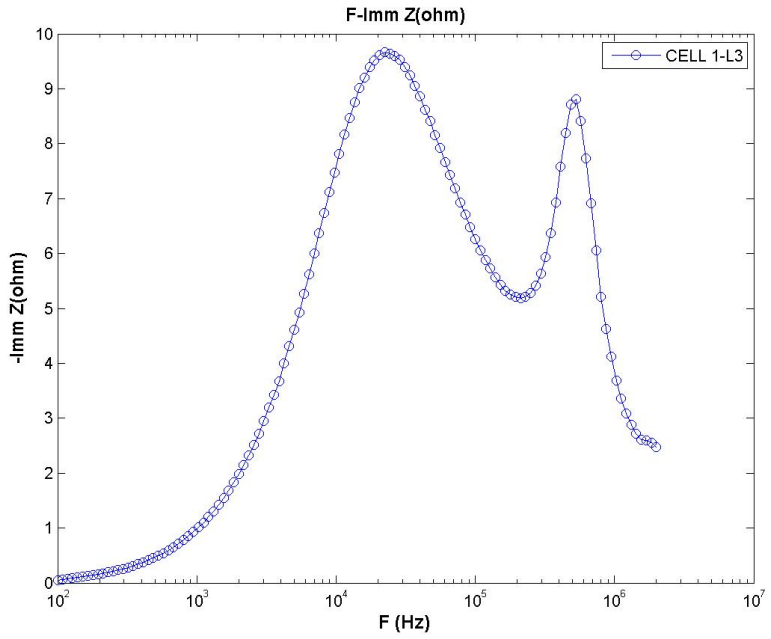

Figure 6.54: Imm Z-Frequency characteristics—TEST ID: L3

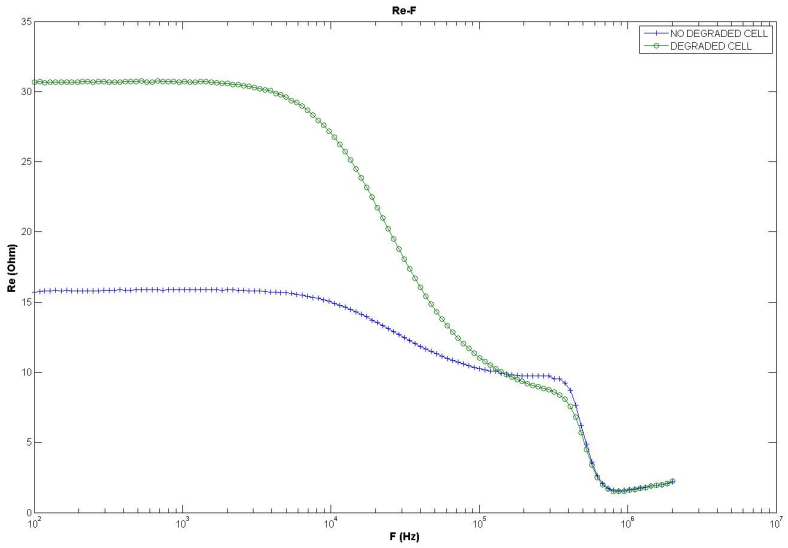

Figure 6.55: Re Z-Frequency characteristics—Comparison between degraded and no degraded cells

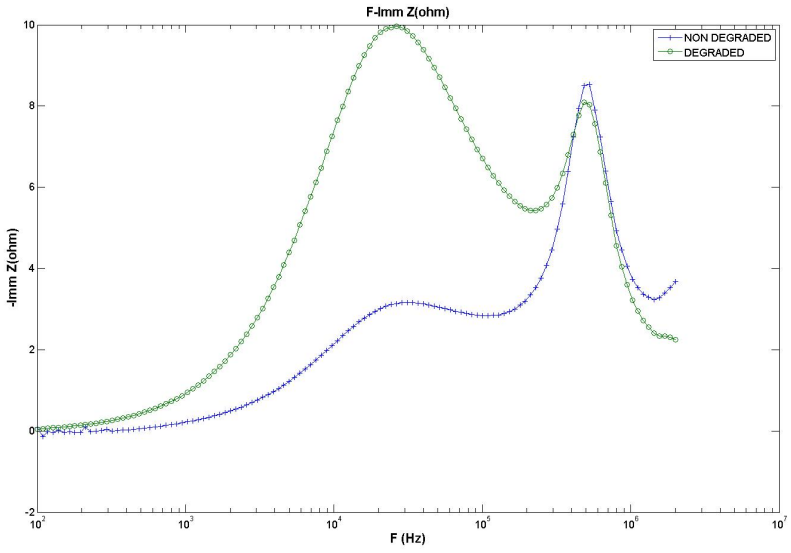

Figure 6.56: Imm Z-Frequency characteristics—Comparison between degraded and no degraded cells

IS curves show that is not possible to find a correlation between the type of degradation and the impedance spectroscopy results.
All the tested devices were not encapsulated; the fast degradation depended on many factors that have determined different degradations for each type of device (on average a cell took 5 minutes to halve its efficiency).
Imaginary-part characteristics (Figure 6.48 , 6.51 and 6.54) show that the low frequency lobe is the mostly affected from degradation of the cell; this is consistent with our hypothesis that low frequency lobe is due to the blend interface.
Figures 6.56 and 6.55 show a comparison between a degraded (cell 1, D3) and a no-degraded cell.
We have reported only one comparison but the result are representative for all tested cells.
Figure 6.56 shows that degradation affects only the low frequency lobe; this confirm that high frequency lobe is not due to PEDOT:PSS-Blend interface because it's very sensitive to humidity.
Figure 6.55 show that the degradation affects also the real part of the impedance; this is probably due to the degradation of the blend and of the PEDOT:PSS layers that could affect the resistivity of the organic material.

High Frequency Lobe-Thickness Variation

With this test we aimed to understand if the lobe on the IS is due to an interface or to a bulk effect. We prepared (during a visit to DTU laboratories) two sets of cells with different thickness of PEDOT (4-6-9 μ m) and ZnO (60-80-160 nm). Interfaces usually have a thickness of few molecular layers; the thinnest layer on our samples (both ZnO and PEDOT layer) is about 60 nm thus if our hypothesis about the interface contribution is right, we expected to see no variation on the frequency of the high frequency peak. On the other hand, if the peak comes from a bulk effect we expected to see variation in the frequency of the lobes peaks and the differences on layers thickness would also permit to establish which layer was responsible of the lobe.
We reported only the imaginary part characteristics and the real part characteristics because we were mostly interested on the frequency variation on both of them (Nyquist plot doesn't give information about frequency).

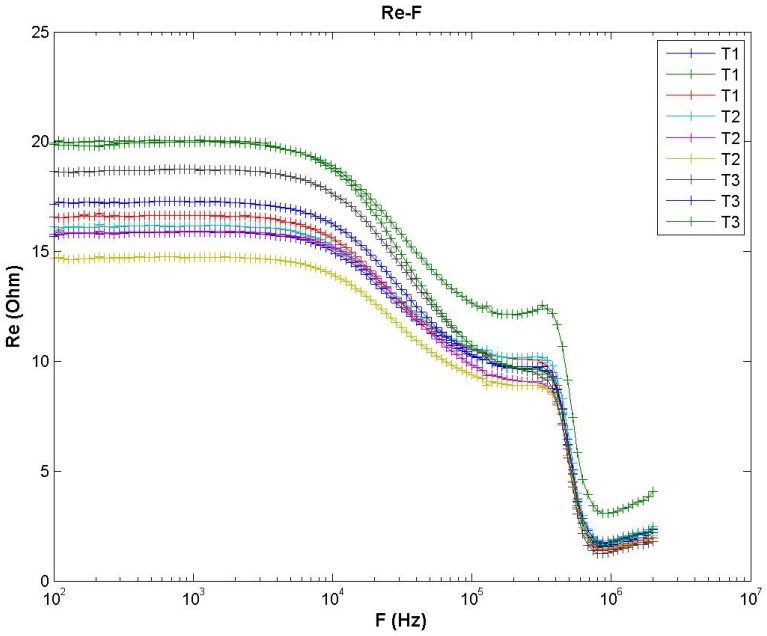

Figure 6.57: Real part characteristics- Different ZnO thickness T1=60nm T2=80nm T3=160nm

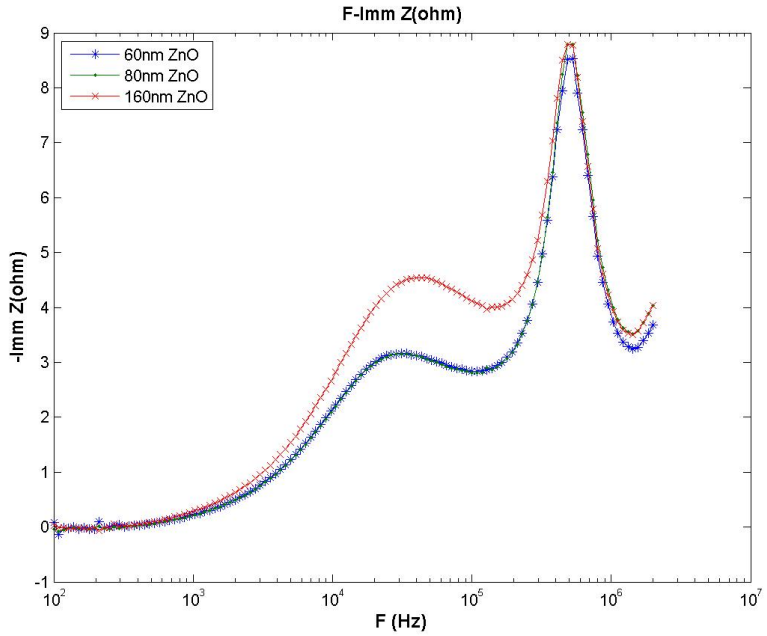

Figure 6.58: Imaginary part characteristics-Different ZnO thickness

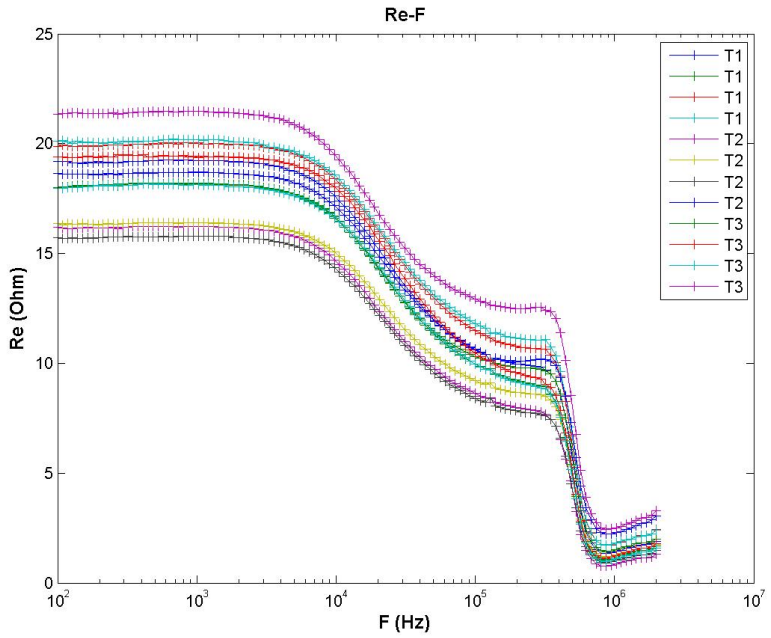

Figure 6.59: Real part characteristics- Different Pedot thickness T1=4μm T T2=6μm T3=9μm

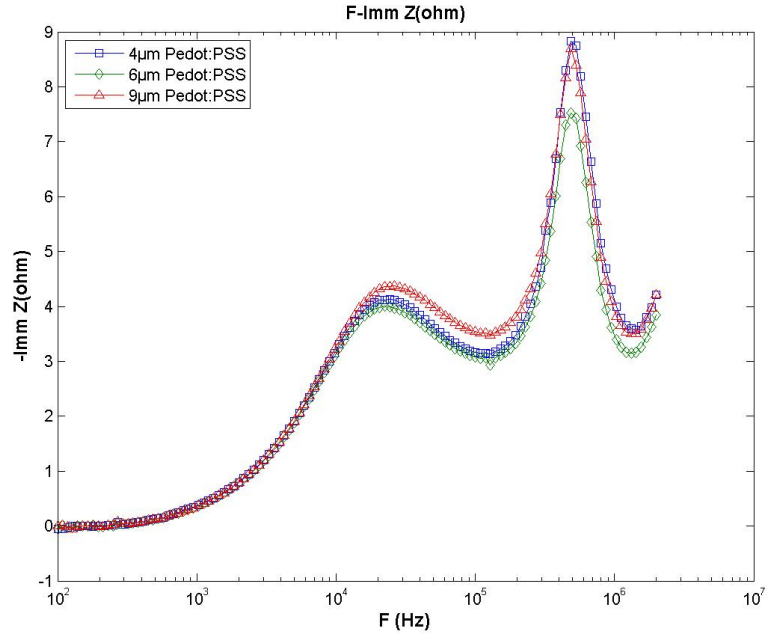

Figure 6.60: Imaginary part characteristics-Different Pedot thickness

Figures 6.58 and 6.60 show that there are no variations on the frequency of HF peak; this confirm that the phenomena we are analysing are all related to interface effects.
Figures 6.57 and 6.59 show that there is not a correlation between ZnO-layer and Pedot:PSS thickness and the DC-resistance of the cell: resistance values are equally distributed from 15 to 20 ohm This behavior could be explained considering the lateral resistance of the cell (see Figure 6.61) and the non-homogeneous distribution of the silver-fingers (see Figure 6.62).

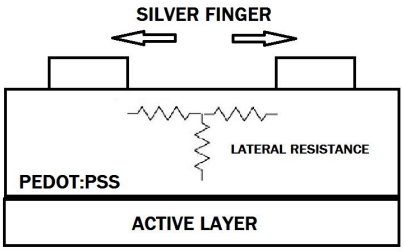

Figure 6.61: Lateral resistance model

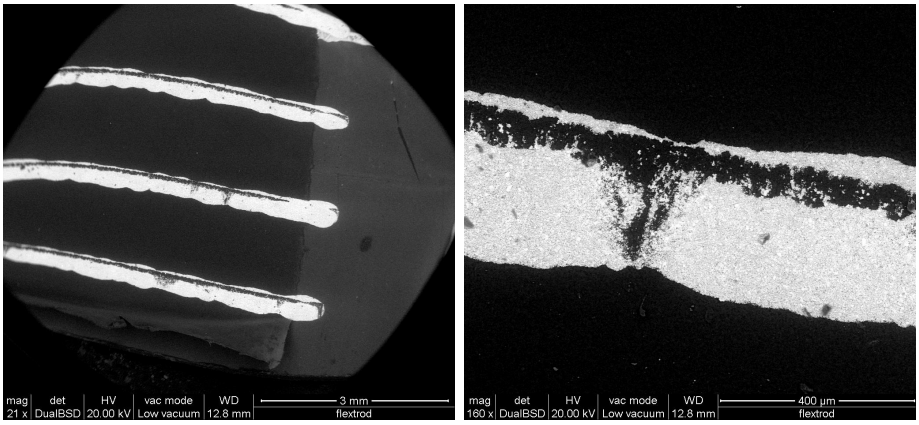

Figure 6.62: SEM image of a silver finger

SEM images shows that all silver fingers present large long-empty areas and all this area are located on the same side of the fingers (this is probably due to an issue during the coating process).
The detail of one the the fingers shows that this is almost completely divided and so the conductive path is really thin; this could explain the difference we found on the resistance measured on cells of the same type.

High Frequency Lobe-Multiple Illumination Sources

First hypothesis was that the HF lobe is due to the ZnO. In this test, we have illuminated the cell using two configuration:

- Only SUN simulator (1 SUN)
- SUN simulator (1 SUN) plus a white high-power LED

Using only the SUN simulator, we obtained a reference measure.

From the measure made with the second configuration we evaluated the variation of IS curves. If the initial hypothesis was right, we had to see two effects:

- Variation on the lobe related with the active layer: PCBM:P3HT absorb the radiation emitted by power led)
- No variation on the lobe related with the ZnO:ZnO has a high energy-gap, ∼3.3 eV, and so it can absorb near-UV radiation; the only UV-source with these configurations is the SUN simulator.

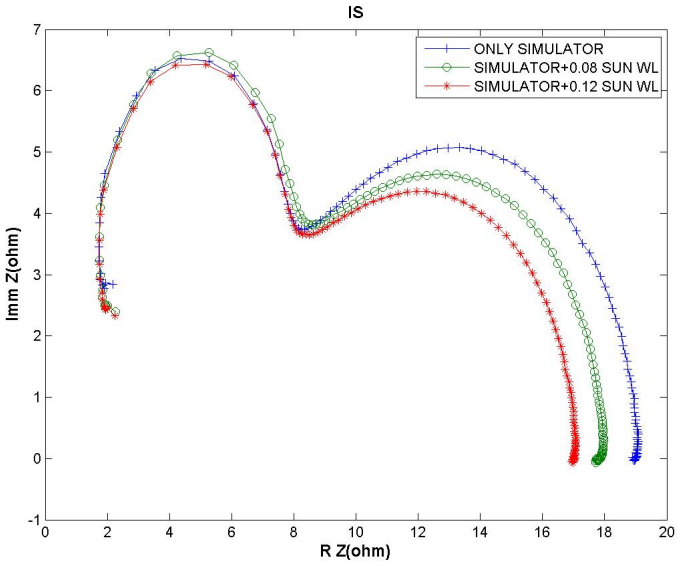

Figure 6.63: IS curve with multiple sources

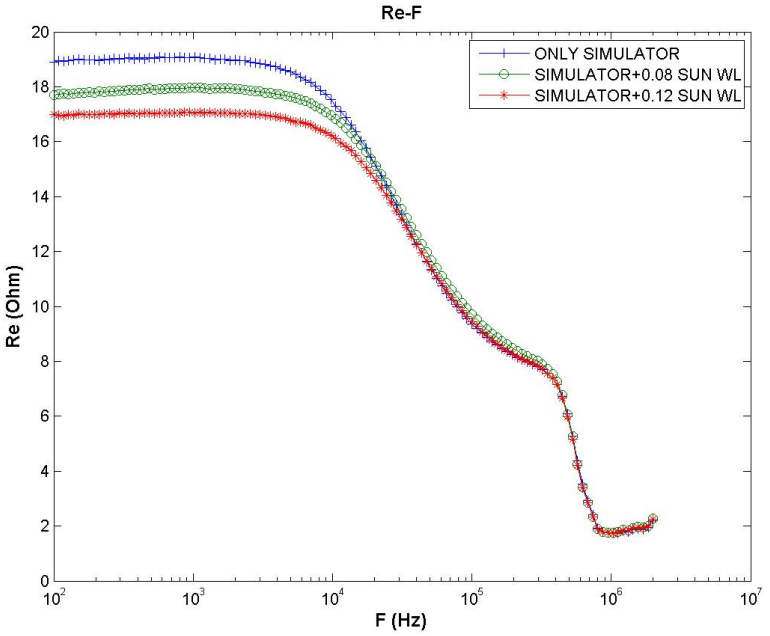

Figure 6.64: Real part characteristics with multiple sources

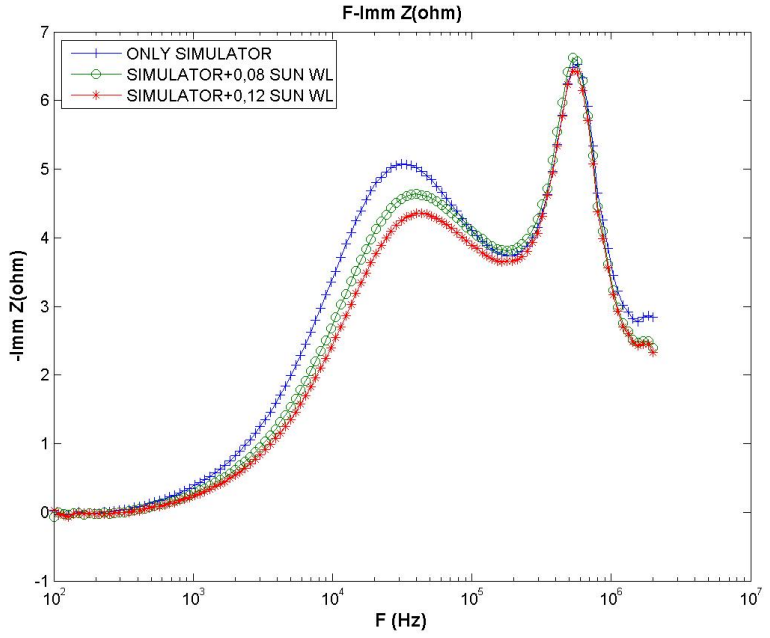

Figure 6.65: Imaginary part characteristics with multiple sources

IS-curves (Figure 6.63) show that the LF lobe varies with different illumination conditions but the HF lobe does not vary.
Also Imaginary-part characteristic (6.65) and Real-part characteristic (Figure 6.64) show variation at low frequency but no variation at high frequency. This could be due to the fact that active layer absorb radiation produced by white led and this means more carriers (lower resistance of the active layer and higher capacitive contribution how see in the previous test).
On the other hand, ZnO cannot absorb visible radiation and so there are no appreciable variation of its resistivity or capacity.
Then we did a test using only the sun simulator (Figures 6.66 and 6.67) and varying the power density: 1 SUN (reference), 0.8 SUN and 0.4 SUN.
In this condition, there are variation on both lobes. It is clear that active layer variations are dominant but Imaginary-part characteristic shows a variation also in the high frequency lobe at higher power density.
Thanks to these tests, we thought that it is possible to attribute the LF-lobe at the active-layer and the HF-lobe at the ZnO.

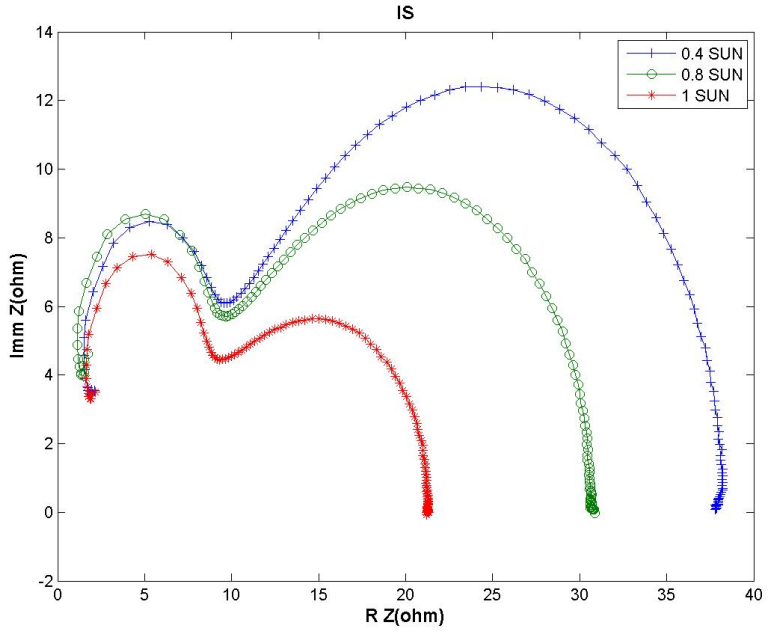

Figure 6.66: IS curve with variation on intensity of the sun simulator

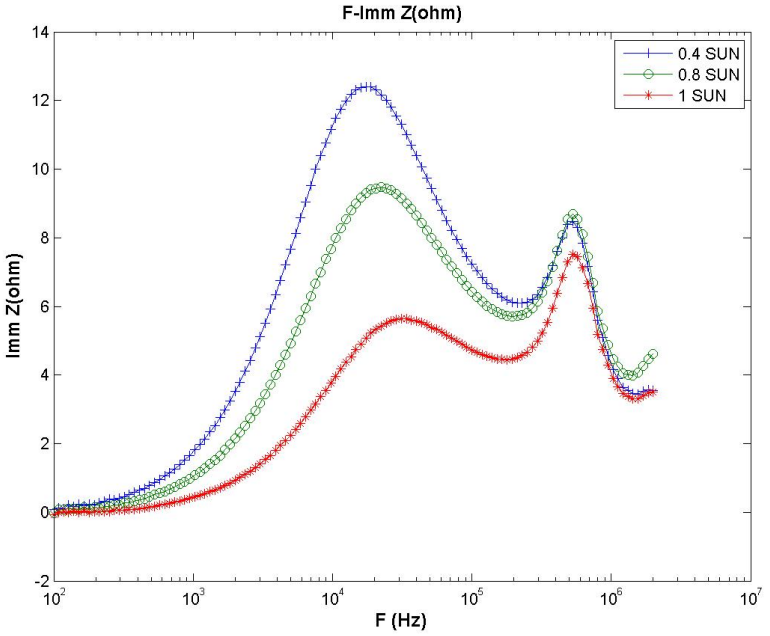

Figure 6.67: Imaginary part characteristics with variation on intensity of the sun simulator

High Frequency Lobe-Illumination from different sides

With this test we aimed to see difference on HF peak due to the difference on absorption spectrum of PEDOT and ZnO (Figure 6.68).
Test procedure:

- Illuminate the cell on ZnO side (right side) and find the Jsc of the cell
- Illuminate the cell on PEDOT:PSS side (wrong side) and adjust the light source in order to obtain the same Jsc

We repeated this test on two devices.

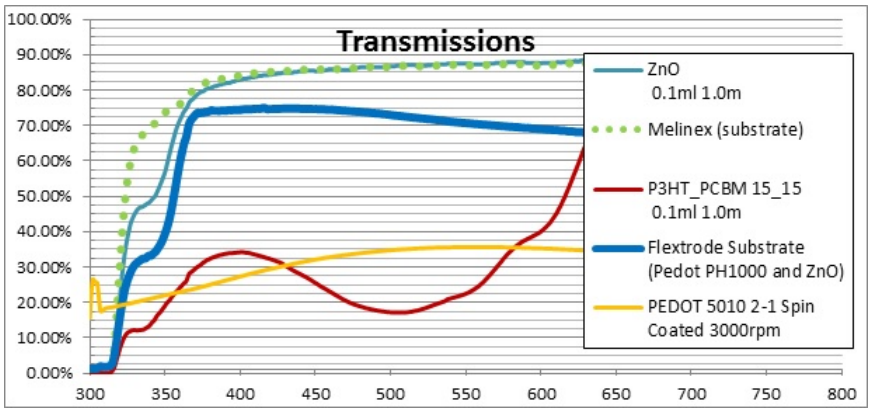

Figure 6.68: Absorption spectrum of PEDOT and ZnO

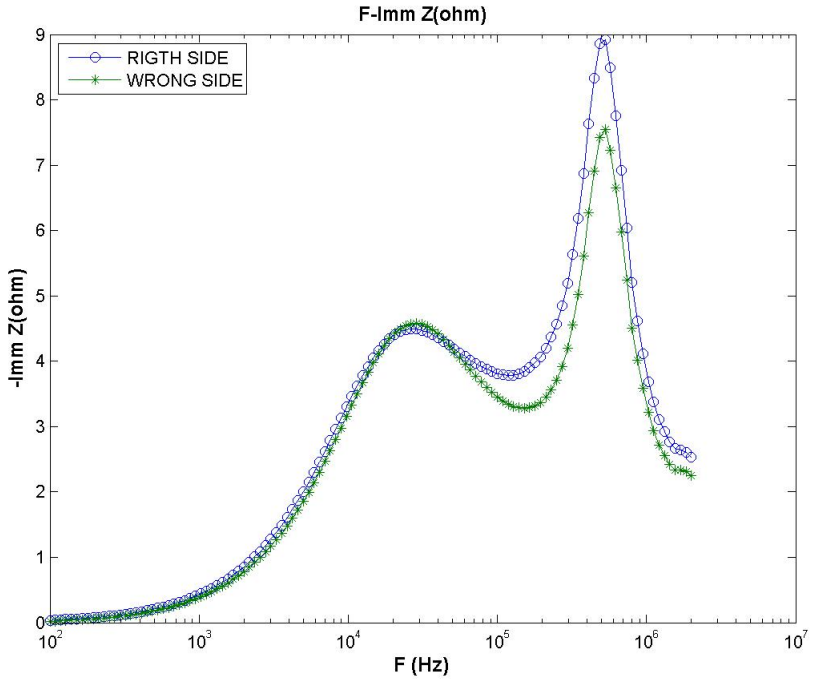

Figure 6.69: Cell illuminated on right and wrong side-Sample 1

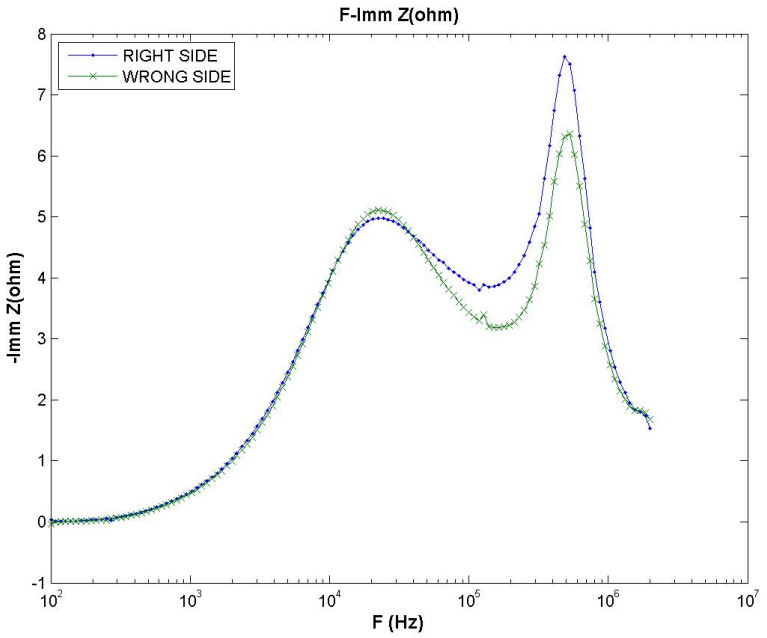

Figure 6.70: Cell illuminated on right and wrong side-Sample 2

Figures 6.69 and 6.70 show the imaginary part characteristics of the two devices.

The low frequencies peak shows that the blend interface in both illumination condition has the same absorption (this confirm again that the low frequency lobe is due to active layer). The high frequencies peak show that the interface related to this lobe has a greater absorption when illuminated on the wrong side. This result could be explained considering the absorption spectrums of PEDOT:PSS and ZnO (Figure 6.68). ZnO absorb radiation at frequencies lower than 370 nm. PEDOT:PSS absorb radiation at frequencies lower than 250-300 nm.

When the cell is illuminated on the PEDOT:PSS side the radiation that is not absorbed by PEDOT:PSS and ACTIVE layer can reach the ZnO and it is absorbed in the ZnO-Blend interfaces. When the cell is illuminated on the ZnO side the radiation with a frequencies lower than 370 nm is immediately absorbed by the ZnO (Bulk region) and not all radiation can reach the ZnO-Blend interface; this means lower absorption on ZnO-Blend interfaces how show by imaginary part characteristic (see Figure for summary picture).

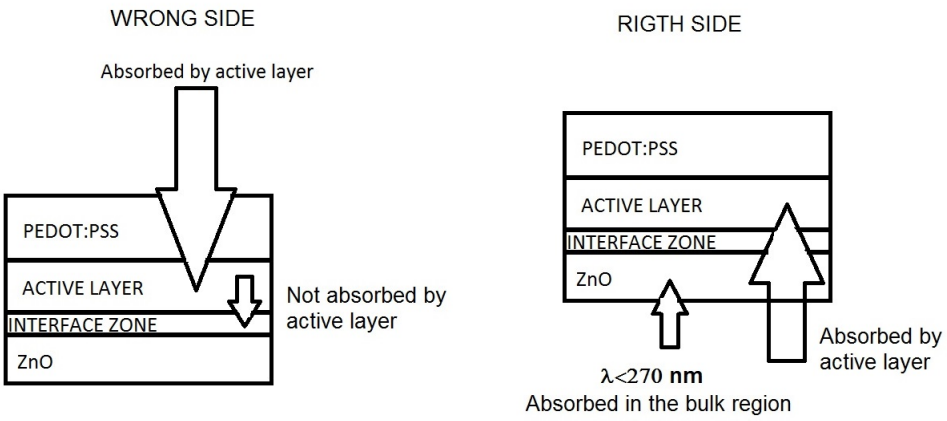

Figure 6.71: Explanation of test results

High Frequency Lobe-Switching on Encapsulated Cells

Cells are always switched before the encapsulation.
We aim to verify if it is possible to encapsulate them before switching in order to avoid the degradation effects that occur during shipping and permit us a better control of the pulse width in our laboratory.
We have applied a pulse of 50 ms of length and an amplitude of 20 V like explain in the previous section.

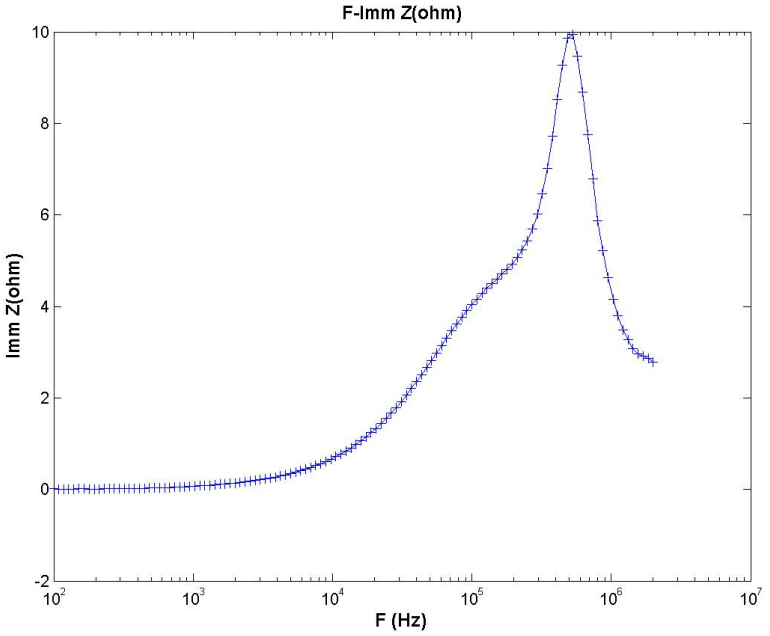

Figure 6.72: Imaginary part characteristics after switching on encapsulated cell-Sample 1

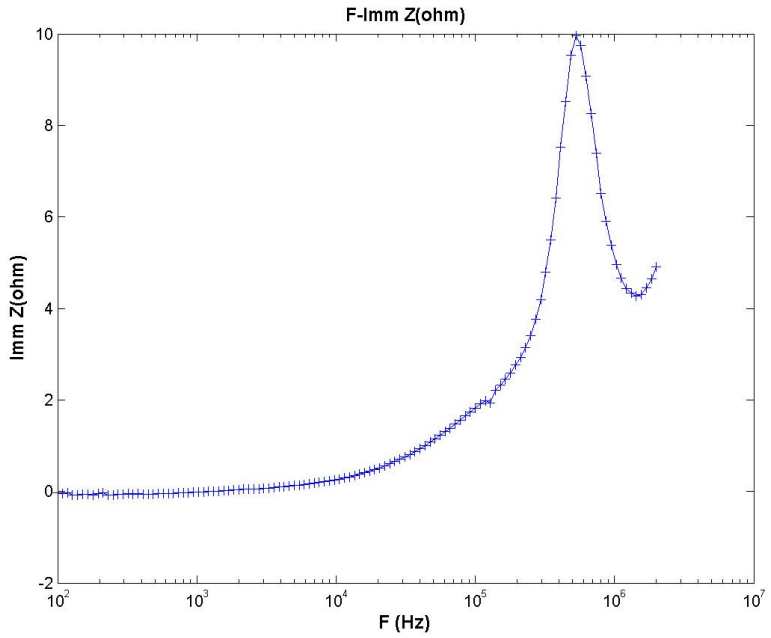

Figure 6.73: Imaginary part characteristics after switching on encapsulated cell-Sample 2

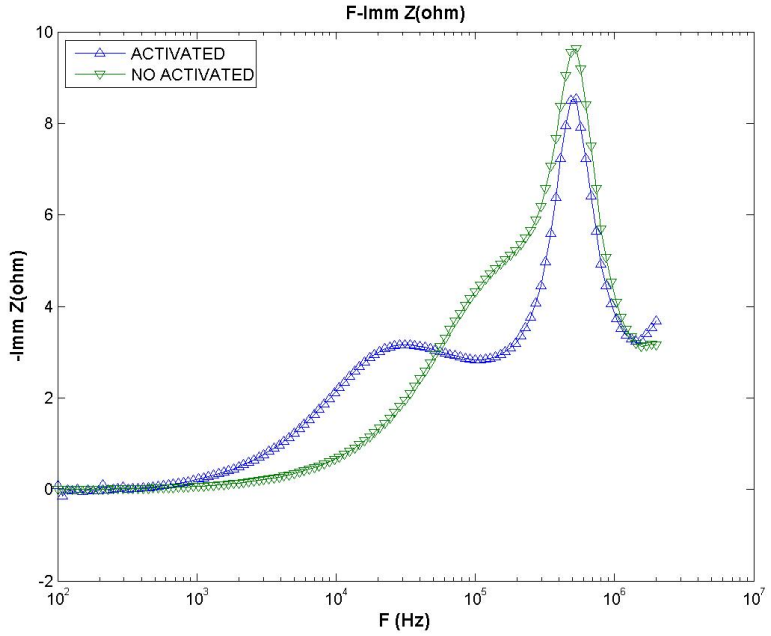

Figure 6.74: Comparison between activated and no activated cells

The activation after encapsulation show a low reproducibility. Cells after switching show two different behaviors:

- Cell-like behavior with low FF due to a low shunt resistance
- Resistance-like behaviour

Figure 6.72 and 6.73 show the Imaginary-part characteristics obtained on cell that present the Resistance-like behaviour. In figure 6.73 is possible to see a low frequency peak probably due to the active layer (blend interface); the frequency of that peak is greater than the typical value because the shunt resistance on cell (due to PEDOT:PSS penetrate into the blend) is really low and it cause the decrease of the RC time constant that model the Blend interface. In Figure 6.73 there isn't a visible low frequency peak because the blend is probably short-circuited by the PEDOT:PSS conductive path.
This test confirm that the high frequency lobe is certainly not due to PEDOT:PSS because in this situation the active layer is short circuited by the PEDOT:PSS penetrated, thus the is not a interface between the PEDOT and the active layer.
But the high frequency peak doesn't show any variation on its value of frequency if compared with an activated device and this mean that the second peak is due to a zone of the cell that is not affected by the conductive path created by the PEDOT:PSS.(see figure 6.74).

6.2.3 Conclusion on Tests made in Padua

Thanks to the tests on the switching technique we have identified a good procedure to obtain from the samples high reproducibility and efficiency. It is worth to remark that in most cases simple IV curves does not show appreciable and clear variations after activation with different conditions. However, by means of IS we see that the pulse length has a crucial role for reproducibility of the cell characteristics.
Thanks to this results now this procedure is a standard on the samples production allowing us to work with devices with similar initial characteristics. Interface identification tests allowed us to understand the phenomena involved.
These results have two important aftermath:

- Obtaining an electrical model for the solar cell; this goal is beyond the scope of this thesis
- Studying the degradation of the cells with the possibility to identify which part of the device is mostly affected; this is important because it allow to understand the direction to follow to improve the stability and durability.

Chapter 7

Production of Solar Cells

After the firsts six months of work on the DTU devices, i had the opportunity to complete my thesis at DTU Riso Campus (Denmark) focusing on the production of the solar cells.
I collaborated with the Solar Cells Group of Frederik C.Krebs, that developed a "mini" Roll to Roll system for the production of small solar cells samples.
The Roll-to-Roll machine enable to coat all the five layer of the device on flexible substrate (for example on the Flextrode) using slot-die coating and the Flexographic printing under ambient condition.
In this chapter i will explained the basic structure of the system and how it works.

7.1 Roll Coater

Figure shows one of the 3 Roll-to-Roll machines of the laboratory. It consists of a 300 mm roll where the substrate is attached.
A slot-die coating head is mounted at the top of the machine and it can be moved in order to adjust height, angle of attack and horizontal position relative to the foil.
A servo motor move the roll and permit to obtain a large range of speed.
An heater system allows to coat at controlled temperature; a fan is mounted in the back for a faster drying.

Figure 7.1: Roll Coater

Coating Head

The coating head is a slot-die coating head with an internal volume of less than 50μl allowing the use of small quantity of solution.
The head is composed of three steel parts held together by 4 screws.
The front side of the head has a 50 mm deep groove milled into it with a width of 13mm (Figure 7.2A), between the brass parts, a 0.25 mm thick stain less steel foil is placed with a meniscus guide of 13 mm width and protruding 0.5 mm from the bottom of the head (Figure 7.2C).

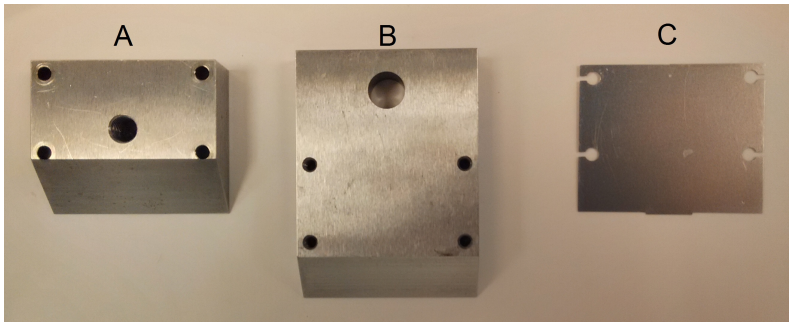

Figure 7.2: Coating Head

Pumping System

The active and the PEDOT:PSS layers are both coated with a siring-pump system (Figure 7.3).
For the active layer a small 1-ml siring and a pipe with an inner diameter of 0.5 mm are used. The PEDOT:PSS is coated using a siring of 5 ml and a pipe with an inner diameter of 1.6 mm (due to the high viscosity of the PEDOT:PSS).

Figure 7.3: Siring Pump system

7.2 Materials

The coating is performed on the Flextrode substrate (Figure 7.4).
The Flextrode is realized with an automated roll-to-roll system on a PET foil. It is composed by three layer (from bottom to top):

- *A silver Grid*: It is the front electrode of the device and it is coated using a screen printing technique
- *PEDOT:PSS layer*: Used to maximize the conduction between the hole electron conductive layer (PCBM) and the silver fingers; it is coated using a slot-die technique and it defers from the PEDOT coated manually on the mini roll-to-roll machine because it is transparent (the cell is illuminated on this side) and less conductive.

The PEDOT:PSS used is called Clevios PH1000 from Heraeus, it is diluted with isopropyl alcohol in the ratio 10:3 and it has a sheet resistance of 60-90 $\Omega square^{-1}$

- *A Zinc Oxide layer*: Used to maximize the exciton dissociation ; it is coated using a slot-die technique.

The active layer is composed of P3HT and 60PCBM in solution with chlorobenzene, chloroform and chloronaphthalene (the recipe is not published).
On the back electrode side an high conductive PEDOT:PSS is used; it has a sheet resistivity of 60 $\Omega square^{-1}$.
The back electrode is then realized using a silver grid screen-printed on the mini roll-to-roll machine; the sheet resistivity of the silver electrode is 0.1 $\Omega square^{-1}$.

To avoid contamination water is used to wash tools utilized with PEDOT:PSS and tetrahydrofuran for the P3HT:PCMB solution.

Figure 7.4: Flextrode

7.3 Coating Procedure

Active Layer

The flextrode is mounted on the roller using tape and aligned with it.
The temperature of the roller is usually of 70 °C to allow a quick and uniform dry of the active layer.
The thickness of the layer is decided changing the rotation speed of the roller and the flow rate of the siring pump. For example to obtain a thickness of 315 nm the rotation speed of the roller is set to 1 m/min and the flow rate to 0.1 ml/min.
Changing the rotation speed and the flow rate of the pump, the height between the head and the substrate need to be changed. It's important to remark that the position of the coating head is done manually.

PEDOT:PSS layer

The coating of the PEDOT:PSS is impossible without a preliminary treatment of the active layer with butanol. In fact, the P3HT is hydrophobic and the PEDOT:PSS is prepared in a water-based solution; trying to coat the PEDOT:PSS without the preliminary treatment cause the de-wetting of the PEDOT:PSS layer that means that the PEDOT:PSS tend to form non-uniform spots without a good adhesion with underlying layer. Using the butanol, the surface of the P3HT layer becomes hydrophilic and this allow to coat the PEDOT:PSS layer without de-wetting effects.
The Flow rate of the pump is set to 1.2 ml/min and the speed of the roller at 0.8 m/min.
The final thickness of the PEDOT:PSS layer is 250 μm.
The layer is then dried for 40 minutes on the roller.

Back Silver Electrode

After the drying of the PEDOT:PSS layer the back silver contact is applied by flexographic printing on the PEDOT:PSS layer.
The pattern of the electrode is shown on Figure 7.5.
It is applied using a master roll with the pattern of the electrode. The silver paste is then applied on the roll manually with a roller brush.

The foil is then dried in the oven with a temperature of 110 °C for 10 minutes.
Any complete device has an active area of 1 cm^2

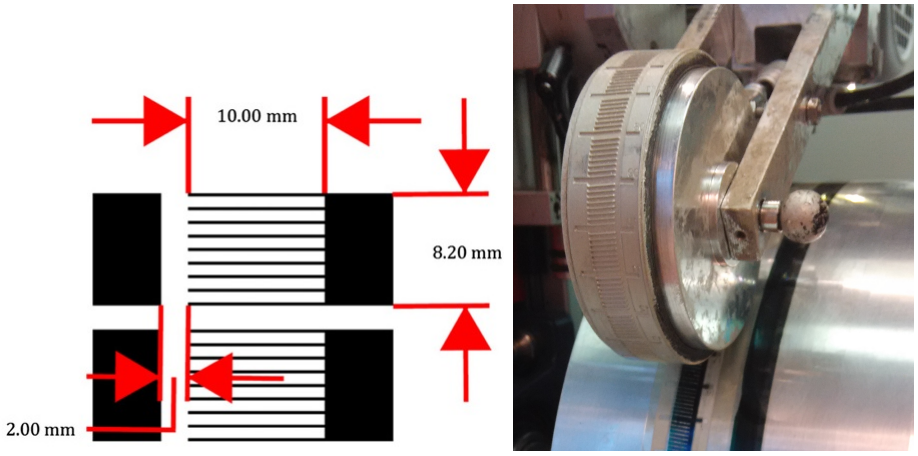

Figure 7.5: Finger Pattern and example of silver coating procedure

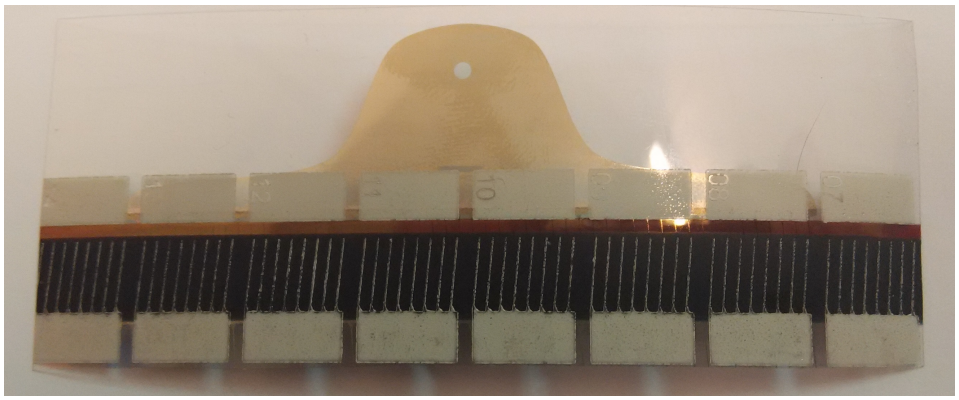

Figure 7.6: Example of some complete devices without encapsulation

Switching and Annealing

Before the encapsulation of the solar cell, like know the cells are activated with the switching technique.
Once activated the cells are usually annealed on a thermal plate at 110 °C in order to increase the efficiency of the device.
This is due to physical changes which occur in the film as result of the thermal annealing process.

An as-cast P3HT:PCBM film is relatively amorphous in structure. This unordered structure severely limits the conduction and charge carrier mobility. As a result, non-annealed OPV devices often show low charge carrier mobility and ultimately low Jsc and fill factor. The purpose of an annealing step is to change the properties of the film from unordered and amorphous to a more homogeneous nature. The film undergoes this transition as a result of an alignment of the polymer chains to form crystallites.
The most important changes that occur in the film after the annealing are basically two:

- **Nano morphology organisation** The local nanoscale organisation of the donor and acceptor in the active layer has a profound impact on the PCE of the device. Intense study of the P3HT:PCBM system as led to an understanding that an annealing treatment induces a more stable nanoscale network with an higher degree of crystallinity and order.

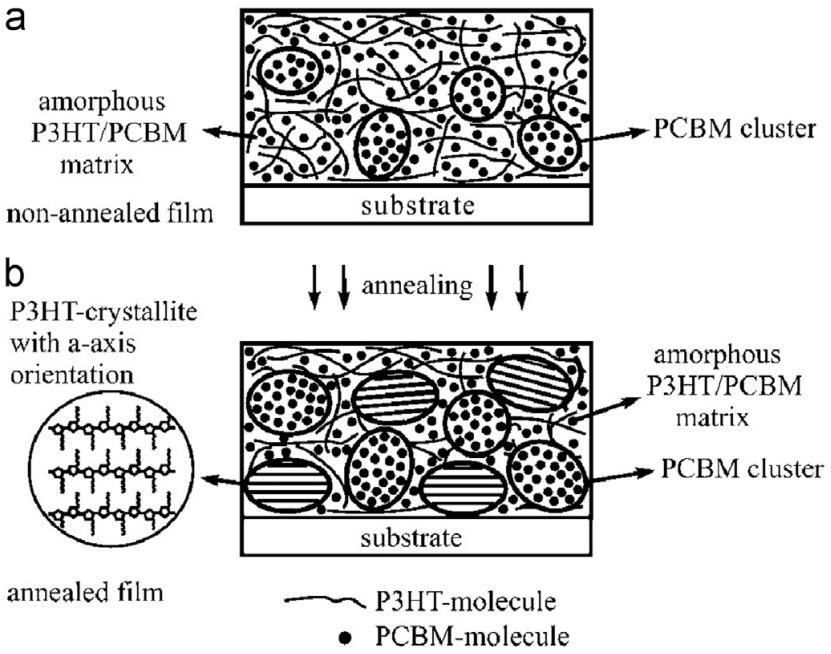

Figure 7.7: Result of the annealing of the solar cell

- **Absorption spectra** Two phenomena are generally observed as a result of thermal annealing. Both a red shift in peak absorption and an increase in magnitude of absorption are observed for a P3HT:PCBM

blend.

Analysis of the P3HT:PCBM films clearly display both of these traits. This will lead to an overall observable increase in useful absorption. With reference to the pure P3HT film, the absorption of the blend is blue-shifted and the vibronic structure of the as-cast P3HT is lost, due to the disruption of the P3HT internal order as a result of the PCMB addition. Upon thermal annealing, the absorption is red-shifted and the vibronic structure is restored.

The magnitude of the absorption also increase by 50 % which is a result of a higher degree of inter-chain interaction. The process of thermal annealing causes P3HT to crystallise which induces a thermodynamically driven alteration of the photoactive layer. This causes a rearrangement of donor and acceptor phases and increase in cristallinity of the P3HT and an improved absorption profile.

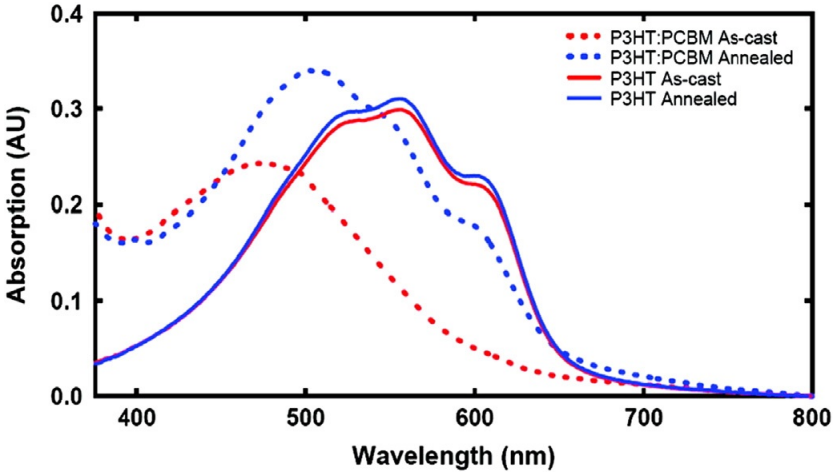

Figure 7.8: Uv-vis spectra for pure P3HT and P3HT:PCBM blend films

Encapsulation

Once realized and tested the devices, usually the working cells are encapsulated using an epoxy glue and small square glass of 15x15 mm in order to avoid the degradation of the cell due to the exposure to oxygen. The glue is left to dry for a few minutes and then the cell can be touched without danger.

Chapter 8

Conclusion

When i started to work on DTU solar cells, it was not yet clear what could be the ultimate goal of my work. In fact, we were the first group that begin to study their devices using the impedance spectroscopy technique and, even if a lot of other group had still worked in similar type of solar cells, our results showed several differences; thus, a direct comparison was not possible. In the beginning the first problem was the non-reproducibility of the results: cells that theoretically should have the same characteristics showed big differences during Impedance Spectroscopy analysis.
The way in which the solar cells are made can definitely affect the reproducibility of the results; many of the parameters of the cell (thickness of the active layer, cell width, width of the PEDOT:PSS back electrode etc.) are actually determined manually e this can cause the differences between devices coated at the same time.
Having no control over the production process of the cells, we start focusing on the switching technique. Also this procedure was realized manually without control on the length of the activation pulse.
The first part of my thesis work was aimed on the realization of the pulse generator circuit and on the test of the influence of the pulse characteristics on the Impedance Spectroscopy curves after the cell activation. We found an optimal value for the length and the voltage of the pulse, demonstrating not only that the cells activated in this way have similar Impedance Spectroscopy curves but also that they have an higher efficiency if compared with the ones activated manually.
Once obtained a good reproducibility, we started with some tests oriented on

the identification of the layers responsible of the different lobe on Impedance Spectroscopy curves in order to obtain an electrical model of the devices.
We start focusing on the active layer because simply changing the illumination condition it was possible to identify which lobe was affected.
For the other lobe the situation was completely different because a direct test was not possible; we start assuming that it was due to the ZnO:P3HT interface, setting up a lot of different experiment trying to affect only that interface.
The first tests proved that the lobe was due to an interface phenomenon (using samples with different ZnO layer thickness).With the other tests we demonstrated that first hypothesis was correct.
Thus after six months of work we had a good knowledge on the phenomena that occurs in the device.
At the first of September i started working with the solar cells group at DTU. In the first period i focused on the production process of the solar cell and on the various type of degradation protocol used. Once obtained a good reproducibility between my samples i start doing some Impedance Spectroscopy test in parallel with the Padua university.
I realized a program (with labview) for the LCR "hioki 3532-50" and a set up for the Impedance Spectroscopy tests using a LED source. We aimed to do some on-site degradation on each layer of the device separately in order to evaluate how the degradation affects each lobe on the Impedance Spectroscopy curves. The first result was good but without a comparison with the Padua results was not still possible to confirm them.

Bibliography

[1] Andrea Cester, *Elettronica organica e Molecolare.*

[2] Gaetan Masson, Marie Latour, Manoel Rekinger, Ioannis-Thomas Theologitis, Myrto Papoutsi, *Global Market Outlook for Photovoltaic 2013-2017.* European Photovoltaic Industries Association 2013

[3] Jeffery L. Gray, *The Physics of the Solar Cell.* Purdue University, West Lafayette, Indiana, USA,2003

[4] Michael C.Petty, *Molecular Electronics,From principle to practice.* Addison Wesley, Massachusetts, Wiley,2007

[5] Juan Carlos Cuevas,Elke Scheer *Molecular Electronics: An Introduciton to Theory and Experiment.* World Scientific,2010

[6] Gamry Instruments *Basics of Electrochemical Impedance Spectroscopy.*

[7] M. Glatthaar, N. Mingirulli, B. Zimmermann, T. Ziegler, R. Kern, M. Niggemann, A. Hinsch, and A. Gombert *Impedance spectroscopy on organic bulk-heterojunction solar cells.* phys.stat.sol. 202, No. 11, 125-127(2005)

[8] M. Glatthaara, M. Riedea, N. Keeganb, K. Sylvester-Hvida, B. Zimmermanna, M. Niggemanna, A. Hinschb, A. Gombertb *Efficiency limiting factors of organic bulk heterojunction solar cells identified by electrical impedance spectroscopy.* Solar Energy Materials and Solar Cells 91 390-393(2007)

[9] Germa Garcia-Belmonte,Antoni Munar, Eva M. Barea, Juan Bisquert, Irati Ugarte, Roberto Pacios *Charge carrier mobility and lifetime of organic bulk heterojunctions analyzed by impedance spectroscopy.* Organic Electronics 9 847-851(2008)

[10] James I. Basham , Thomas N. Jackson , and David J. Gundlach *Predicting the J-V Curve in Organic Photovoltaics Using Impedance Spectroscopy.* Adv. Energy Mater. 1400499 (2014)

[11] Germa Garcia-Belmonte, Antoni Munar, Eva M. Barea, Juan Bisquert, Irati Ugarte, Roberto Pacios *Charge carrier mobility and lifetime of organic bulk heterojunctions analyzed by impedance spectroscopy.* Organic Electronics 9,847-851 (2008)

[12] Frederik C. Krebs, Markus Hosel, Michael Corazza, Brenger Roth, Morten V. Madsen,Suren A. Gevorgyan, Roar R. SÃ¸ndergaard, Dieter Karg and Mikkel JÃ¸rgensen *Freely available OPV-The fast way to progress.* Energy Technol. 1,378-381 (2013)

[13] Henrik F.Dam, Frederik C.Krebs *Simple roll coater with variable coating and temperature control for printed polymer solar cells.* Solar Energy Materials and Solar Cells 97, 191-196 (2012)

[14] Jon E.Carle, ThomasR.Andersen, Martin Holgesen, Eva Bundgaard, Mikkel Jorgensen, Frederik C.Krebs *A laboratory scale approach to polymer solar cells using one coating/printing machine, flexible substrates, no ITO, no vacuum and no spin coating.* Solar Energy Materials and Solar Cells 108, 126-128 (2013)

[15] Xiaohan Yang n, Ashraf Uddin *Effect of thermal annealing on P3HT:PCBM bulk-hetero junction organic solar cells: A critical review.* Renewable and Sustainable Energy Reviews 30, 324-336 (2014)

[16] Thomas R.Andersen,Henrik F.Dam, Birgitta Andreasen, Markus Hosel, Morten V.Madsen, Suren A.Gevorgyan, Roar R. Sondergaard, Mikkel Jorgensen, Frederik C.Krebs *A rational method for developing and testing stable flexible indium-and vacuum-free multi layer tandem polymer solar cells comprising up to twelve roll processed layers.* Solar Energy Materials and Solar Cells 120, 735-743 (2014)